# Investigation of the Surface Tension of Atmospheric Liquids by Molecular Dynamics Simulations

Dissertation

zur Erlangung des Ges

‘Doktor rerum naturalium (Dr. rer.nat.)’

im Promotionsfach Chemie

am Fachbereich Chemie, Pharmazie und Geowissenschaften

der Johannes Gutenberg-Universität in Mainz

Paul Crutzen Graduate School

**Xiaoxiang Wang**

geb. am 21. 09. 1989 in Wenzhou, China

Mainz, Germany. March, 2019

I hereby declare that I wrote the dissertation without any unauthorized external assistance. I used only sources acknowledged in the work. All textual passages which are appropriated verbatim or paraphrased from published and unpublished texts as well as all information obtained from oral sources are duly indicated and listed in accordance with bibliographical rules. In carrying out this research, I complied with the rules of standard scientific practice as formulated in the statutes of Johannes Gutenberg-University Mainz to insure standard scientific practice.

Xiaoxiang Wang

March, 2019.

**Abstract**

The surface tension of liquids is important for many processes in the atmosphere. However, a lot of uncertainties exist over its influencing factors. For example, people are still debating whether the "second inflection point (SIP)" exists in the temperature dependence of the surface tension of water in the supercooled regime. Controversies can also be found in the discussions about the concentration-of-solutes dependence and size dependence in the nano-regime. In this PhD project, these uncertainties are clarified by using molecular dynamics (MD) simulations.

In the first part of this work, we use MD simulations of the SPC/E water model to study the surface tension of water ($\sigma_w$) as a function of temperature down to 198.15 K, and find a minimum point of surface excess entropy per unit area around ~240-250 K. Hence, we predict a second inflection point (SIP) of $\sigma_w$ roughly in this region, at the boundary where the "no man's land" happens. Furthermore, we find that $\sigma_w$ has a near-linear correlation with the interfacial width, which can be well explained by the capillary wave theory. Deep in the supercooled regime, a compact water layer in the interface is detected in our simulations.

The second part is about the surface tension of aqueous NaCl solution ($\sigma_{NaCl,sol}$) and the concentration dependence. We show that the linear approximation of concentration dependence of $\sigma_{NaCl,sol}$ at molality scale can be extended to the supersaturated NaCl solution until a molality of ~10.7 mol $kg^{-1}$ (i.e., solute mass fraction ($x_{NaCl}$) of ~0.39). After that, the simulated $\sigma_{NaCl,sol}$ remains almost unchanged until $x_{NaCl}$ of ~0.47 (near the concentration upon efflorescence). After a "second inflection point" at $x_{NaCl}$ of ~0.47, the $\sigma_{NaCl,sol}$ gradually regains a strong concentration dependence with a tendency to approach the surface tension of molten NaCl (~175.58 mN $m^{-1}$ at 298.15 K).

Finally, the vapor pressure and surface tension of water nano-droplets are studied by MD simulations. We found the value of $\ln\frac{P_{sat}(r)}{P_{sat\_0}}$ increases from 0.46 to 2.1 when the radius decreases from ~1.92 nm to ~0.4 nm. The size dependence of the surface tension was analyzed by using a modified form of Tolman equation. The Tolman length is conjectured to be -0.12 nm.

In conclusion, several anomalies exist in the temperature dependence, concentration dependence and size dependence of the surface tension, and these anomalies are analyzed from the perspective of energy and structure.

# Contents

# 1. Introduction

## 1.1 Surface tension and its significance in the atmosphere

According to the International Union of Pure and Applied Chemistry (IUPAC), surface tension (σ) is the work required to increase a surface area divided by that area (*1*). From the perspective of mechanics, σ is the attractive force that tends to draw the surface molecules into the inner part of the liquid and makes the liquid having the least surface area. Dimensions of σ are energy/area or force/length, and the units are typically joules per metre squared (J m$^{-2}$) or newtons per metre (N m$^{-1}$) (*2*). In term of phases we studied, σ may be liquid-vapor, liquid-liquid, liquid-solid or solid-vapor surface tension. In this thesis, we mainly study liquid-vapor surface tension, thus we use "surface tension" and "σ" to represent the liquid-vapor surface tension. Many experimental methods can be used in the measurement of liquid-vapor surface tension, mainly including Du Noüy ring method, Wilhelmy plate method, Spinning drop method, Pendant drop method, Maximum bubble pressure method, Capillary rise method and Stalagmometric method (*3-9*). The brief introduction of these methods was summarized in Table 1-1.

Surface tension (σ) plays a vital role in various processes in the atmosphere. Firstly, σ affects the thermodynamic equilibrium during the process of cloud formation, thereby influencing effects relevant for the climate change (*10*). It is well-known that aerosols act as cloud condensation nuclei (CCN) during the process of cloud formation. The value of σ can affect equilibrium between an aerosol and the vapor over the aerosol's curved surface due to the Kelvin effect (Eq. 1-1) (*11*).

$$P = P_0 \cdot \exp(\frac{2\sigma V_m}{rRT}) \quad (1\text{-}1)$$

Here, P is the saturated vapor pressure of the droplet with a radius of r; $P_0$ is the vapor pressure of a planar surface; $V_m$ is the molar volume of the studied liquid; R is the gas constant and T the temperature in Kelvin. Through the Kelvin effect (Eq. 1-1) and Raoult's law (*12*, *13*), σ can determine the activation states of particles, i.e. hygroscopicity. Recently, Giordano et al. observed in situ that changes of σ affected the hygroscopicity of corresponding biomass burning aerosols (*14*). Secondly, σ is

important for the kinetics of the nucleation of atmospheric droplets/particles. In the nucleation theory (*15*), the rate of homogeneous nucleation from an ideal supersaturated vapor, J, is related to σ. It is because the surface energy (σ×surface area) is the main energy barrier from the gas phase to the condensed phase during the nucleation.

Table 1-1. Experimental approaches used to measure the liquid-vapor surface tension.

| Name (references) | Brief introduction |
|---|---|
| Du Noüy ring method (*3*) | It involves lifting a ring from the surface of a liquid. The force required to raise the ring from the surface is measured and used to calculate σ. |
| Wilhelmy plate method (*4*) | A vertical plate is oriented to the surface, and the force exerted on this plate is measured. After that, σ can be calculated. |
| Spinning drop method (*5*) | A gas bubble is placed inside a rotating horizontal tube which contains a liquid. The centrifugal forces from rotation make the bubble to deform into an elongated shape. This deformation stops when σ and centrifugal forces are balanced. Then σ can be derived from the shape of the bubble at this point. |
| Pendant drop method (*6*) | At the end of a tube, the force due to σ suspends the drop of liquid. This force is proportional to the length of the boundary between the liquid and the tube. Thus, σ can be calculated. |
| Maximum bubble pressure method (*7*) | Bubbles are produced and blown through a capillary. The maximum pressure inside is obtained when the bubble has the hemispherical shape whose radius is exactly same to the one of the capillary. By using Young–Laplace equation, σ is obtained. |
| Capillary rise method (*8*) | A capillary is immersed into the liquid. The height that the liquid reaches inside the end of capillary is related σ. |
| Stalagmometric method (*9*) | It is to measure the weight of drops of liquid falling from a capillary glass tube, and then calculate σ based on Tate's law. |

### 1.2 Influencing factors of the surface tension

Several pivotal factors, including temperature, vapor pressure and components, and the size of droplets can change the value of σ for the same liquid. First of all, σ is negatively correlated with the temperature of the given liquid (*16*). Thus, temperature must be explicitly stated when a value is given for σ. A number of equations were developed to describe the temperature dependence of σ. For example, Eötvös (*16*) proposed Eq. 1-2.

$$\sigma \cdot V^{\frac{2}{3}} = \mathrm{k} \cdot (T - T_\mathrm{c}) \quad (1\text{-}2)$$

Here, V is the molar volume of a substance, $T_C$ is the critical temperature and k is a constant valid for almost all substances. Of course, now one knows that this simple relation does not hold quantitatively. The International Association for the Properties of Water and Steam (IAPWS) provided an accurate equation to describe the temperature dependence of surface tension of water ($\sigma_w$) (*17*):

$$\sigma_\mathrm{w}(T) = B \cdot \left(\frac{T_\mathrm{c}-T}{T_\mathrm{c}}\right)^{\mu} \cdot (1 + b \cdot \frac{T_\mathrm{c}-T}{T_\mathrm{c}}) \quad (1\text{-}3)$$

Here, $\sigma_\mathrm{w}(T)$ is in mN m$^{-1}$ and T is the temperature in Kelvin. The critical temperature $T_C$ is 647.096 K. B, μ and b are 235.8 mN m$^{-1}$, 1.256 and -0.625, respectively. Secondly, species and the concentration of dissolved solutes can also affect the surface tension of the liquid (solvent) (*18-20*). For example, the majority of inorganic salts can increase σ of water (*18*), while alcohols decrease σ of water (*20*). For the concentration dependence, different models have been developed to describe it. Dutcher et al. built a model that predicts σ of electrolyte solutions as well as their mixtures whose concentrations range from dilute to infinite (*21*). This model is employed in the extended aerosol inorganics model (E-AIM), which is frequently used in atmospheric investigations. Szyskowski proposed Eq. 1-4 to describe the decrease of σ for aqueous solutions of dissolved organic surfactant at low concentrations (*22*).

$$\sigma = \sigma_0 - \vartheta RT\Gamma_\infty \ln(1 + K_L C) \quad (1\text{-}4)$$

where $\sigma_0$ is surface tension of pure water, ϑ represents the number of species produced by surfactants, $\Gamma_\infty$ and $K_L$ are constants specific for each surfactant, and C is the value of the concentration. Thirdly, the size of droplets can affect the value of σ of the corresponding droplets as well. By using thermodynamic interpretation, Rice predicted that increasing vapor pressure could reduce the value of σ (*23*). Experimental results supported this relationship (*24*). For instance, the value of σ of water-$CO_2$ surface under 60 atm pressure is half of the one under a zero pressure. Given that the vapor pressure over a droplet can be affected by the size of this droplet, thus the size of droplet can also affect the value of σ indirectly. The relation between

σ and the radius of droplet (r) was derived by Tolman (*25*):

$$\sigma(r) = \frac{\sigma_\infty}{1+2\frac{\delta}{r}} \quad (1\text{-}5)$$

$\sigma(r)$ is σ of a droplet with a radius of r; $\sigma_\infty$ denotes the planar σ; and $\delta$ is the so-called Tolman length. This size dependence of σ attracted a lot of discussions (*26-30*), and further studies would be helpful for understanding it.

### 1.3 Research objectives and questions to be resolved

Water normally freezes at 0 ℃ (273.15 K), however it can be "supercooled" and remain non-frozen at standard pressure down to about 235K, i.e. the homogeneous nucleation temperature, without heterogeneous nucleation sites (*31, 32*). Supercooled water receives considerable attention from atmospheric chemistry and physics. It was widely detected in atmospheric systems, such as in cirrostratus (*33*), orographic wave clouds (*34*) and deep convective clouds (*35*). In the latter study, Rosenfeld and Woodley reported that most of the condensed water in deep convective clouds remains liquid down to -37.5 °C, and these droplets have a median diameter of 17 μm and amount to 1.8 $g \cdot m^{-3}$ (*35*). IAPWS has proposed Eq. 1-3 to describe the temperature dependence of $\sigma_w$ (*17*). This quantitative relationship is, however, only based on the experimental data of $\sigma_w$ above 0 ℃ (273.15K), and it is still under debate if the $\sigma_w$ of supercooled water follows the IAPWS equation. Many studies showed an anomaly in the dependency of the $\sigma_w$ on temperature (*36-40*). According to these studies, $\sigma_w$ has a stronger increase along with decreasing temperature below a specific temperature in the vicinity of 0 ℃, and the corresponding point is thus defined as the "second inflection point (SIP)". However, recent laboratory studies showed contrasting results, where no SIP was found by different methods (*41-43*). Thus, we calculated $\sigma_w$ over a temperature range from 198.15 K to 348.15 K to determine (Q1) if SIP exists and where it is. Indeed, the physical chemistry behind the temperature dependence of $\sigma_w$ is still unclear. The driving forces (enthalpic or entropic part of surface free energy) of the changes of $\sigma_w$ and structural factors determining the temperature dependence have not been elucidated clearly. According

to the energetic and structure analyses, (Q2) the causes of temperature dependence of $\sigma_w$ were investigated.

The second study of this PhD project regards to the surface tension of supersaturated NaCl solution. The aqueous NaCl solution droplet was reported to be involved in several processes of the atmosphere (*44-51*). These processes are: I) Phase transition: below the efflorescence point (~45% RH), the crystallization of NaCl salt occurs in the aqueous solution (*44*). Recently, Cheng et al. showed that the efflorescence point of NaCl solution was dependent on the size of the solution droplet (*52*), which means NaCl salt may be generated at a higher RH condition. II) Ice nucleation: after the efflorescence, solid NaCl in the atmosphere can provide a heterogeneous site for nucleation of supercooled water (*46*). III) Cloud activation: Bilde and Svenningsson have revealed the significance of NaCl in the cloud activation (*45*). They found that small amounts of NaCl salt may have a dramatic effect on the critical supersaturation of soluble organic compounds, and this result explained the apparent gap between experimental data and theory in the form of the modified Köhler equation for acids (*45*). IV) Aqueous-phase chemistry: in the solution, several types of reactions lead to the depletion of $Cl^-$ and the formation of gas-phase chlorine compounds. Among these reactions, 5 types were considered to be the most important ones by Finlayson-Pitts (*50*): acid displacement reactions, reactions initiated by $O_3$, reaction with OH, reactions with sulfur compounds, and reactions with $NO_3$ and $N_2O_5$ (*50*). V) Heterogeneous chemistry: both of the aqueous NaCl solution and the solid NaCl from the efflorescence participate in heterogeneous chemistry of aerosols (*47*, *48*). By using experiments, molecular dynamics (MD) simulations, and the kinetics modeling, Knipping et al. found that $Cl^-$ ions prefer to stay on the surface of aqueous NaCl solution droplets and attract hydroxl radicals (*47*). As a result, the ion-enhanced interactions with gases at aqueous surfaces produce large amount of gas-phase chlorine compounds. Similarly, several reactions on the surface of solid NaCl have been reported, e.g. generation of nitrosyl chloride from nitrogen dioxide (*48*), generation of molecular chlorine from chlorine nitrate (*49*), and generation of molecular chlorine induced by OH (*51*). Due to the significance of aqueous NaCl

solution, the concentration-dependent $\sigma_{NaCl,sol}$ is essential to determine the equilibrium between NaCl solution droplet and water vapor. Below the saturation point (~6.15 mol $kg^{-1}$), $\sigma_{NaCl,sol}$ shows a near linear dependence on molality (*53*, *54*) with a slope of 1.73±0.17 (*18*, *55*). Due to the energy barrier of crystallization during dehydration and size-effects at the nanoscale (*44*, *52*, *56*), supersaturated aqueous NaCl solution droplets can exist under atmospheric conditions. It is a matter of debate to which extent the approximation of a near linear dependence of surface tensions on molality can still be used for NaCl droplets. Therefore, $\sigma_{NaCl,sol}$ of solution with different concentration from infinitely dilute ($x_{NaCl}$ = 0) to highly supersaturated solution to molten salt ($x_{NaCl}$ = 1) was calculated to determine (Q3) concentration dependence of $\sigma_{NaCl,sol}$. More importantly, the physical chemistry behind the concentration dependence is also unclear. (Q4) The change was also explained from the perspective of energy and structure, e.g. the profile of surface enthalpy and the distribution of ions. Last but not least, surface tension of the water nano-droplet was investigated.

The third study is about water nano-droplets. The droplets studied here, whose size is at the scale of a few nanometers, may not be very pertinent to the atmosphere directly, while the results and conclusion based on them have the implications for many atmospheric processes, e.g. new particle formation. Because of the significance of the vapor pressure and surface tension atmospheric nano-particles, (Q5) we developed a method, based on the MD simulation, to calculate the vapor pressure and surface tension of nano-droplets. Another question concerns the size dependence of these 2 properties. Tolman has showed that the surface tension of spherical droplets can be written as a simple function of radius of the droplets (Eq. 1-5) (*25*). Currently, many debates are carried out about Tolman length, although it is agreed that this value should be of the order of the inter-molecular distance. The value of water proposed by Tolman was 0.1 nm originally (*57*). However, a work based on MD simulations for the TIP4P/2005 water model reported a negative $\delta$ of -0.056 nm, and in this case, the surface tension should increase when the droplet becomes smaller (*26*). This inconsistency might be explained by the different assumptions in the data processing.

Besides the debates about $\delta$, the validity of Eq. 1-5 is also disputed (*58-60*). Therefore, (Q6) we studied the size dependence of vapor pressure and surface tension of nano-droplets based on the developed method.

### 1.4 Molecular dynamics (MD) simulations and calculation of surface tension

Measuring the surface tension of highly supercooled water, supersaturated NaCl solution and nano-droplets is quite difficult. At the same time, the mechanisms behind the observed trends are also essential to be interpreted. Molecular dynamics (MD) simulations would be a useful tool to obtain these goals. MD simulations describe the physical movements of atoms/molecules using Newton's equations of motion (*61, 62*). In MD simulations, interactions between studied atoms/molecules are given (namely, the force field), and then the Newton's equations of motion are solved to evolve atoms/molecules. MD simulations have several advantages. This technique can provide detailed information about a system at the atomic level, such as the structure and thermodynamic properties. In addition, conditions of interests, such as pressure and temperature, for a system can be controlled very accurately in MD simulations. This method gained popularity in materials science and biophysics. In materials science, MD simulations are carried out to investigate the dynamics of phenomena that cannot be observed by experiments, as well as physical properties of nano-materials, e.g. growth of the thin film (*63*). In biophysics, the method is frequently applied to study the behaviors of proteins or nucleic acids (*64*), which can be used to interpret the results of experiments and model interactions with other molecules. In the last decade, more and more MD simulations are performed to study topics of atmospheric chemistry and physics. Loukonen et al. investigated the nucleation of sulfuric acid in the presence of water by employing MD simulations (*65*). Karadima et al. studied the local structure and local concentration in atmospheric nanoparticles consisting of cis-pinonic acid, sulfate and ammonium ions, and water (*66*). Mass accommodation of water on particles was also studied by Julin et al. (*67*) and Takahama and Russell (*68*). Knipping at al. (*47*) and Ghosal et al. (*69*) found chloride, bromide and iodide ions can enrich on the surface of aerosols, and this

phenomenon explains the ion-enhanced interfacial chemistry of aerosols. We can expect that, obviously, more investigations about atmospheric particles would employ the technique of MD simulations in the future.

Several types of techniques based on MD simulation have been developed to determine σ for the liquid-vapor surface. The mostly used technique involves a mechanical route which requires the calculation of the pressure tensor (*70*). Thus, this method was named as the "pressure tensor" method. In the case of a planar surface, σ is given by Eq. 1-6,

$$\sigma = \int_{-\infty}^{\infty} dz[P_N(z) - P_T(z)] \quad (1\text{-}6)$$

where $P_N$ (z) and $P_T$ (z) are the normal and tangential components of the pressure. According to Alejandre (*71*), in the context of MD simulations, Eq, 1-6 can also be presented as Eq. 1-7.

$$\sigma = \frac{1}{2} L_z[\langle P_{zz}\rangle - \frac{1}{2}\big(\langle P_{xx}\rangle + \langle P_{yy}\rangle\big)] \quad (1\text{-}7)$$

Here, $L_z$ is the length of the simulation cell in the longest direction (more descriptions about simulation cells are shown in the next chapter), and $P_{aa}$ (a=x,y,z) denotes the diagonal component of the pressure tensor. The < > refers to time average. The factor of 1/2 outside the bracket arises from the presence of two surfaces in the system. Currently, pressure tensors can be obtained directly by the majority of molecular simulation software directly. The second class of methods to calculate σ involves a thermodynamic way. The difference of free energy between two or more systems with different surface areas is determined to estimate σ (*72*). This concept can be presented as Eq. 1-8.

$$\sigma = (\frac{\partial F}{\partial A})_{NVT} \quad (1\text{-}8)$$

i.e., σ is the change of free energy for an infinitesimal change in the surface area. Here, F is the free energy; A is the surface area; and NVT means that studied systems have a constant volume and temperature. After the first work of free energy-difference method by Bennett (*72*), a number of researchers developed advanced methods, such as Moody and Attard (*73*), and Laird and Davidchack (*74*). Test-area method developed by Gloor et al. (*75*) provides a significant reduction in computational costs

by comparing with methods above. This method is related to the energy-difference method, while it relies on estimating the change of free energy from perturbations in the surface area within an individual simulation. Last but not least, one class of methods is related to the concept of finite-size scaling. For instance, Binder estimated σ between 2 phases with a flat surface from the variation of certain probability distribution functions of finite blocks with block size (*76*).

## 2. Results and discussion

### 2.1 Overview

The main results of this PhD project are described in three first-author manuscripts which are attached in Appendix B. Two of these have already been published and one is prepared to be submitted. Figure 2-1 provides an overview of the studies, and the main results and conclusions are summarized in the following sections. In addition to the research and results presented in this thesis, the PhD project also includes investigations of the size dependence of solubility of NaCl nano-particles and the development of a new method to observe atmospheric particles based on the scanning force microscopy (SFM). These additional studies are still in progress and thus not included in this thesis.

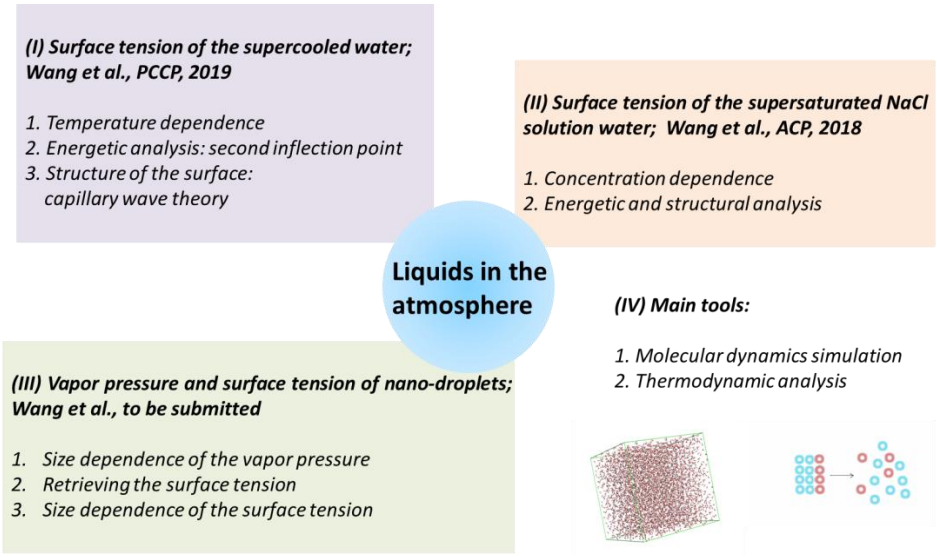


Figure 2-1. Structure of the PhD thesis. In the middle, the object of the project is schematically presented. In the panel I, II and III, the topics, corresponding papers and main studied questions are shown. In the pane IV, tools used in this thesis are mentioned.

## 2.2 Individual studies

### 2.2.1 Surface tension of the supercooled water

The surface tension of supercooled water is of fundamental importance in physical chemistry and material and atmospheric sciences. Controversy, however, exists over its temperature dependence in the supercooled regime, especially on the existence of the "second inflection point (SIP)". Here, we predict an SIP of $\sigma_w$ roughly in the region of ~240 K-250 K, at the boundary where the "no man's land" happens. The increase of surface entropy with decreasing temperature in the region below the inflection point clearly is an anomalous behavior, unknown for simple liquids. Furthermore, we find that $\sigma_w$ has a near-linear correlation with the interfacial width, which can be well explained by the capillary wave theory. Deep in the supercooled regime, a compact water layer in the interface is detected in our simulations, which may be a key component that contributes to the deviation of surface tension from the International Association for the Properties of Water and Steam relationship.

### 2.2.2 Surface tension of the supersaturated NaCl solution

Sodium chloride (NaCl) is one of the key components of atmospheric aerosols. The surface tension of aqueous NaCl solution ($\sigma_{NaCl,sol}$) and its concentration dependence are essential to determine the equilibrium water vapor pressure of aqueous NaCl droplets. Supersaturated NaCl solution droplets are observed in laboratory experiments and under atmospheric conditions, but the experimental data for $\sigma_{NaCl,sol}$ are mostly limited up to sub-saturated solutions. In this study, we show that the linear approximation of concentration dependence of $\sigma_{NaCl,sol}$ at molality scale can be extended to the supersaturated NaCl solution until a molality of ~10.7 mol $kg^{-1}$ (i.e., solute mass fraction ($x_{NaCl}$) of ~0.39). Energetic analyses show that this monotonic increase of surface tension is driven by the increase of excess surface enthalpy ($\Delta H$) as the solution becomes concentrated. After that, the simulated $\sigma_{NaCl,sol}$ remains almost unchanged until $x_{NaCl}$ of ~0.47 (near the concentration upon efflorescence). The existence of the "inflection point" at $x_{NaCl}$ of ~0.39 and the stable surface tension of $x_{NaCl}$ between ~0.39 and ~0.47 can be attributed to the nearly unchanged excess surface entropy term ($T \cdot \Delta S$) and the excess surface enthalpy term ($\Delta H$). After a "second inflection point" at $x_{NaCl}$ of ~0.47, the simulated $\sigma_{NaCl,sol}$ gradually regains momentum stronger concentration dependence with a tendency to approach the surface tension of molten NaCl (~175.58 mN $m^{-1}$ at 298.15 K, MD simulation based extrapolation). This fast increase of $\sigma_{NaCl,sol}$ at $x_{NaCl}$ > 0.47 is a process driven by excess surface enthalpy and excess surface entropy. Our results reveal different regimes of concentration dependence of the surface tension of aqueous NaCl at 298.15 K: a water-dominated regime ($x_{NaCl}$ from 0 to ~0.39), a transition regime ($x_{NaCl}$ from ~0.39 to ~0.47) and a molten NaCl-dominated regime ($x_{NaCl}$ from ~0.47 to 1).

### 2.2.3 Vapor pressure and surface tension of nano-droplets

The vapor pressure and surface tension of water nano-droplets play key roles in many different processes. There are still many different debates about the size dependence of these properties. In this part, we used MD simulation to address some

questions involved in these debates. We found SPC water model is the best model to reproduce the vapor pressure of water among 6 studied models. The vapor pressure of nano-droplets with different size was calculated, and we found the value of $\ln\frac{P_{sat}(r)}{P_{sat\_0}}$ increases from 0.46 to 2.1 when the radius decreases from ~1.92 nm to ~0.4 nm. Then a method of retrieving surface tension based on the data of vapor pressure from MD simulations was developed. The size dependence of surface tension was analyzed by using a modified form of Tolman equation. The Tolman length is conjectured to be -0.12 nm. Additionally, a compression in the nano-droplet was found, and this compression might be related to the size dependence of vapor pressure and surface tension.

**3. References**


1. H. Lehmann, X. Fuentes-Arderiu, L. Bertello, Glossary of terms in quantities and units in Clinical Chemistry (IUPAC-IFCC Recommendations 1996). *Pure and Applied Chemistry* **68**, 995 (1996).
2. P. Atkins, J. De Paula, J. Keeler, *Atkins' physical chemistry* (Oxford university press, 2018).
3. P. L. du Noüy, An interfacial tensiometer for universal use. *J. Gen. Physiol.* **7**, 625 (1925).
4. L. Wilhelmy, About the dependence of capillary constants of alcohols on substance and shapes of moistened solid bodies. *Ann. Phys.* **195**, 177-217 (1863).
5. H. Princen, I. Zia, S. Mason, Measurement of interfacial tension from the shape of a rotating drop. *J. Colloid Interface Sci.* **23**, 99-107 (1967).
6. J. Andreas, E. Hauser, W. Tucker, Boundary tension by pendant drops1. *J. Phys. Chem.* **42**, 1001-1019 (1938).
7. S. Sugden, V. The determination of surface tension from the maximum pressure in bubbles. Part II. *J. Chem. Soc. Transactions* **125**, 27-31 (1924).
8. W. D. Harkins, F. Brown, The determination of surface tension (free surface

energy), and the weight of falling drops: The surface tension of water and benzene by the capillary height method. *J. Am. Chem. Soc.* **41**, 499-524 (1919).

9. A. Taylor, E. J. Boell, Studies of the electromotive force in biological systems. II. The surface activity of homologous carbamate solutions. *J. Cell. Physiol.* **3**, 385-395 (1933).
10. M. C. Facchini, M. Mircea, S. Fuzzi, R. J. Charlson, Cloud albedo enhancement by surface-active organic solutes in growing droplets. *Nature* **401**, 257 (1999).
11. W. Thomson, On the equilibrium of vapour at a curved surface of liquid. *P. Roy. Soc. Edinb.* **7**, 63-68 (1872).
12. F.-M. Raoult, Loi générale des tensions de vapeur des dissolvants. *CR Hebd, Seances Acad. Sci* **104**, 1430-1433 (1887).
13. H. Köhler, The nucleus in and the growth of hygroscopic droplets. *Trans. Faraday Soc.* **32**, 1152-1161 (1936).
14. M. R. Giordano, D. Z. Short, S. Hosseini, W. Lichtenberg, A. A. Asa-Awuku, Changes in droplet surface tension affect the observed hygroscopicity of photochemically aged biomass burning aerosol. *Environ. Sci. Technol.* **47**, 10980-10986 (2013).
15. S. L. Girshick, C. P. Chiu, Kinetic nucleation theory: A new expression for the rate of homogeneous nucleation from an ideal supersaturated vapor. *J. Chem. Phys.* **93**, 1273-1277 (1990).
16. R. Eötvös, Ueber den Zusammenhang der Oberflächenspannung der Flüssigkeiten mit ihrem Molecularvolumen. *Ann. Phys.* **263**, 448-459 (1886).
17. IAPWS, *IAPWS release on surface tension of ordinary water substance* (International Association for the Properties of Water and Steam (IAPWS), Moscow, Russia, 2014).
18. L. M. Pegram, M. T. Record, Hofmeister salt effects on surface tension arise from partitioning of anions and cations between bulk water and the air-water interface. *J. Phys. Chem. B* **111**, 5411-5417 (2007).

19. K. Habrdová, Š. Hovorka, L. Bartovská, Concentration dependence of surface tension for very dilute aqueous solutions of organic nonelectrolytes. *J. Chem. Eng. Data.* **49**, 1003-1007 (2004).

20. G. Vazquez, E. Alvarez, J. M. Navaza, Surface tension of alcohol water+ water from 20 to 50. degree. C. *J. Chem. Eng. Data.* **40**, 611-614 (1995).

21. C. S. Dutcher, A. S. Wexler, S. L. Clegg, Surface tensions of inorganic multicomponent aqueous electrolyte solutions and melts. *J. Phys. Chem. A* **114**, 12216-12230 (2010).

22. B. von Szyszkowski, Experimentelle Studien über kapillare Eigenschaften der wässerigen Lösungen von Fettsäuren. *Z. Phys. Chem.* **64**, 385-414 (1908).

23. O. K. Rice, The effect of pressure on surface tension. *J. Chem. Phys.* **15**, 333-335 (1947).

24. R. Massoudi, A. King Jr, Effect of pressure on the surface tension of water. Adsorption of low molecular weight gases on water at 25 °. *J. Phys. Chem.* **78**, 2262-2266 (1974).

25. R. C. Tolman, The effect of droplet size on surface tension. *J. Chem. Phys.* **17**, 333-337 (1949).

26. M. N. Joswiak, N. Duff, M. F. Doherty, B. Peters, Size-dependent surface free energy and Tolman-corrected droplet nucleation of TIP4P/2005 water. *J. Phys. Chem. Lett.* **4**, 4267-4272 (2013).

27. Y. A. Lei, T. Bykov, S. Yoo, X. C. Zeng, The Tolman length: Is it positive or negative? *J. Am. Chem. Soc.* **127**, 15346-15347 (2005).

28. L. Granásy, Semiempirical van der Waals/Cahn–Hilliard theory: size dependence of the Tolman length. *J. Chem. Phys.* **109**, 9660-9663 (1998).

29. F. P. Buff, J. G. Kirkwood, Remarks on the surface tension of small droplets. *J. Chem. Phys.* **18**, 991-992 (1950).

30. N. Bruot, F. Caupin, Curvature dependence of the liquid-vapor surface tension beyond the Tolman approximation. *Phys. Rev. Lett.* **116**, 056102 (2016).

31. C. Angell, Supercooled water. *Annu. Rev. Phys. Chem.* **34**, 593-630 (1983).

32. O. Mishima, H. E. Stanley, Decompression-induced melting of ice IV and the

liquid–liquid transition in water. *Nature* **392**, 164 (1998).

33. K. Sassen, K. N. Liou, S. Kinne, M. Griffin, Highly supercooled cirrus cloud water: Confirmation and climatic implications. *Science* **227**, 411-413 (1985).
34. A. J. Heymsfield, L. M. Miloshevich, Homogeneous ice nucleation and supercooled liquid water in orographic wave clouds. *J. Atmos. Sci.* **50**, 2335-2353 (1993).
35. D. Rosenfeld, W. L. Woodley, Deep convective clouds with sustained supercooled liquid water down to-37.5 C. *Nature* **405**, 440 (2000).
36. W. J. Humphreys, J. F. Mohler, Surface tension of water at temperatures below zero degree centigrade. *Phys. Rev.* **2**, 387-391 (1895).
37. P. T. Hacker, *Experimental values of the surface tension of supercooled water* (National Advisory Committee for Aeronautics, Washington, 1951).
38. M. Floriano, C. Angell, Surface tension and molar surface free energy and entropy of water to -27.2 ℃. *J. Phys. Chem.* **94**, 4199-4202 (1990).
39. E. Trinh, K. Ohsaka, Measurement of density, sound velocity, surface tension, and viscosity of freely suspended supercooled liquids. *Int. J. Thermophys.* **16**, 545-555 (1995).
40. V. Holten, C. Bertrand, M. Anisimov, J. Sengers, Thermodynamics of supercooled water. *J. Chem. Phys.* **136**, 094507 (2012).
41. J. Hrubý, V. c. Vinš, R. Mareš, J. Hykl, J. Kalová, Surface tension of supercooled water: no inflection point down to −25 °C. *J. Phys. Chem. Lett.* **5**, 425-428 (2014).
42. V. c. Vinš, M. Fransen, J. Hykl, J. Hrubý, Surface tension of supercooled water determined by using a counterpressure capillary rise method. *J. Phys. Chem. B* **119**, 5567-5575 (2015).
43. V. c. Vinš, J. Hošek, J. í. Hykl, J. Hrubý, Surface tension of supercooled water: inflection point-free course down to 250 K confirmed using a horizontal capillary tube. *J. Chem. Eng. Data.* **62**, 3823-3832 (2017).
44. S. T. Martin, Phase transitions of aqueous atmospheric particles. *Chem. Rev.* **100**, 3403-3454 (2000).

45. M. Bilde, B. Svenningsson, CCN activation of slightly soluble organics: the importance of small amounts of inorganic salt and particle phase. *Tellus B* **56**, 128-134 (2004).

46. R. Wagner, O. Möhler, H. Saathoff, M. Schnaiter, T. Leisner, New cloud chamber experiments on the heterogeneous ice nucleation ability of oxalic acid in the immersion mode. *Atmos. Chem. Phys.* **11**, 2083-2110 (2011).

47. E. Knipping, M. Lakin, K. Foster, P. Jungwirth, D. Tobias, R. Gerber, D. Dabdub, B. Finlayson-Pitts, Experiments and simulations of ion-enhanced interfacial chemistry on aqueous NaCl aerosols. *Science* **288**, 301-306 (2000).

48. W. H. Schroeder, P. Urone, Formation of nitrosyl chloride from salt particles in air. *Environ. Sci. Technol.* **8**, 756-758 (1974).

49. R. S. Timonen, L. T. Chu, M.-T. Leu, L. F. Keyser, Heterogeneous reaction of ClONO2 (g)+ NaCl (s). fwdarw. Cl2 (g)+ NaNO3 (s). *J. Phys. Chem.* **98**, 9509-9517 (1994).

50. B. Finlayson-Pitts, The tropospheric chemistry of sea salt: A molecular-level view of the chemistry of NaCl and NaBr. *Chem. Rev.* **103**, 4801-4822 (2003).

51. A. Ivanov, Y. M. Gershenzon, F. Gratpanche, P. Devolder, J.-P. Sawerysyn, in *Annales Geophysicae*. (Springer, 1996), vol. 14, pp. 659-664.

52. Y. Cheng, H. Su, T. Koop, E. Mikhailov, U. Pöschl, Size dependence of phase transitions in aerosol nanoparticles. *Nat. Commun,* **6**, 5923 (2015).

53. N. L. Jarvis, M. A. Scheiman, Surface potentials of aqueous electrolyte solutions. *J. Phys. Chem.* **72**, 74-78 (1968).

54. N. Matubayasi, K. Tsunetomo, I. Sato, R. Akizuki, T. Morishita, A. Matuzawa, Y. Natsukari, Thermodynamic quantities of surface formation of aqueous electrolyte solutions: IV. Sodium halides, anion mixtures, and sea water. *J. Colloid Interface Sci.* **243**, 444-456 (2001).

55. L. M. Pegram, M. T. Record, Partitioning of atmospherically relevant ions between bulk water and the water/vapor interface. *P. Natl. Acad, Sci.* **103**, 14278-14281 (2006).

56. G. Biskos, A. Malinowski, L. Russell, P. Buseck, S. Martin, Nanosize effect on

the deliquescence and the efflorescence of sodium chloride particles. *Aerosol Sci. Tech.* **40**, 97-106 (2006).

57. R. C. Tolman, The superficial density of matter at a liquid-vapor boundary. *J. Chem. Phys.* **17**, 118-127 (1949).

58. S. K. Das, K. Binder, Universal critical behavior of curvature-dependent interfacial tension. *Phys. Rev. Lett.* **107**, 235702 (2011).

59. K. Binder, B. J. Block, P. Virnau, A. Tröster, Beyond the van der Waals loop: What can be learned from simulating Lennard-Jones fluids inside the region of phase coexistence. *Am. J. Phys.* **80**, 1099-1109 (2012).

60. B. J. Block, S. K. Das, M. Oettel, P. Virnau, K. Binder, Curvature dependence of surface free energy of liquid drops and bubbles: A simulation study. *J. Chem. Phys.* **133**, 154702 (2010).

61. B. J. Alder, T. E. Wainwright, Studies in molecular dynamics. I. General method. *J. Chem. Phys.* **31**, 459-466 (1959).

62. H. J. Berendsen, D. van der Spoel, R. van Drunen, GROMACS: a message-passing parallel molecular dynamics implementation. *Comput. Phys. Commun.* **91**, 43-56 (1995).

63. F.-J. M. Zu Heringdorf, M. Reuter, R. Tromp, Growth dynamics of pentacene thin films. *Nature* **412**, 517 (2001).

64. W. D. Cornell, P. Cieplak, C. I. Bayly, I. R. Gould, K. M. Merz, D. M. Ferguson, D. C. Spellmeyer, T. Fox, J. W. Caldwell, P. A. Kollman, A second generation force field for the simulation of proteins, nucleic acids, and organic molecules. *J. Am. Chem. Soc.* **117**, 5179-5197 (1995).

65. V. Loukonen, T. Kurtén, I. Ortega, H. Vehkamäki, A. A. Padua, K. Sellegri, M. Kulmala, Enhancing effect of dimethylamine in sulfuric acid nucleation in the presence of water–a computational study. *Atmos. Chem. Phys.* **10**, 4961-4974 (2010).

66. K. S. Karadima, V. G. Mavrantzas, S. N. Pandis, Molecular dynamics simulation of the local concentration and structure in multicomponent aerosol nanoparticles under atmospheric conditions. *Phys. Chem. Chem. Phys.* **19**,

16681-16692 (2017).

67. J. Julin, M. Shiraiwa, R. E. Miles, J. P. Reid, U. Pöschl, I. Riipinen, Mass accommodation of water: Bridging the gap between molecular dynamics simulations and kinetic condensation models. *J. Phys. Chem. A* **117**, 410-420 (2013).

68. S. Takahama, L. Russell, A molecular dynamics study of water mass accommodation on condensed phase water coated by fatty acid monolayers. *J. Geophys. Res.-Atmos.* **116**, (2011).

69. S. Ghosal, J. C. Hemminger, H. Bluhm, B. S. Mun, E. L. Hebenstreit, G. Ketteler, D. F. Ogletree, F. G. Requejo, M. Salmeron, Electron spectroscopy of aqueous solution interfaces reveals surface enhancement of halides. *Science* **307**, 563-566 (2005).

70. J. Rowlinson, B. Widom, Molecular Theory of Capillarity, The International Series of Monographs on Chemistry. *Clarendon: Oxford, UK*, (1982).

71. J. Alejandre, D. J. Tildesley, G. A. Chapela, Molecular dynamics simulation of the orthobaric densities and surface tension of water. *J. Chem. Phys.* **102**, 4574-4583 (1995).

72. C. H. Bennett, Efficient estimation of free energy differences from Monte Carlo data. *J. Comput. Phys.* **22**, 245-268 (1976).

73. M. P. Moody, P. Attard, Monte Carlo simulation methodology of the ghost interface theory for the planar surface tension. *J. Chem. Phys.* **120**, 1892-1904 (2004).

74. B. B. Laird, R. L. Davidchack, Direct Calculation of the Crystal− Melt Interfacial Free Energy via Molecular Dynamics Computer Simulation. *J. Phys. Chem. B* **109**, 17802-17812 (2005).

75. G. J. Gloor, G. Jackson, F. J. Blas, E. de Miguel, Test-area simulation method for the direct determination of the interfacial tension of systems with continuous or discontinuous potentials. *J. Chem. Phys.* **123**, 134703 (2005).

76. K. Binder, Monte Carlo calculation of the surface tension for two-and three-dimensional lattice-gas models. *Phys. Rev. A* **25**, 1699 (1982).

## A. Personal List of Publications

### A.1 Journal Articles

**1. Wang, X.**, Binder, K., Chen, C., Koop, T., Pöschl, U., Su, H., Cheng, Y.: Second inflection point of water surface tension in deeply supercooled regime revealed by entropy anomaly and surface structure using molecular dynamics simulations[J], Physical Chemistry Chemical Physics, 2019.

**2. Wang, X.**, Chen, C., Binder, K., Kuhn, U., Pöschl, U., Su, H., Cheng, Y.: Molecular dynamics simulation of the surface tension of aqueous sodium chloride: from dilute to highly supersaturated solutions and molten salt [J], Atmospheric Chemistry and Physics, 2018, 18(23), 17077-17086.

**3. Wang, X.**, Chen, C., Binder, K., Pöschl, U., Su, H., Cheng, Y.: Studying the vapor pressure and surface tension of water nano-droplets by MD simulations (to be submitted)

**4. Wang, X.**, Lei, H., Berger, R., Cheng, Y., Zhang, Y., Su, H.: Hygroscopic properties of NaCl nanoparticles on the surface: a scanning force microscopy study (to be submitted)

**5. Wang, X.**, Yang, H., Hu, X., Zhang, X., Zhang, Q., Jiang, H., Wei, S., Yu, H.: Effects of HO-/MeO-PBDEs on androgen receptor: in vitro investigation and helix 12-involved MD simulation [J], Environmental Science & Technology, 2013, 47(20), 11802-11809.

**6.** Zhang, R.[1], **Wang, X.[1]**, Zhang, X., Song, C., Letcher, R. J., Liu, C.: Polychlorinated diphenylsulfides activate aryl hydrocarbon receptor 2 in zebrafish embryos: potential mechanism of developmental toxicity [J], Environmental Science & Technology, 2018, 52 (7), 4402-4412. ([1] Contribute equally)

**7.** Meusel, H., Elshorbany, Y., Kuhn, U., Bartels-Rausch, T., Reinmuth-Selzle, K., Kampf, C., Li, G., **Wang, X.**, Lelieveld, J., Pöschl, U., Hoffmann, T., Su, H., Ammann, M., Cheng, Y.: Light-induced protein nitration and degradation with HONO emission [J], Atmospheric Chemistry and Physics, 2017, 17(19), 11819-11833.

**8.** Su, H., Cheng, Y., Ma, N., Wang, Z., **Wang, X.**, Pöhlker, M., Nillius, B., Wiedensohler, A., Pöschl, U.: A broad supersaturation scanning (BS2) approach for rapid measurement of aerosol particle hygroscopicity and cloud condensation nuclei activity [J], Atmospheric Measurement Techniques, 2016, 9(10), 5183-5192.

**A.2 Oral Presentations**

**1. Wang, X.**, Binder, K., Chen, C., Koop, T., Pöschl, U., Su, H., Cheng, Y.: Temperature dependence of the surface tension of supercooled water determined by molecular dynamics simulations, General Assembly of the European Geoscience Union, Vienna, Austria, 8-13, April, 2018.

**2. Wang, X.**, Chen, C., Pöschl, U., Su, H., Cheng, Y.: Molecular dynamics simulation of surface tension of NaCl aqueous solution at 298.15K: from diluted to highly supersaturated concentrations, General Assembly of the European Geoscience Union, Vienna, Austria, 23-28, April, 2017.

**3. Wang, X.**, Su, H., Pöschl, U., Cheng, Y.: The surface tension of NaCl solution: molecular dynamics simulation on the concentration and temperature dependence, American Chemical Society National Meeting & Exposition, Philadelphia, Pennsylvania, USA, 21-25, August, 2016.

**A.3 Poster Presentations**

**Wang, X.**, Su, H., Pöschl, U., Cheng, Y.: MD simulation of surface tension of organic aerosol based on energy difference method and evaporation correction, European Aerosol Conference, Milan, Italy, 6-11, September, 2015.

**B. Selected Publications**

**B1. Wang, X.,** Binder, K., Chen, C., Koop, T., Pöschl, U., Su, H., Cheng, Y.: Second inflection point of water surface tension in deeply supercooled regime revealed by entropy anomaly and surface structure using molecular dynamics simulations[J], Physical Chemistry Chemical Physics, 2019.

**B2. Wang, X.,** Chen, C., Binder, K., Kuhn, U., Pöschl, U., Su, H., Cheng, Y.: Molecular dynamics simulation of the surface tension of aqueous sodium chloride: from dilute to highly supersaturated solutions and molten salt [J], Atmospheric Chemistry and Physics, 2018, 18(23), 17077-17086.

**B3. Wang, X.,** Chen, C., Binder, K., Pöschl, U., Su, H., Cheng, Y.: Studying the vapor pressure and surface tension of water nano-droplets by MD simulations (to be submitted)

## B.1 Wang et al., Phys. Chem. Chem. Phys., 2019

# Second inflection point of water surface tension in deeply supercooled regime revealed by entropy anomaly and surface structure using molecular dynamics simulations

Xiaoxiang Wang,[a] Kurt Binder,[b] Chuchu Chen,[a] Thomas Koop,[c] Ulrich Pöschl,[a] Hang Su,[*a,d] Yafang Cheng[*a]

[a] Multiphase Chemistry Department, Max Planck Institute for Chemistry, Hahn-Meitner-Weg 1, 55128 Mainz, Germany

[b] Institut für Physik, Johannes Gutenberg-Universität, Staudinger Weg 7, 55128 Mainz, Germany

[c] Faculty of Chemistry, Bielefeld University, 33615 Bielefeld, Germany

[d] Center for Air Pollution and Climate Change Research (APCC), Institute for Environmental and Climate Research (ECI), Jinan University, 510632 Guangzhou, China

* Corresponding author. E-mail: yafang.cheng@mpic.de (Y.C.); h.su@mpic.de (H.S.)

DOI: 10.1039/C8CP05997G

### Author contributions

Y.C. and H.S. conceived and led the study. X.W. performed the MD simulation and analyzed the data. X.W., Y.C., K.B. and H.S. interpreted the results. U.P., T.K. and C.C. discussed the results and commented on the manuscript. X.W., Y.C., K.B. and H.S. wrote the manuscript with inputs from all coauthors.

PCCP

PAPER

View Article Online
View Journal | View Issue





Cite this: *Phys. Chem. Chem. Phys.*, 2019, **21**, 3360

# Second inflection point of water surface tension in the deeply supercooled regime revealed by entropy anomaly and surface structure using molecular dynamics simulations†

Xiaoxiang Wang,[a] Kurt Binder,[b] Chuchu Chen,[a] Thomas Koop,[c] Ulrich Pöschl,[a] Hang Su*[ad] and Yafang Cheng*[a]

Received 24th September 2018,
Accepted 12th January 2019

DOI: 10.1039/c8cp05997g

rsc.li/pccp

The surface tension of supercooled water is of fundamental importance in physical chemistry and materials and atmospheric sciences. Controversy, however, exists over its temperature dependence in the supercooled regime, especially on the existence of the "second inflection point (SIP)". Here, we use molecular dynamics simulations of the SPC/E water model to study the surface tension of water ($\sigma_w$) as a function of temperature down to 198.15 K, and find a minimum point of surface excess entropy per unit area around ~240–250 K. Additional simulations with the TIP4P/2005 water model also show consistent results. Hence, we predict an SIP of $\sigma_w$ roughly in this region, at the boundary where the "no man's land" happens. The increase of surface entropy with decreasing temperature in the region below the inflection point is clearly an anomalous behavior, unknown for simple liquids. Furthermore, we find that $\sigma_w$ has a near-linear correlation with the interfacial width, which can be well explained by the capillary wave theory. Deep in the supercooled regime, a compact water layer at the interface is detected in our simulations, which may be a key component that contributes to the deviation of surface tension from the International Association for the Properties of Water and Steam relationship. Our findings may advance the understanding of the origin of the anomalous properties of liquid water in the supercooled regime.

## Introduction

Supercooled water widely exists in atmospheric systems, such as in cirrus and orographic wave clouds.[1] Water micro- and nano-droplets can even retain their liquid phase at much lower temperatures, in the so called "no-man's land" (<240 K),[2–4] which has a large impact on multiphase reactions in aerosols and activations of cloud droplets.[5,6] Surface tension of supercooled water is essential for understanding the gas–liquid partitioning, homogeneous nucleation and aerosol–cloud interactions[7–9] in the supercooled regime. However, it is difficult to measure the surface tension of supercooled water due to the limitation of measurement techniques. This is because, while homogeneous nucleation of ice from supercooled water is often not the dominating mechanism limiting the stability of supercooled water due to the relatively low nucleation rates,[10–12] the heterogeneous nucleation and crystallization of ice could be induced when a solid container or piece is in contact with the studied supercooled water.[13,14] The experimental measurement of the surface tension of nano-droplets in the "no-man's land" would thus be much more difficult and even unavailable to perform at this time.

To describe the temperature ($T$) dependence of surface tension of water ($\sigma_w$), the International Association for the Properties of Water and Steam (IAPWS) equation has been proposed:[15]

$$\sigma_w(T) = B \cdot \left(\frac{T_c - T}{T_c}\right)^{\mu} \cdot \left(1 + b \cdot \frac{T_c - T}{T_c}\right) \quad (1)$$

where $\sigma_w(T)$ is in mN m$^{-1}$ and $T$ is in Kelvin. The critical temperature $T_c$ is 647.096 K. $B$, $\mu$ and $b$ are 235.8 mN m$^{-1}$, 1.256 and −0.625, respectively. It should be noted that the standard

[a] *Multiphase Chemistry Department, Max Planck Institute for Chemistry, Hahn-Meitner-Weg 1, 55128 Mainz, Germany. E-mail: yafang.cheng@mpic.de, h.su@mpic.de*
[b] *Institut für Physik, Johannes Gutenberg-Universität, Staudinger Weg 7, 55128 Mainz, Germany*
[c] *Faculty of Chemistry, Bielefeld University, 33615 Bielefeld, Germany*
[d] *Center for Air Pollution and Climate Change Research (APCC), Institute for Environmental and Climate Research (ECI), Jinan University, 510632 Guangzhou, China*

† Electronic supplementary information (ESI) available: All data needed to evaluate the conclusions in the paper are present in the paper and/or the electronic supplementary information. Additional data related to this paper may be requested from the authors. See DOI: 10.1039/c8cp05997g

IAPWS equation is based on the data of Vargaftik *et al.*[16] This quantitative relationship is, however, only based on the experimental data of water surface tension above 0 °C (273.15 K), and it is still under debate whether the surface tension of supercooled water follows the IAPWS equation. For example, Humphreys and Mohler[17] measured the surface tension of supercooled water down to −8 °C (265.15 K) and showed an anomaly in the dependency of surface tension on temperature. Anomalies in a similar temperature range have also been found by later experimental studies.[18–21] According to these studies, surface tension has a stronger increase with decreasing temperature below a specific temperature in the vicinity of 0 °C, and the corresponding point is thus defined as the ''second inflection point (SIP)''. Note that the ''first inflection point'' is at about 520–530 K.[22,23] However, recent laboratory studies showed contrasting results, where no SIP was found in the measurable temperature range down to −25 °C (248.15 K) by using capillary elevation,[24] counter-pressure capillary rise[25] and horizontal capillary tube[26] methods.

In view of the significance of surface tension of supercooled water and the ongoing debate on the existence of an SIP, we performed molecular dynamics (MD) simulations to study the surface tension of water over a temperature range from 198.15 K to 348.15 K. The results are then compared with the IAPWS equation and existing experimental data. The temperature dependence of surface tension and its driving forces are elucidated by analyzing the energetic and structural parameters of the simulated systems. According to the energetic and structure analyses, a second inflection point of surface tension of water was revealed at around 240–250 K, the edge of the ''no-man's land''.

## Methods

### MD simulation

The MD simulations were carried out with the GROMACS v5.1 package.[27] The SPC/E water model (Extended Simple Point Charge Model)[28] was selected to represent the water molecules. We have opted to choose the SPC/E water model of water, for three reasons: (i) it is the most widely used model in previous simulation studies of the surface tension of water (*e.g.* Sakamaki *et al.*, Chen and Smith, Vins *et al.*, and Alejandre *et al.*[29–32]). Due to the long range of electrostatic forces, and the need to use a slab geometry for simulating the liquid coexisting with its vapor, such simulations are technically very difficult, and actually some early results are presumably invalid, as pointed out in ref. 30. For other force fields of water, less extensive data would be available for comparison. (ii) Some other force fields of water (*e.g.* ST2 model) are known to imply a critical anomaly in the predictions for the bulk properties of supercooled water (2nd critical point)[33] and for such models a corresponding anomaly of the surface tension is likely. However, it is still unclear that whether real supercooled water at low enough temperatures (if they become accessible) will show such critical anomaly of bulk properties. We do not wish to bias our study of surface tension by using such a model which perhaps overemphasizes such critical behavior in the bulk. The SPC/E water model, however, does not produce a 2nd bulk critical point in the accessible temperature region, and hence is less biased. (iii) A recent study by Shvab and Sadus[34] has reported that the SPC/E water model yields reasonable values for most quantities of water. By contrast, some other specific models may reproduce one property of water very well while fail to reproduce other ones. In this study, we do not only investigate the value of surface tension, but also discuss the surface excess enthalpy, surface excess entropy, density profile and the thickness of the surface. Therefore, we need to use a model to avoid any irrational results for these parameters.

Water molecules were added into the simulation cell (a cube with lengths at *x*-, *y*- and *z*-directions of 5 nm, $L_x = L_y = L_z =$ 5 nm; the number of water molecules is 4142) to generate the initial structure for simulation of water. Water was then equilibrated in the *NVT* ensemble and *NPT* ensemble (pressure = 1 bar) at different temperatures (198.15–348.15 K with an interval of 10 K) with periodic boundary conditions in all three directions. The temperature was controlled by using a Nosé–Hoover thermostat.[35,36] The volume of the simulation cell may slightly change due to the difference in density at different temperatures, and the length of the cubic cell ranged from 4.9 nm to 5.1 nm. After equilibrium was reached, the cubic simulation cell was elongated along the *z*-direction with $L_z$ = 20 nm to create two surfaces. The water was equilibrated and simulated with the *NVT* ensemble in the rectangular parallelepiped cell at the corresponding temperature. Simulations at each temperature were performed for five individual times. All simulations were carried out for at least 50 ns by using a 1 fs time step, and configurations for analysis were saved every 2 ps. Both electrostatic interactions and van der Waals interactions were calculated using the particle mesh Ewald (PME) algorithm,[37,38] because PME has been found to give an accurate calculation of long-range interactions.[38]

### Calculation of surface tension

For each MD simulation at a certain temperature, the water surface tension at the interface, $\sigma_w$, was then calculated with the ''pressure tensor'' method as we did in our previous study,[39] using the mechanical definition of the atomic pressure:[32]

$$\sigma_w = \frac{1}{2}L_z\left[\langle P_{zz}\rangle - \frac{1}{2}\left(\langle P_{xx}\rangle + \langle P_{yy}\rangle\right)\right] \quad (2)$$

Here, $L_z$ is the length of the simulation cell in the longest direction (along *z*-direction, $L_z$ = 20 nm in our case) and $P_{aa}$ ($a = x, y, z$) denotes the diagonal component of the pressure tensor. The $\langle\cdots\rangle$ refers to time average. The factor $\frac{1}{2}$ outside the square brackets takes into account the two interfaces in the system.

To check whether the size of our simulation system is large enough to get an accurate prediction of $\sigma_w$, we performed sensitivity simulations of systems with different $L_x$ ($L_y$) and thickness of the water slab at 298.15 K. As shown in Fig. S1 (ESI†), with fixed $L_z$ (= 20 nm) and thickness of the water slab (5 nm), the predicted $\sigma_w$ from the systems with $L_x$ and $L_y \geq 3$ nm

are converged to be ~62 mN m$^{-1}$. With a fixed cell dimension (*i.e.*, $L_x = L_y = 5$ nm and $L_z = 20$ nm), the simulated $\sigma_w$ quickly reaches ~62 mN m$^{-1}$ at a water slab thickness of ~2 nm and becomes almost constant upon further enlarging the thickness. These results suggest that the size of the system used in our study should be sufficient.

### Energetic analysis

Surface tension is defined as the excess surface free energy per unit area with the following equation:[40]

$$\sigma(T) = \frac{\Delta G_s(T)}{A} = \frac{\Delta H_s(T) - T \cdot \Delta S_s(T)}{A} \quad (3)$$

Here, $\Delta G_s(T)$ is the incremental part of free energy due to the surfaces at temperature $T$, $A$ is the total area of the surface we created, so $A = 2 \times A'$ and $A'$ is the area of each created surface. $\frac{\Delta S_s}{A}(T)$ and $\frac{\Delta H_s}{A}(T)$ are the excess surface entropy and enthalpy per unit area at temperature $T$, respectively. By using eqn (4) and (5),[40] $\frac{\Delta S_s}{A}(T)$ and $\frac{\Delta H_s}{A}(T)$ can be further calculated as:

$$\frac{\Delta S_s}{A}(T) = -\frac{d[\sigma(T)]}{dT} \quad (4)$$

$$\frac{\Delta H_s}{A}(T) = \sigma(T) - T \cdot \frac{d[\sigma(T)]}{dT} \quad (5)$$

To obtain $\frac{\Delta S_s}{A}(T)$, we apply a discrete differential method to the simulated surface tension of water at different temperatures. In this approach, we firstly use eqn (6) to fit the data of $\sigma_w(T_0)$, $\sigma_w(T_0 - 10\ K)$ and $\sigma_w(T_0 + 10\ K)$ to get the fitting parameters $a$ and $b$ for a given $T_0$, *i.e.*, $a(T_0)$ and $b(T_0)$, respectively.

$$\sigma_w(T) = \sigma_w(T_0) + a \times (T - T_0) + b \times (T - T_0)^2 \quad (6)$$

Together with eqn (4), we have

$$\frac{\Delta S_s}{A}(T_0) = -a(T_0) \quad (7)$$

$\frac{T \cdot \Delta S_s}{A}$ and $\frac{\Delta H_s}{A}$ are then obtained and they were used to interpret the change of surface tension with temperature. Note that $\frac{\Delta S_s}{A}$ at 198.15 K and 348.15 K cannot be calculated by using the discrete differential approach because we do not have the surface tension data at 188.15 K and 358.15 K.

### Structural analysis

To calculate the distribution of density of water along the $z$-direction, the simulation cell is divided into slabs with a thickness of 0.2 Å, and the density of each slab is statistically averaged over the simulation time. The density profiles were fitted to a hyperbolic tangent function:[41]

$$\rho(z) = \frac{1}{2}(\rho_L + \rho_V) - \frac{1}{2}(\rho_L - \rho_V)\tanh\left[\frac{z - z_0}{d}\right] \quad (8)$$

where $\rho_L$ and $\rho_V$ are densities of water and vapor, $z_0$ is the position of the Gibbs-dividing surface, and $d$ is a parameter about surface thickness. It is often not recognized that parameters, such as $d$, are not intrinsic properties of a surface, but depend on the linear dimension of the surface that is studied, due to capillary wave broadening of the density profile (see more details in the main results).

## Results and discussion

### Surface tension of water above 0 °C

Fig. 1 shows the simulated and observed temperature dependence of $\sigma_w$. Above 0 °C (273.15 K), our simulated temperature dependence (red circles) agrees well with the observation-based IAPWS parameterization (blue solid line, commonly used as a reliable description of $\sigma_w$ at this temperature range),[15,16] though the absolute values of modelled $\sigma_w$ show a systematic shift. Compared to previous MD studies where the SPC/E water model has also been applied, our results (red circles) are consistent with the ones from Vega and de Miguel[41] (light green triangles), Sega and Dellago[42] (dark green triangles), Sakamaki *et al.*[29] (brown triangles), Chen and Smith[30] (grey triangles), and Vins *et al.*[31] (light blue triangles). The surface tension of water against water vapor was also calculated by Ismail *et al.*[43] using the SPC/E potential, but their results are consistently about 10 mN m$^{-1}$ smaller than all the other data (by three groups of authors) shown in Fig. 1, which are in very good mutual agreement.

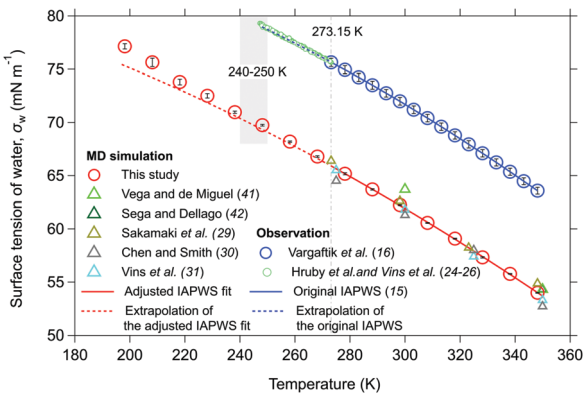


Fig. 1 Simulated and observed temperature dependence of surface tension of water. The red open circles represent the molecular dynamics (MD) simulated surface tension of water ($\sigma_w$) in this study. The black error bars are the standard deviations of five individual simulations. The red solid line is the adjusted IAPWS fit based on the MD simulated $\sigma_w$ above 273.15 K, and the red dashed line shows the extrapolation. The blue solid line is the original IAPWS parameterization based on the measured $\sigma_w$ above 273.15 K by Vargaftik *et al.*[16] (blue open circles with black error bars), and the blue dashed line shows the extrapolation. Light green circles represent the measured surface tension in the supercooled regime down to about −25 °C from Hruby, Vins and their colleagues.[24–26] More measurement data can be found in the review of Holten *et al.*[21] The triangles represent the MD simulated $\sigma_w$ with the SPC/E water model from Vega and de Miguel (ref. 41, light green), Sega and Dellago (ref. 42, dark green), Sakamaki *et al.* (ref. 29, brown), Chen and Smith (ref. 30, grey), and Vins *et al.* (ref. 31, light blue), respectively. The light grey dashed line and shade mark the 0 °C (273.15 K) and 240–250 K temperature range, respectively.

To explore the source of this model discrepancy, we carefully compared the relevant settings in the MD simulations of Ismail *et al.*'s,[43] Vega and de Miguel's,[41] Sega and Dellago's[42] and our studies. Firstly, although Alejandre *et al.*[32] found that the simulation of surface tension depended on the reciprocal-space mesh refinement, Ismail *et al.*[43] reported that the accuracy of the reciprocal-space mesh did not affect the calculation of surface tension of the SPC/E water model when it was averaged over sufficiently long times. The averaging time in our study ($\sim$50 ns), in Vega and de Miguel[41] (1.5–2 ns) and in Sega and Dellago[42] (50 ns) are longer than or comparable to the 1–2 ns used in Ismail *et al.*,[43] and thus should be long enough to avoid the effect of reciprocal-space mesh on surface tension. The second potential reason lies in the different choice of cutoff parameters, such as the Lennard-Jones (LJ) potentials and the short-range cutoff for the electrostatic potentials. The corresponding values were both set to 1 nm in Ismail *et al.*,[43] but 1.3 nm in Vega and de Miguel[41] and Sega and Dellago.[42] In our study, the cutoff values were both 1 nm, the same as in Ismail *et al.*[43] But we adopted the particle mesh Ewald (PME) algorithm, which may work similarly to longer cutoff values for interactions and bring our simulation results closer to those of Vega and de Miguel[41] and Sega and Dellago.[42] The different techniques used to calculate electrostatic interactions may also play a role. For example, both Vega and de Miguel[41] and Sega and Dellago,[42] as well as our studies used the PME algorithm, while Ismail *et al.*[43] used the particle-particle particle-mesh (PPPM) technique. Finally, the PME algorithm has been found to give an accurate calculation of long-range interactions.[38] Since we have used the PME algorithm to calculate both electrostatic interactions and van der Waals interactions, a tail correction for surface tension was thus not made in our study. However, in the current case, the tail correction should not play a significant role in explaining the difference of surface tension in the two previous studies, because it has been applied in both studies. Overall, despite more systematic research being still needed to clarify what parameters in MD simulations can affect and how they affect the simulation of the surface tension of the water slab, our simulation should be able to reflect the trend of surface tension with temperature.

The systematic differences between the modeled and simulated $\sigma_w$ may be attributed to the fact that the critical temperature $T_c$ predicted by the water models applied in the MD simulations is different from the experimental one. A similar shift in the opposite direction has been found by Rogers *et al.*[44] with a different water model (*i.e.*, WAIL, Water potential from Adaptive force matching for Ice and Liquid) and a different $T_c$ of $\sim$711 K. Following Vega and de Miguel's[41] and Rogers *et al.*'s[44] approach, an adjusted IAPWS equation (red solid line in Fig. 1) was thus obtained by fitting the original form of the IAPWAS equation (as in eqn (1)) to the MD simulated values (red circles in Fig. 1) at temperatures above 273.15 K. The critical exponent $\mu$ is fixed at 11/9.[45] The new equation becomes:

$$\sigma_w(T) = 192.82\left(\frac{T_c' - T}{T_c'}\right)^{11/9} \cdot \left(1 - 0.554\frac{T_c' - T}{T_c'}\right) \qquad (9)$$

here, $T_c'$ (= 627.16 K) is the simulated critical temperature of SPC/E water, which is similar to the ones from previous studies where the SPC/E water was also applied, *e.g.*, 625.7 K from Vega and de Miguel[41] and 630.6 K from Errington and Panagiotopoulos.[46] As shown in Fig. 1, the adjusted IAPWS equation can well describe the simulated $\sigma_w$ above 273.15 K.

### Surface tension of water in the supercooled regime

In the supercooled regime ($T$ < 273.15 K), we find that the simulated $\sigma_w$ (red circles in Fig. 1) and the extrapolation of the adjusted IAPWS relationship (red dashed line in Fig. 1) well converge until $\sim$250 K. In this range (above 250 K), our simulations show no obvious deviation from the adjusted IAPWS equation. Consistently, recent experimental results also show that the surface tension between $\sim$250 K and 273.15 K follows the extrapolation of IAPWS correlation (blue dashed line) very well.[24–26] At about 240 K to 250 K, the extrapolation begins to deviate from the MD simulation, and the deviations become more significant when the temperature further decreases. Rogers *et al.*[44] performed a MD simulation by using the WAIL water model and found the deviation to the extrapolation of the IAPWS equation in a similar temperature range (*i.e.*, $\sim$243 K). This consistency is supported by findings from simulations using other force fields for water. Thus, it should be very interesting to extend the range of measurement for real water to somewhat lower temperature than so far possible. For real water, Taschin *et al.*[47] have reported a time-resolved optical Kerr effect down to $T$ = 247 K, showing that a slowing down occurs, compatible with a mode-coupling critical temperature of a glass transition at $T_c$ = 227 K. They interpret this finding as the interplay of two local configurations, namely, high-density and low-density water forms, as suggested by Anisimov *et al.*[48] It could be that this mechanism is also relevant for the density maximum of SPC/E, implying that below $T_c$, the fraction of the low-density component increases. To identify the low density liquid (LDL) in water, we used distance to the fifth nearest neighbor (d5) criterion by following Cuthbertson *et al.* and Singh *et al.*[49,50] The d5 criterion assigns molecules to belong to ''low density'' when d5 is greater than the cutoff distance of 0.35 nm. The fractions of LDL at different temperatures were obtained (Fig. 2). The fractions of LDL increase as the temperature decreases in the studied region. However, the momentums below and above the $\sim$240–250 K range are quite different from each other. From $\sim$350 K to $\sim$250 K, the fraction increases gradually. Below this temperature, the fraction increases sharply as the temperature decreases. This result indicates that the existence of deviation of surface tension from IAPWS might be related to the rapid increase in the fraction of LDL.

According to our results, the IAPWS equation is suitable and accurate enough to describe the surface tension of supercooled water down to $\sim$250 K ($-$23 °C), below which the surface tension begins to deviate from IAPWS. However, supercooled water nano-droplets can still exist at a temperature as low as 200 K.[2] Thus, the relationship between surface tension and temperature should be further studied in this low temperature range. Note that, in the nano-size range, the size dependence of

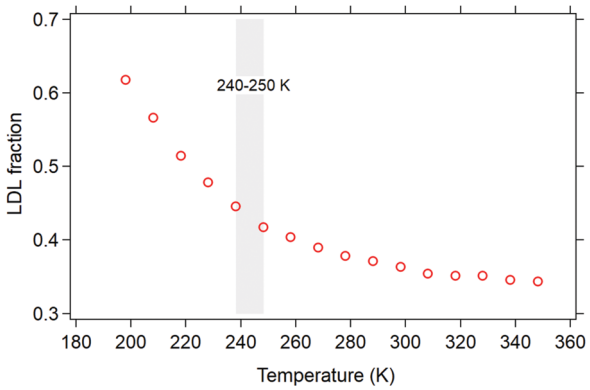


Fig. 2 The fractions of LDL at different temperatures. Red circles represent the fraction of LDL at different temperatures.

surface tension should also be introduced to study the surface tension of water nano-droplets or clusters.[51,52] The apparent deviation of $\sigma_w$ from the adjusted IAPWS may suggest an SIP at about 240–250 K. Therefore, we performed further energetic and structure analysis in the next sections to discuss and address the following two questions: (i) whether an SIP exists in the supercooled regime; and (ii) what are the driving forces controlling the change of $\sigma_w$ against temperature?

### Entropy anomaly and driving forces of temperature dependence

By definition, an "inflection point" in the temperature–surface tension curve shall locate at the temperature where $\frac{d^2[\sigma_w(T)]}{dT^2} = 0$. Because $\frac{\Delta S_s(T)}{A} = -\frac{d[\sigma_w(T)]}{dT}$ (see eqn (4) in Methods), if an SIP exists, one should see a local minimum or maximun in the temperature–surface excess entropy curve. Thus, we calculated the surface excess entropy $\frac{\Delta S_s}{A}$ and enthalpy $\frac{\Delta H_s}{A}$ by the discrete differential method based on the simulated $\sigma_w(T)$.

As presented in Fig. 3A, our data show a clear local minimum of $\frac{\Delta S_s}{A}(T)$ at a temperature around ~240–250 K, indicating an SIP of $\sigma_w(T)$ roughly in this region, at the boundary of the "no man's land" in real water. Above ~240 K, the surface excess entropy $\frac{\Delta S_s}{A}$ and enthalpy $\frac{\Delta H_s}{A}$ determined from our MD simulations compare well with the respective ones from the adjusted IAPWS equation (eqn (9)). Below ~240 K, however, the IAPWS equation fails to describe the temperature dependence of $\frac{\Delta S_s}{A}$ and $\frac{\Delta H_s}{A}$, leading to the aforementioned deviation of $\sigma_w(T)$ in Fig. 1.

From an energy perspective, surface tension ($\sigma$) can be decomposed into an entropy term $\left(-\frac{T\cdot\Delta S_s}{A}\right)$ and an enthalpy term $\left(\frac{\Delta H_s}{A}\right)$ as by definition $\sigma = \frac{\Delta H_s - T\cdot\Delta S_s}{A}$. Fig. 3B shows the variations of two driving forces, *i.e.*, $\frac{\Delta H_s}{A}$ and $-\frac{T\cdot\Delta S_s}{A}$ that

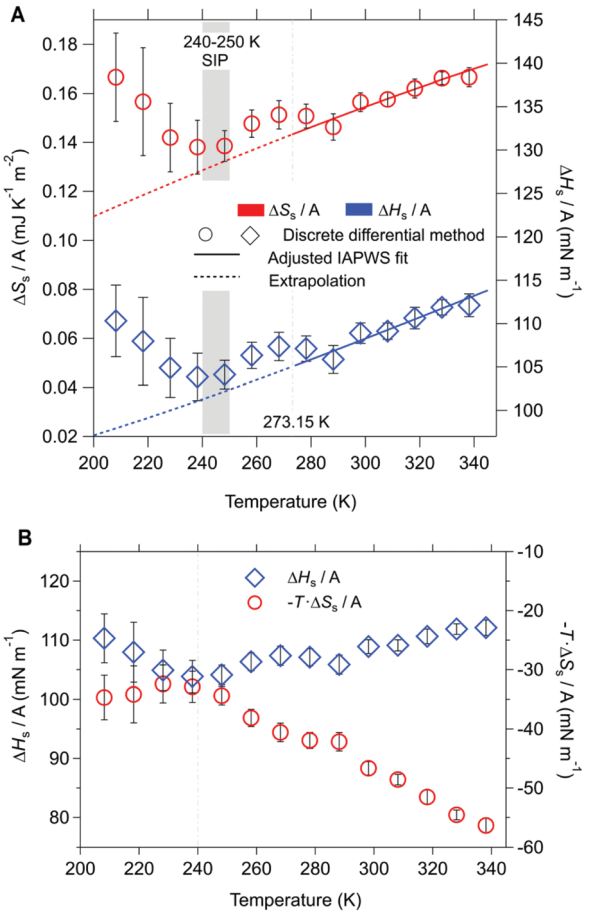


Fig. 3 Entropy anomaly and driving forces of the temperature dependence of the surface tension of water. (A) Temperature dependent surface excess entropy $\left(\frac{\Delta S_s}{A}\right)$ and enthalpy $\left(\frac{\Delta H_s}{A}\right)$ per unit of area. $\frac{\Delta S_s}{A}$ and $\frac{\Delta H_s}{A}$ derived from the MD simulated surface tension of water ($\sigma_w$) with the discrete differential method are marked with red open circles and blue open diamonds, respectively. The data derived from direct differential of the IAPWS fit (above 273.15 K) are marked with red and blue solid lines, respectively. The dashed lines denote the extrapolations. (B) Decomposed temperature dependent enthalpy $\left(\frac{\Delta H_s}{A}\right)$ and entropy $\left(-\frac{T\cdot\Delta S_s}{A}\right)$ terms of $\sigma_w$. The black error bars are the inherited error from the standard deviations of the MD simulated $\sigma_w$ from five individual simulations.

control the change of surface tension, with temperature. Above ~240 K, $-\frac{T\cdot\Delta S_s}{A}$ shows a stronger negative temperature dependence, while $\frac{\Delta H_s}{A}$ shows a much weaker positive dependence. Thus the increase of $\sigma_w$ from ~350 K to ~240 K is an entropy-driven process, which is consistent with the current understanding that an entropy change is the major driving force of negative temperature dependence of $\sigma_w$.[53] However, below ~240 K, $-\frac{T\cdot\Delta S_s}{A}$ remains almost unchanged, and therefore does not contribute to the negative temperature dependence of $\sigma_w$. In contrast, the enthalpy term $\frac{\Delta H_s}{A}$ begins to show a strong negative dependence on temperature. Thus

the amplification of the increasing tendency of surface tension below ~240 K and the deviation from the IAPWS relationship is an enthalpy-driven process.

### Influence of surface thickness

To understand the temperature dependence of $\sigma_w$ from a molecular level, we compared the structures of water at different temperatures, *i.e.*, the density profile of water along the $z$-direction ($\rho(z)$, see Structure analysis in Methods). By fitting the density profile with a hyperbolic tangent function (eqn (8)), the surface thickness parameter $d$ can be obtained. The "10–90" thickness of the interface ($t$) is defined as the distance along the interface, over which the density changes from a value of 10% to 90% of water's bulk density, and mathematically $t$ is equal to $2.1972d$.[41] As presented in Fig. 4A, there is an almost perfect linear correlation between the surface thickness and surface tension, *i.e.*, with increasing temperature, thickness increases while surface tension decreases. We also find that water has a thinner surface at a lower temperature, and the surface thickness near linearly correlates with decreasing temperature, also shown as blue solid circles in Fig. 4B. This is consistent with the results from previous studies involving planar macroscopic water and nano-droplets.[41,43,54]

In these previous studies, the general trends of the change in surface thickness with temperature are almost the same; the absolute values of thickness are however quite different (see results from Vega and de Miguel[41] (black solid diamonds) and Sega and Dellago[42] (black solid triangles) as examples, Fig. 4B). One obvious reason for the observed differences is the use of different force fields or different choice of cutoff parameters for the same force field, which may also cause systematic differences. However, another important reason why different groups reported different results for the same force field is that there is a systematic dependence of the interfacial thickness on the lateral linear dimension ($L$) of the interface, caused by the so-called "capillary waves".[55] While the capillary wave broadening of interfacial profiles has been extensively discussed for binary polymer mixtures,[56,57] for water surfaces, it has only recently been discussed.[43,58–60] Here, we shall demonstrate that this concept is useful to correlate the temperature dependence of surface tension and thickness.

The capillary wave fluctuations lead to a logarithmic variation of $d$ with $L$,[56]

$$d_L^2 = d_{\text{intr}}^2 + \frac{k_B T}{4\sigma_w(T)} \ln\left(\frac{L}{d_0}\right) \qquad (10a)$$

where $d_{\text{intr}}$ is the so-called "intrinsic" thickness, $d_0$ is a minimum lateral length for which eqn (10a) can be used. Neither $d_{\text{intr}}$ nor $d_0$ is predicted by the theory (sometimes $d_0 = d_{\text{intr}}$ is assumed, but this is questionable, see ref. 57). $\sigma_w(T)$ is the surface tension at temperature $T$ and the value is the same for systems with $L'$ and $L$. $k_B$ is the Boltzmann constant. Note also that eqn (10a) does not apply to macroscopic surfaces of real water in nature, since their long wavelength capillary waves are suppressed by gravity, unlike in MD simulations, where no gravitational potential is included. A useful consequence of eqn (10a) is that one can relate the thicknesses for two different choices $L'$ and $L$ as follows

$$d_{L'}^2 = d_L^2 + \frac{k_B T}{4\sigma_w(T)} \ln\left(\frac{L'}{L}\right) \qquad (10b)$$

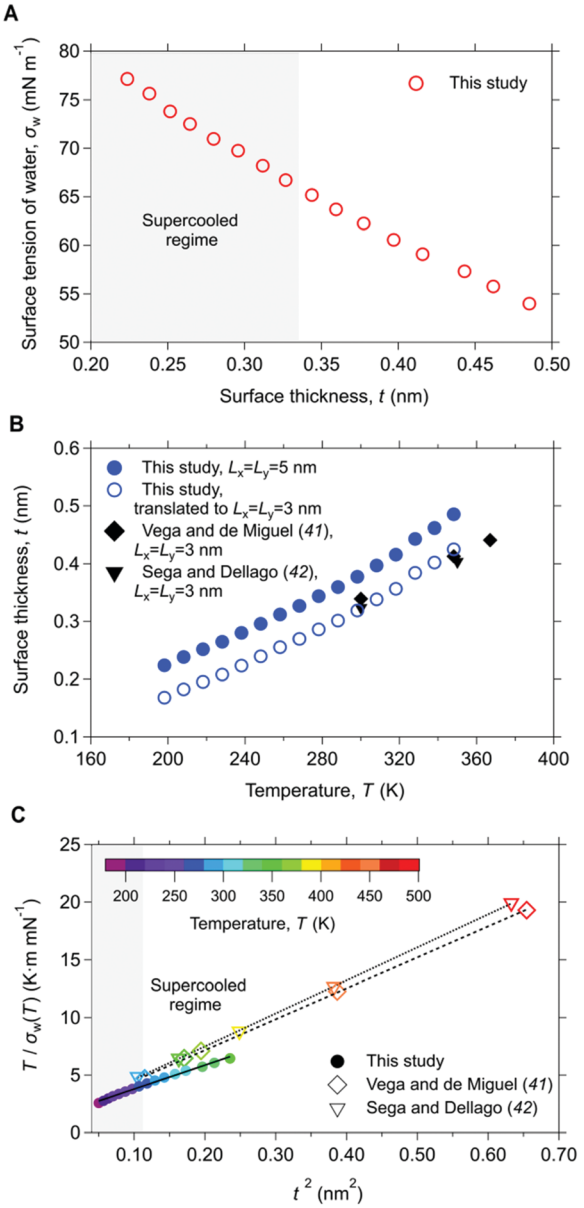


Fig. 4 Compact correlations between temperature dependent surface tension of water and surface thickness. (A) The MD simulated surface tension of water ($\sigma_w$) as a function of the surface thickness ($t$). (B) The thickness of surface $t$ as a function of temperature. The blue solid circles represent the surface thickness simulated in this study in a cell with $L_x = L_y = 5$ nm. The blue open circles represent the surface thickness translated to a simulation cell with $L_x = L_y = 3$ nm for comparison with Vega and de Miguel[41] (black solid diamonds) and Sega and Dellago[42] (black solid triangles) who used also $L_x = L_y = 3$ nm. (C) Positive near-linear relationship between $t^2$ and $\frac{T}{\sigma_w(T)}$. The solid circles and open diamonds and triangles represent data from this study, Vega and de Miguel[41] and Sega and Dellago,[42] respectively. The data points are color coded with temperature. The solid, dashed and dotted black lines are linear fitting to the corresponding data sets. The grey areas mark the supercooled regime.

Note here that both $d_{intr}$ and $d_0$ in this relation have been cancelled out. $d_{L'}$ and $d_L$ represent $d$ of the surface of the water slab whose $L_x$ ($L_y$) are $L'$ and $L$, respectively.

Fig. 4B compares the thickness, $t$, from our simulation ($L$ = 5 nm, blue solid circles) with the corresponding data of Vega and de Miguel[41] (black solid diamonds) and Sega and Dellago[42] (black solid triangles), who used also the SPC/E water model but $L'$ = 3 nm. One sees that the trends with temperature are similar, while the actual absolute values differ. However, when one uses eqn (10b) to "translate" our data from a thickness $L$ = 5 nm to a thickness $L'$ = 3 nm (shown as blue open circles), there is an almost perfect agreement between our values and those of Vega and de Miguel[41] and Sega and Dellago.[42] This also serves as a demonstration that it does not make sense to quote values for the surface thicknesses without mentioning to which surface lateral linear dimension, $L$, they belong.

According to the capillary wave theory, one may disregard the temperature dependence of $d_{intr}$ and $d_0$ in eqn (10) and plot $\frac{T}{\sigma_w(T)}$ *versus* $t^2$, as shown in Fig. 4C. It is seen that indeed over a wide range, *e.g.*, ~198 to 348 K in this study, 300 to 500 K in Vega and de Miguel[41] and 300 to 550 K in Sega and Dellago,[42] an almost straight line is found. The slope implies that $d_0 \approx 0.75$ nm, corresponding to a size of just a few water molecules, which is reasonable. Taking the compact near-linear relationship between surface thickness and $T$ into account, the compact correlation between surface tension and surface thickness can thus be also expected. It is interesting to note that these results still apply in the regime of supercooled water, where an oscillatory density profile at the water rich side of the interface appears (see more details in the next section). Actually, the number of water molecules in the simulation can affect the value of $t$; more discussions about this relationship are presented in the ESI.†

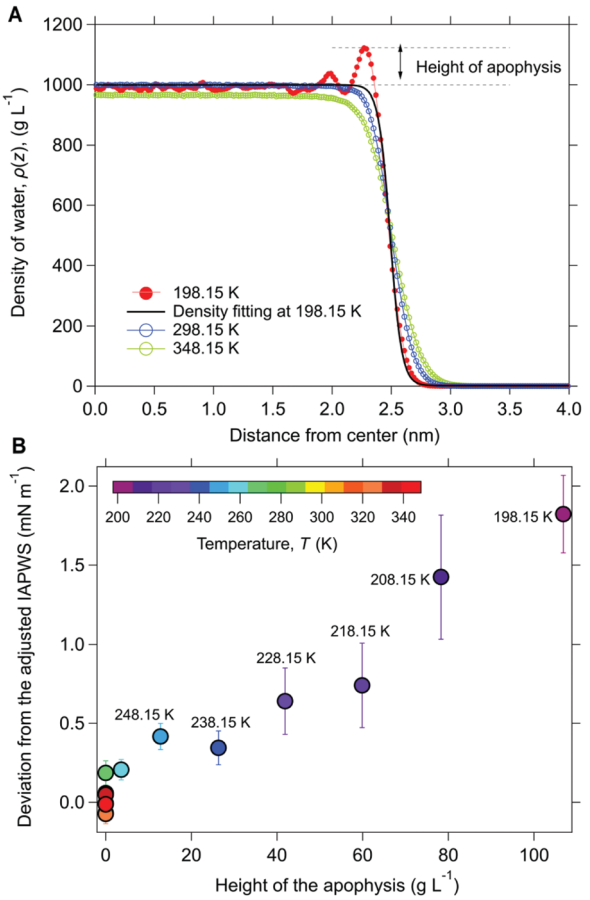


Fig. 5 Compact water layer near the surface and its influence on the surface tension of water in deeply supercooled regime. (A) The MD simulated density profiles of water at 198.15 K (red open circles), 298.15 K (blue open circles) and 348.15 K (green open circles). The black solid line is the fitting of the density profile at 198.15 K with the hyperbolic tangent function. The difference between the largest density at the surface and the fitted bulk density is defined as the height of "apophysis". (B) Positive correlation between the height of the apophysis and deviation of the MD simulated surface tension of water from the adjusted IAPWS relationship. The data points are color coded with temperature.

### Compact water layer near the surface in the deeply supercooled regime

By analyzing the density profiles of water at different temperatures, we find a compact water layer near the surface below ~250 K. By a "compact water layer", we mean that the water density near the surface exceeds the water density in the bulk. Here, the density profile at 298.15 K was selected as the reference and compared to the ones for different temperatures in panels of Fig. 5A and Fig. S2 (ESI†). Above ~250 K, a continuous density drop exists between the bulk water and the vapor, which indicates that a water–vapor interface forms. However, a small "apophysis" (an example of the apophysis is in Fig. 5A for the density profile of water slab at 198.15 K) occurs near the surface when the temperature drops to 248.15 K (Fig. S2F, ESI†). The apophysis becomes more pronounced with decreasing temperature (Fig. 5B and Fig. S2, ESI†). This means that the compact water layer, existing between the interface and interior part, becomes even more compact when the temperature decreases. To prove that this phenomenon is not an artifact induced by insufficient simulation time and/or the finiteness of the simulation cell, we have also performed simulation with a larger system ($L_x = L_y$ = 10 nm, $L_z$ = 30 nm) for 250 ns at 198.15 K for two individual times, and the apophysis persists at a similar level in the density profiles, although the density fluctuation in the bulk seems to be slightly smoother to some extent (Fig. S3, ESI†). Such apophysis was also found before by Matsubara *et al.*,[61] Li *et al.*,[62] Abe *et al.*,[63] Haji-Akbari *et al.*[64] and Haji-Akbari and Debenedetti.[65] The latter authors found that in the center of the liquid slab, where the density already agrees with its bulk value, the bond-orientational order is still significantly different from the bulk, and they therefore suggested that the proximity of a water–vapor surface facilitates ice nucleation, although this does not occur right at the surface, but rather at a distance of a few nanometers inside.

Interestingly, the temperature at which this compact water layer occurs is similar to the temperature where the surface

tension begins to deviate from IAPWS extension. To further explore the potential influence of the apophysis on the deviation of surface tension from the IAPWS relationship, we defined the difference between the largest density in the compact water layer and the bulk density ($\rho_L$) as the height of apophysis, as exampled in Fig. 5A. At each temperature, $\rho_L$ is obtained by fitting the simulated density profile with a hyperbolic tangent function. As shown in Fig. 5B, in the temperature range below ~240–250 K, the deviation increases as the height of the apophysis increases. This strongly positive relationship demonstrates that the compact water layer may be a key component that contributes to the deviation of surface tension from the IAPWS relationship.

## Conclusions

The surface tension of pure water was studied as a function of temperature at zero pressure from about 200 K to 350 K by using the SPC/E water model and extensive MD simulation. We carefully assert that for the chosen linear dimensions of the water slab (about 5 nm), finite size effects are negligible, and show that for $T \geq \sim 250$ K, the surface tension can be fitted well by an equation of the IAPWS form,[15] hence ruling out the appearance of an SIP in this temperature regime. As a caveat, we call attention to the fact that several competing water models exist, and none of them can reproduce all the measured physical properties of real water accurately. However, in the temperature regime where reliable measurements of the surface tension of water exist, the predicted temperature dependence of the surface tension for the SPC/E water model is similar to both the experimental data (Fig. 1) and to predictions from other water models. Thus, it appears reasonable to rely on our model predictions also in the deeply supercooled region, where neither reliable experimental data nor predictions of the surface tension from the other water models are available. We find that, in the deeply supercooled region, there is a significant deviation from the IAPWS relationship that fits the result at high temperature ($T > 273.15$ K). Using a thermodynamic relation and separating contributions to surface tension into the enthalpic and entropic parts, we predict that (in our model), an SIP occurs in the region from ~240–250 K, because $\frac{\Delta S_s}{A}$ has a minimum value around this temperature. This conclusion is based on the SPC/E water model. To examine if it is applicable for other water models, we calculated the surface tension and surface excess entropy at different temperatures based on TIP4P/2005, the one that produces the closest values of surface tension to the observation. As shown in Fig. S4A (ESI†), the simulated surface tension also begins to deviate from the adjusted IAPWS fit based on the data above 273.15 K when the temperature is in the region ~240–250 K. $\frac{\Delta S_s}{A}$ of TIP4P/2005 also presents a minimum point around this temperature range (Fig. S4B, ESI†). While the temperature dependence of the surface tension at temperatures below the SIP is mostly controlled by the surface excess enthalpy, at higher temperature the decrease of the surface tension with temperature to a large extent is caused by the surface excess entropy. The occurrence of an SIP in the deeply supercooled region of water clearly is a somewhat anomalous property, and it is an intriguing question, if this is somehow related to other anomalous properties of deeply supercooled water. In this context, we draw attention to recent findings of maxima of the correlation length and compressibility in rapidly supercooled micrometer-sized droplets at $T = 229$ K.[66] This observation was attributed to the presence of a Widom line associated with a liquid–liquid critical point in supercooled water at lower temperature and higher pressure.

At very low temperatures (close to the border line of the "no man's land" of supercooled water), the water surface simulated using the SPC/E potential exhibits a compact layer (*i.e.* a clearly higher local density of the water than the one in the bulk range at these temperatures). The consequences of this phenomenon on the nucleation behavior of water droplets from deeply supercooled vapor remain to be explored. In a broad temperature regime, a strong and nearly linear correlation between the surface thickness (which increases with temperature) and the surface tension (which decreases with temperature) is found and interpreted with capillary wave theory. The latter term allows us to relate our results for surface thickness to other simulations for the same model, where different linear dimensions of the surface were used.

## Author contributions

Y. C. and H. S. conceived and led the study. X. W. performed the MD simulation and analyzed the data. X. W., Y. C., K. B. and H. S. interpreted the results. U. P., T. K. and C. C. discussed the results and commented on the manuscript. X. W., Y. C., K. B. and H. S. wrote the manuscript with inputs from all coauthors.

## Conflicts of interest

There are no conflicts to declare.

## Acknowledgements

We would like to acknowledge the following funding resources: the National Natural Science Foundation of China (91644218), the National Key R&D Program of China (2017YFC0210104) and Guangdong Innovative and Entrepreneurial Research Team Program (2016ZT06N263). X. W. acknowledges the support from the China Scholarship Council (CSC, 201406190170). This study was supported by the Max Planck Society (MPG). Y. C. would also like to acknowledge the Minerva Program of MPG. Open Access funding provided by the Max Planck Society.

## Notes and references

1 D. Rosenfeld and W. L. Woodley, *Nature*, 2000, **405**, 440–442.
2 J. Huang and L. S. Bartell, *J. Phys. Chem.*, 1995, **99**, 3924–3931.

3 A. Manka, H. Pathak, S. Tanimura, J. Wölk, R. Strey and B. E. Wyslouzil, *Phys. Chem. Chem. Phys.*, 2012, **14**, 4505–4516.
4 H. Laksmono, T. A. McQueen, J. A. Sellberg, N. D. Loh, C. Huang, D. Schlesinger, R. G. Sierra, C. Y. Hampton, D. Nordlund and M. Beye, *J. Phys. Chem. Lett.*, 2015, **6**, 2826–2832.
5 J. H. Slade, M. Shiraiwa, A. Arangio, H. Su, U. Pöschl, J. Wang and D. A. Knopf, *Geophys. Res. Lett.*, 2017, **44**, 1583–1591.
6 Q. Mu, M. Shiraiwa, M. Octaviani, N. Ma, A. Ding, H. Su, G. Lammel, U. Pöschl and Y. Cheng, *Sci. Adv.*, 2018, **4**, eaap7314.
7 H. R. Pruppacher and J. D. Klett, *Microphysics of clouds and precipitation*, Springer, New York, 1997.
8 J. H. Seinfeld and S. N. Pandis, *Atmospheric chemistry and physics: from air pollution to climate change*, John Wiley & Sons, 2006.
9 Y. Cheng, H. Su, T. Koop, E. Mikhailov and U. Pöschl, *Nat. Commun.*, 2015, **6**, 5923.
10 T. Koop and B. J. Murray, *J. Chem. Phys.*, 2016, **145**, 211915.
11 T. Koop, *Z. Phys. Chem.*, 2004, **218**, 1231–1258.
12 L. Ickes, A. Welti, C. Hoose and U. Lohmann, *Phys. Chem. Chem. Phys.*, 2015, **17**, 5514–5537.
13 B. Murray, D. O'sullivan, J. Atkinson and M. Webb, *Chem. Soc. Rev.*, 2012, **41**, 6519–6554.
14 R. P. Sear, *CrystEngComm*, 2014, **16**, 6506–6522.
15 IAPWS, IAPWS release on surface tension of ordinary water substance, International Association for the Properties of Water and Steam (IAPWS), Moscow, Russia, 2014.
16 N. Vargaftik, B. Volkov and L. Voljak, *J. Phys. Chem. Ref. Data*, 1983, **12**, 817–820.
17 W. J. Humphreys and J. F. Mohler, *Phys. Rev.*, 1895, **2**, 387–391.
18 P. T. Hacker, *Experimental values of the surface tension of supercooled water*, National Advisory Committee for Aeronautics, Washington, 1951.
19 M. Floriano and C. Angell, *J. Phys. Chem.*, 1990, **94**, 4199–4202.
20 E. Trinh and K. Ohsaka, *Int. J. Thermophys.*, 1995, **16**, 545–555.
21 V. Holten, C. Bertrand, M. Anisimov and J. Sengers, *J. Chem. Phys.*, 2012, **136**, 094507.
22 J. Pellicer, V. García-Morales, L. Guanter, M. Hernández and M. Dolz, *Am. J. Phys.*, 2002, **70**, 705–709.
23 J. Kalova and R. Mares, *Int. J. Thermophys.*, 2012, **33**, 992–999.
24 J. Hrubý, V. c. Vinš, R. Mares, J. Hykl and J. Kalová, *J. Phys. Chem. Lett.*, 2014, **5**, 425–428.
25 V. c. Vinš, M. Fransen, J. Hykl and J. Hruby, *J. Phys. Chem. B*, 2015, **119**, 5567–5575.
26 V. c. Vinš, J. Hošek, J. í. Hykl and J. Hruby, *J. Chem. Eng. Data*, 2017, **62**, 3823–3832.
27 S. Pronk, S. Páll, R. Schulz, P. Larsson, P. Bjelkmar, R. Apostolov, M. R. Shirts, J. C. Smith, P. M. Kasson and D. Van Der Spoel, *Bioinformatics*, 2013, **29**, 845–854.
28 H. Berendsen, J. Grigera and T. Straatsma, *J. Phys. Chem.*, 1987, **91**, 6269–6271.
29 R. Sakamaki, A. K. Sum, T. Narumi and K. Yasuoka, *J. Chem. Phys.*, 2011, **134**, 124708.
30 F. Chen and P. E. Smith, *J. Chem. Phys.*, 2007, **126**, 221101.
31 V. Vinš, D. Celný, B. Planková, T. Němec, M. Duška and J. Hrubý, *EPJ Web Conf.*, 2016, **114**, 02136.
32 J. Alejandre, D. J. Tildesley and G. A. Chapela, *J. Chem. Phys.*, 1995, **102**, 4574–4583.
33 Y. Liu, A. Z. Panagiotopoulos and P. G. Debenedetti, *J. Chem. Phys.*, 2009, **131**, 104508.
34 I. Shvab and R. J. Sadus, *Fluid Phase Equilib.*, 2016, **407**, 7–30.
35 S. Nosé, *Mol. Phys.*, 1984, **52**, 255–268.
36 W. G. Hoover, *Phys. Rev. A: At., Mol., Opt. Phys.*, 1985, **31**, 1695–1697.
37 U. Essmann, L. Perera, M. L. Berkowitz, T. Darden, H. Lee and L. G. Pedersen, *J. Chem. Phys.*, 1995, **103**, 8577–8593.
38 N. M. Fischer, P. J. van Maaren, J. C. Ditz, A. Yildirim and D. van der Spoel, *J. Chem. Theory Comput.*, 2015, **11**, 2938–2944.
39 X. Wang, C. Chen, K. Binder, U. Kuhn, U. Pöschl, H. Su and Y. Cheng, *Atmos. Chem. Phys.*, 2018, **18**, 17077–17086.
40 L. D. Landau and E. M. Lifshitz, *Statistical physics*, Pergamon Press, 1969.
41 C. Vega and E. De Miguel, *J. Chem. Phys.*, 2007, **126**, 154707.
42 M. Sega and C. Dellago, *J. Phys. Chem. B*, 2017, **121**, 3798–3803.
43 A. E. Ismail, G. S. Grest and M. J. Stevens, *J. Chem. Phys.*, 2006, **125**, 014702.
44 T. R. Rogers, K.-Y. Leong and F. Wang, *Sci. Rep.*, 2016, **6**, 33284.
45 E. A. Guggenheim, *J. Chem. Phys.*, 1945, **13**, 253–261.
46 J. R. Errington and A. Z. Panagiotopoulos, *J. Phys. Chem. B*, 1998, **102**, 7470–7475.
47 A. Taschin, P. Bartolini, R. Eramo, R. Righini and R. Torre, *Nat. Commun.*, 2013, **4**, 2401.
48 M. A. Anisimov, M. Duška, F. Caupin, L. E. Amrhein, A. Rosenbaum and R. J. Sadus, *Phys. Rev. X*, 2018, **8**, 011004.
49 M. J. Cuthbertson and P. H. Poole, *Phys. Rev. Lett.*, 2011, **106**, 115706.
50 R. S. Singh, J. W. Biddle, P. G. Debenedetti and M. A. Anisimov, *J. Chem. Phys.*, 2016, **144**, 144504.
51 R. C. Tolman, *J. Chem. Phys.*, 1949, **17**, 333–337.
52 R. Massoudi and A. King Jr, *J. Phys. Chem.*, 1974, **78**, 2262–2266.
53 S. R. Palit, *Nature*, 1956, **177**, 1180.
54 S. Thompson, K. Gubbins, J. Walton, R. Chantry and J. Rowlinson, *J. Chem. Phys.*, 1984, **81**, 530–542.
55 F. Buff, R. Lovett and F. Stillinger Jr, *Phys. Rev. Lett.*, 1965, **15**, 621–623.
56 A. Werner, F. Schmid, M. Müller and K. Binder, *Phys. Rev. E: Stat. Phys., Plasmas, Fluids, Relat. Interdiscip. Top.*, 1999, **59**, 728–738.
57 K. Binder, M. Müller, F. Schmid and A. Werner, *Adv. Colloid Interface Sci.*, 2001, **94**, 237–248.
58 D. E. Otten, P. R. Shaffer, P. L. Geissler and R. J. Saykally, *Proc. Natl. Acad. Sci. U. S. A.*, 2012, **109**, 701–705.

59 D. L. McCaffrey, S. C. Nguyen, S. J. Cox, H. Weller, A. P. Alivisatos, P. L. Geissler and R. J. Saykally, *Proc. Natl. Acad. Sci. U. S. A.*, 2017, **114**, 13369–13373.
60 F. Sedlmeier, D. Horinek and R. R. Netz, *Phys. Rev. Lett.*, 2009, **103**, 136102.
61 H. Matsubara, T. Koishi, T. Ebisuzaki and K. Yasuoka, *J. Chem. Phys.*, 2007, **127**, 214507.
62 T. Li, D. Donadio, G. Russo and G. Galli, *Phys. Chem. Chem. Phys.*, 2011, **13**, 19807–19813.
63 K. Abe, T. Sumi and K. Koga, *J. Chem. Phys.*, 2014, **141**, 18C516.
64 A. Haji-Akbari, R. S. DeFever, S. Sarupria and P. G. Debenedetti, *Phys. Chem. Chem. Phys.*, 2014, **16**, 25916–25927.
65 A. Haji-Akbari and P. G. Debenedetti, *Proc. Natl. Acad. Sci. U. S. A.*, 2017, **114**, 3316–3321.
66 K. H. Kim, A. Späh, H. Pathak, F. Perakis, D. Mariedahl, K. Amann-Winkel, J. A. Sellberg, J. H. Lee, S. Kim, J. Park, K. H. Nam, T. Katayama and A. Nilsson, *Science*, 2017, **358**, 1589–1593.

# Second inflection point of water surface tension in deeply supercooled regime revealed by entropy anomaly and surface structure using molecular dynamics simulations

Xiaoxiang Wang,[a] Kurt Binder,[b] Chuchu Chen,[a] Thomas Koop,[c] Ulrich Pöschl,[a] Hang Su,[*a,d] Yafang Cheng[*a]

[a] Multiphase Chemistry Department, Max Planck Institute for Chemistry, Hahn-Meitner-Weg 1, 55128 Mainz, Germany
[b] Institut für Physik, Johannes Gutenberg-Universität, Staudinger Weg 7, 55128 Mainz, Germany
[c] Faculty of Chemistry, Bielefeld University, 33615 Bielefeld, Germany
[d] Center for Air Pollution and Climate Change Research (APCC), Jinan University, 510632 Guangzhou, China

* Corresponding author. E-mail: yafang.cheng@mpic.de (Y.C.); h.su@mpic.de (H.S.)

## Electronic supplementary information (ESI†)

### Relationship between the thickness of surface and the number of molecules in the simulated systems

Vins et al. [1] compared their results for 4 choices of N (the number of water molecules in the simulation, and the one in our study is 4142 as pointed out in our main text). They find that the surface tension is independent of N, but the interface thickness t increases systematically with N. Here, we plot $t^2$ against $ln(N)$ at ~350 K, and these data are from Vins et al.'s [1], Vega and Miguel [2], Sega and Dellago's [3] and our studies (Fig. S5). The relationship between them is as Eq. S1

$$t^2 = 0.0408 \times ln(N) - 0.1066 \quad \text{(S1)}$$

This N-dependence of $t^2$ is a simple consequence of Eq. 10a. Of course, writing N as the product of the bulk water density times the volume of the water slab, and noting that volume scales with the third power of the linear dimension L, one has that $ln(N) = 3\ln(L) + constant$. The prefactor 0.0408 indeed is rather close to the prefactor that Eq. 10a then would predict. Thus, the N-dependence of $t^2$ provides a further independent test of the estimated surface tension.

**List of figures.**

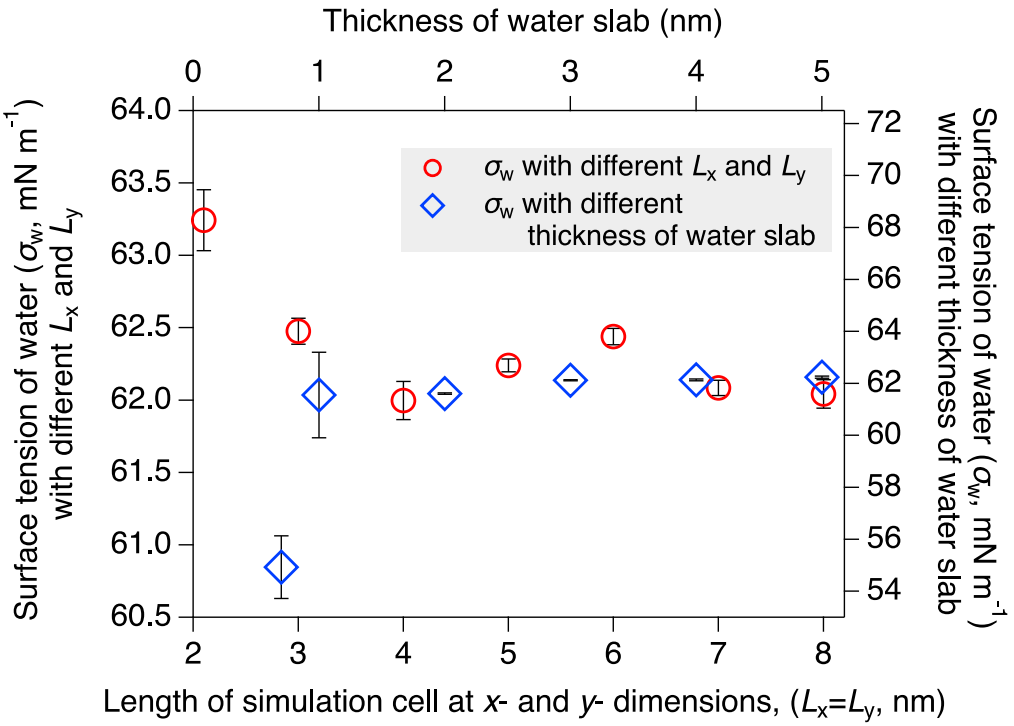


**Fig. S1. Surface tension of water ($\sigma_w$) at 298.15 K for systems with different sizes.** The red circles represent the simulated $\sigma_w$ with different length of simulation cell at *x*- and *y*- directions ( $L_x = L_y$), but the length at z-direction ($L_z$) and the thickness of water are fixed with 20 nm and 5 nm, respectively. The blue diamonds represent the simulated $\sigma_w$ with different thickness of water slab, but simulation cell is with a fix size ($L_x = L_y$ = 5 nm and $L_z$ = 20 nm). The black error bars are the standard error of three individual simulations.

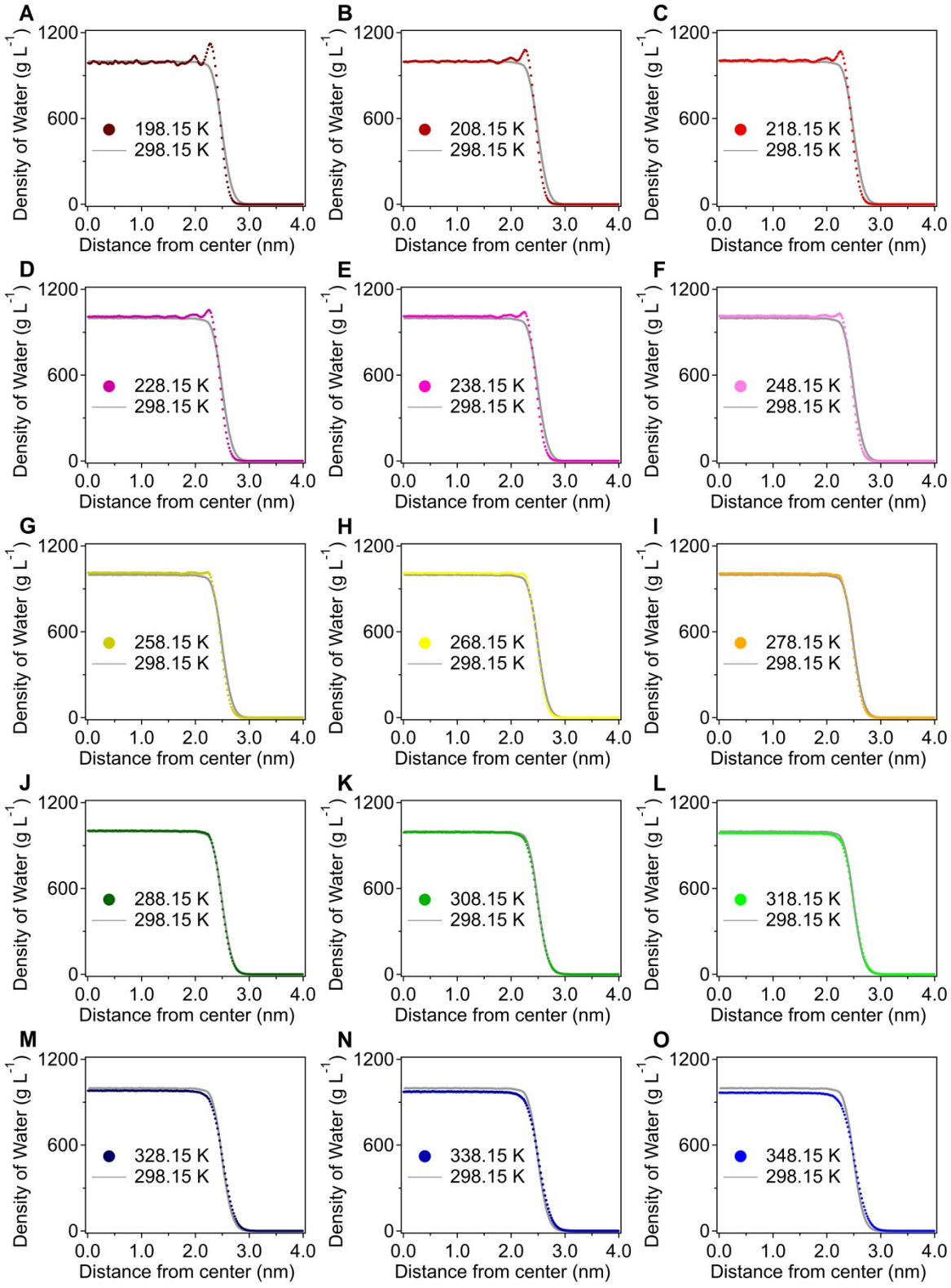


**Fig. S2. The MD simulated density profiles of water at different temperature.** The density profile at 298.15 K is always plotted with grey line as a reference.

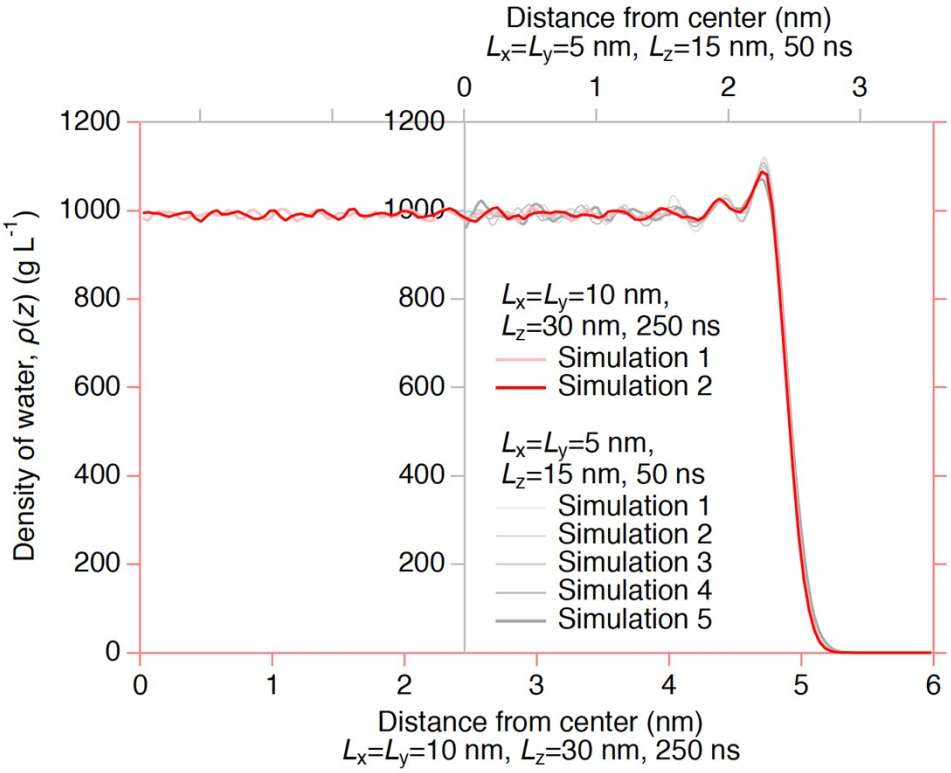


**Fig. S3. Stability and repeatability of the 'apophysis' and the compact water layer near the surface.** The density profiles of the supercooled water at 198.15 K obtained from two individual simulations in a larger cell ($L_x = L_y$ = 10 nm, $L_z$ = 30 nm, 250 ns, reddish colored lines), as well as from five individual simulations in a smaller cell ($L_x = L_y$ = 5 nm, $L_z$ = 15 nm, 50 ns, greyish colored lines), which is the one that we used in our study.

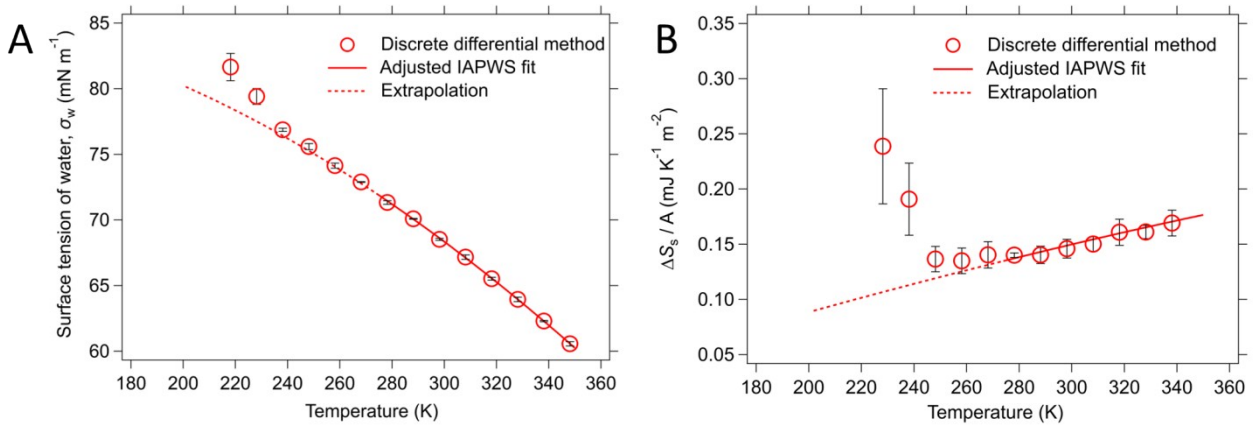


**Fig. S4. Temperature dependence of surface tension of water (A) and surface excess entropy per unit of area (B) simulated with the TIP4P/2005 water model.**

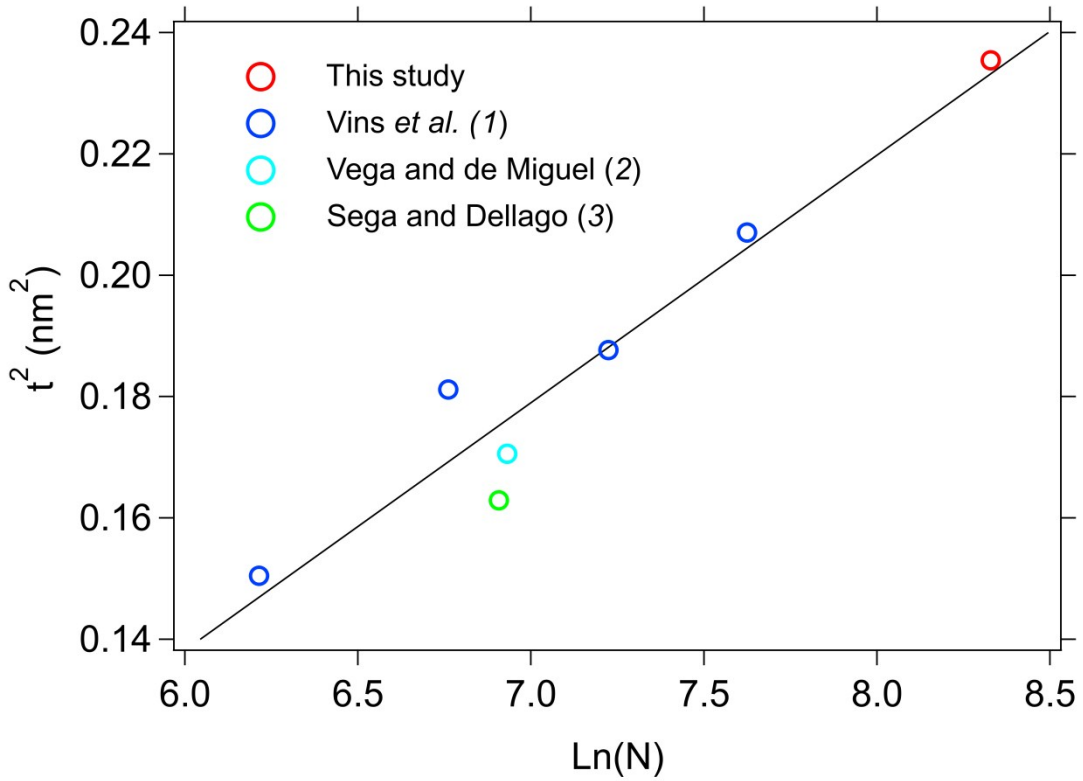


**Fig. S5. The relationship between the natural logarithm of number of water molecules in simulations and the square of thickness of surface at ~350 K.**

**Notes and references**


1. V. Vinš, D. Celný, B. Planková, T. Němec, M. Duška and J. Hrubý, *EPJ Web of Conferences*, 2016, **114**, 02136.
2. C. Vega and E. De Miguel, *J. Chem. Phys.*, 2007, **126**, 154707.
3. M. Sega and C. Dellago, *J. Phys. Chem. B*, 2017, **121**, 3798-3803.

## B.2 Wang et al., Atmos. Chem. Phys., 2018

# Molecular Dynamics Simulation of the Surface Tension of Aqueous Sodium Chloride: from Dilute to Highly Supersaturated Solutions and Molten Salt

Xiaoxiang Wang[1], Chuchu Chen[1], Kurt Binder[2], Uwe Kuhn[1], Ulrich Pöschl[1], Hang Su[3,1]*, Yafang Cheng[1,3*]

[1] Max Planck Institute for Chemistry, Multiphase Chemistry Department, Hahn-Meitner-Weg 1, 55128 Mainz, Germany

[2] Institut für Physik, Johannes Gutenberg-Universität, Staudinger Weg 7, 55128 Mainz, Germany

[3] Institute for Environmental and Climate Research, Jinan University, 510632 Guangzhou, China

* Corresponding author. E-mail: yafang.cheng@mpic.de (Y.C.); h.su@mpic.de (H.S.)

DOI:10.5194/acp-15-2969-2015

### Author contributions

Y.C. and H.S. conceived and led the study. X.W. performed the MD simulation and analyzed the data. X.W., Y.C., K.B. and H.S. interpreted the results. U.P. and C.C. discussed the results and commented on the manuscript. X.W., Y.C., K.B. and H.S. wrote the manuscript with inputs from all coauthors.

Atmos. Chem. Phys., 18, 17077–17086, 2018
https://doi.org/10.5194/acp-18-17077-2018


Atmospheric Chemistry and Physics
Open Access
EGU

# Molecular dynamics simulation of the surface tension of aqueous sodium chloride: from dilute to highly supersaturated solutions and molten salt

**Xiaoxiang Wang[1], Chuchu Chen[1], Kurt Binder[2], Uwe Kuhn[1], Ulrich Pöschl[1], Hang Su[3,1], and Yafang Cheng[1,3]**

[1]Max Planck Institute for Chemistry, Multiphase Chemistry Department, Hahn-Meitner-Weg 1, 55128 Mainz, Germany
[2]Institut für Physik, Johannes Gutenberg-Universität, Staudinger Weg 7, 55128 Mainz, Germany
[3]Institute for Environmental and Climate Research, Jinan University, 510632 Guangzhou, China

**Correspondence:** Yafang Cheng (yafang.cheng@mpic.de) and Hang Su (h.su@mpic.de)

Received: 30 October 2017 – Discussion started: 8 November 2017
Revised: 29 October 2018 – Accepted: 21 November 2018 – Published: 4 December 2018

**Abstract.** Sodium chloride (NaCl) is one of the key components of atmospheric aerosols. The surface tension of aqueous NaCl solution ($\sigma_{NaCl,sol}$) and its concentration dependence are essential to determine the equilibrium water vapor pressure of aqueous NaCl droplets. Supersaturated NaCl solution droplets are observed in laboratory experiments and under atmospheric conditions, but the experimental data for $\sigma_{NaCl,sol}$ are mostly limited up to subsaturated solutions. In this study, the surface tension of aqueous NaCl is investigated by molecular dynamics (MD) simulations and the pressure tensor method from dilute to highly supersaturated solutions. We show that the linear approximation of concentration dependence of $\sigma_{NaCl,sol}$ at molality scale can be extended to the supersaturated NaCl solution until a molality of $\sim 10.7\,mol\,kg^{-1}$ (i.e., solute mass fraction ($x_{NaCl}$) of $\sim 0.39$). Energetic analyses show that this monotonic increase in surface tension is driven by the increase in excess surface enthalpy ($\Delta H$) as the solution becomes concentrated. After that, the simulated $\sigma_{NaCl,sol}$ remains almost unchanged until $x_{NaCl}$ of $\sim 0.47$ (near the concentration upon efflorescence). The existence of the "inflection point" at $x_{NaCl}$ of $\sim 0.39$ and the stable surface tension of $x_{NaCl}$ between $\sim 0.39$ and $\sim 0.47$ can be attributed to the nearly unchanged excess surface entropy term ($T \cdot \Delta S$) and the excess surface enthalpy term ($\Delta H$). After a "second inflection point" at $x_{NaCl}$ of $\sim 0.47$, the simulated $\sigma_{NaCl,sol}$ gradually regains the growing momentum with a tendency to approach the surface tension of molten NaCl ($\sim 175.58\,mN\,m^{-1}$ at 298.15 K, MD simulation-based extrapolation). This fast increase in $\sigma_{NaCl,sol}$ at $x_{NaCl} > 0.47$ is a process driven by excess surface enthalpy and excess surface entropy. Our results reveal different regimes of concentration dependence of the surface tension of aqueous NaCl at 298.15 K: a water-dominated regime ($x_{NaCl}$ from 0 to $\sim 0.39$), a transition regime ($x_{NaCl}$ from $\sim 0.39$ to $\sim 0.47$) and a molten NaCl-dominated regime ($x_{NaCl}$ from $\sim 0.47$ to 1).

## 1 Introduction

Sodium chloride (NaCl) is one of the most important components of atmospheric aerosol particles (Finlayson-Pitts, 2003; Lewis and Schwartz, 2004). The aqueous NaCl solution droplet could participate in many atmospheric processes, such as phase transition, cloud activation, ice crystallization, long-range transport and chemical aging (Martin, 2000; Finlayson-Pitts, 2003; Ghorai et al., 2014; Wagner et al., 2015; Chen et al., 2016). To better understand these processes, the concentration-dependent surface tension of aqueous NaCl solution ($\sigma_{NaCl,sol}$) is essential to determine the equilibrium between NaCl solution droplet and water vapor (Jarvis and Scheiman, 1968; Dutcher et al., 2010).

Below the saturation point ($\sim 6.15\,mol\,kg^{-1}$), $\sigma_{NaCl,sol}$ shows a near-linear dependence on molality (Jarvis and Scheiman, 1968; Johansson and Eriksson, 1974; Aveyard and Saleem, 1976; Weissenborn and Pugh, 1995; Matubayasi et al., 2001) with a slope of $1.73 \pm 0.17$ (Pegram and Record, 2006, 2007). Because of the energy barrier of crystallization during dehydration and size effects at the nanoscale (Martin,

**Published by Copernicus Publications on behalf of the European Geosciences Union.**

2000; Biskos et al., 2006; Cheng et al., 2015), supersaturated aqueous NaCl solution droplets can exist under atmospheric conditions. However, direct measurements of surface tension of supersaturated droplets are challenging due to technical difficulties (Harkins and Brown, 1919; Vargaftik et al., 1983; Richardson and Snyder, 1994; Kumar, 2001). Only recently, Bzdek et al. (2016) overcame these limitations with an optical tweezer method and extended the concentration range to $\sim 8\,\mathrm{mol\,kg^{-1}}$, where the near-linear relationship still holds (Bzdek et al., 2016).

It is a matter of debate to what extent the approximation of a near-linear dependence of surface tension on molality can still be used for NaCl droplets. Cheng et al. (2015) used the differential Köhler analyses (DKA) method to retrieve the surface tension of NaCl aqueous droplets, and revealed a large deviation from the near-linear increase at a molality of $\sim 10\,\mathrm{mol\,kg^{-1}}$. In literature, such a deviation in concentrated solution has also been found for other compounds, such as $HNO_3$ (Weissenborn and Pugh, 1996), and it is believed to be typically true for most highly soluble electrolytes (Dutcher et al., 2010). The reason for such deviation remains unclear.

Several models about surface tension have been developed for highly concentrated solutions, e.g., Li and Lu (2001), Li et al. (1999) and Levin and Flores-Mena (2001). Li and Lu (2001) developed a model based on the Gibbs dividing surface concept, where the adsorption and desorption rate constants, saturated surface excess, stoichiometric coefficient of ions and mean ionic activity coefficient are needed. For NaCl aqueous solutions, this model is suitable for solutions with concentrations up to $\sim 5.5\,\mathrm{mol\,kg^{-1}}$. Li et al. (1999) uses a Debye–Hückel parameter, osmotic coefficient and a proportionality constant from the fitting of measured values to calculate the surface tension, which covers the concentration until the saturation point of bulk NaCl aqueous solutions. The remaining models are mostly only suitable for the dilute electrolyte solutions, such as the one proposed by Levin and Flores-Mena (2001). In their valid concentration range, these surface tension models produce linear or near-linear concentration dependence of $\sigma_{\mathrm{NaCl,sol}}$ that agrees well with currently available observations.

One surface tension model that is able to predict $\sigma_{\mathrm{NaCl,sol}}$ in the whole concentration range from infinitely dilute ($x_{\mathrm{NaCl}} = 0$) to highly supersaturated solution to molten salts ($x_{\mathrm{NaCl}} = 1$) was proposed by Dutcher et al. (2010), which has been adopted into the widely used Extended Aerosol Inorganics Model (E-AIM; Wexler and Clegg, 2002). This model is based on the following concept: ions are solvated by the water at low salt concentrations, which means that water molecules form hydration shells around the ions; while at very high salt concentration the water is considered as "solute" that is solvated by the ions, which means that ions form shells around the water molecules (Dutcher et al., 2010). Accordingly, for a diluted solution, the surface tension of water dominates and the surface tension of the solution equals the surface tension of water adjusted by a term that is proportional to the solute concentration. For a highly supersaturated solution, a similar relationship can be applied with the surface tension of molten salt as governing element. Legitimately, the model is then constrained by the surface tensions of water and molten salt. The parameterization of this model is obtained by fitting the data of subsaturated solutions. When the aqueous NaCl solution gets concentrated, this model shows a nonlinear monotonically increasing trend of $\sigma_{\mathrm{NaCl,sol}}$ generally in good agreement with observations, but no inflection point was introduced. It should be noted that the surface tension as a function of mole fraction of NaCl according to the Dutcher et al. (2010) model is essentially a linear interpolation between the surface tensions of water and molten NaCl.

In this study, we applied molecular dynamics (MD) simulations and the pressure tensor method to calculate the concentration dependence of $\sigma_{\mathrm{NaCl,sol}}$ from infinitely dilute ($x_{\mathrm{NaCl}} = 0$) to highly supersaturated solution to molten salt ($x_{\mathrm{NaCl}} = 1$). The concentration dependence of $\sigma_{\mathrm{NaCl,sol}}$ is divided into 3 regimes: a water-dominated regime, a transition regime and a molten NaCl-dominated regime. We compare our results with the Dutcher et al. (2010) model, and present the principal underlying physical chemistry (driving forces) behind the change of surface tension along concentration changes.

## 2 Methods

### 2.1 MD simulation

MD simulations were carried out with the GROMACS 5.1 package (Abraham et al., 2015). The $Na^+$ ions, $Cl^-$ ions and water molecules were added into a cubic box ($L = 5\,\mathrm{nm}$) to imitate the NaCl solution. The concentrations of simulated solutions are summarized in Table 1. To simulate the surface tension of supersaturated NaCl aqueous solution, we make use of the time window in the MD simulations before the crystallization starts in the system. The highest $x_{\mathrm{NaCl}}$ we can reach is $\sim 0.64$ (the corresponding concentration is $\sim 30.39\,\mathrm{mol\,kg^{-1}}$), below which the simulated surface tensions in three independent runs stably converge after 50 to 100 ns (Fig. 1). For more concentrated solutions, stable convergence cannot be reached, e.g., large fluctuations are shown in Fig. 1d at $x_{\mathrm{NaCl}}$ of 0.75.

According to Dutcher et al. (2010), surface tension of liquid or molten NaCl at 298.15 K (corresponding $x_{\mathrm{NaCl}}$ is 1, infinite concentrated solution) can be regarded as the upper boundary of $\sigma_{\mathrm{NaCl,sol}}$. However, a direct simulation of surface tension of molten NaCl at 298.15 K would not be possible, due to excessively large relaxation times of this system at this temperature. It has been found that surface tensions of a very wide range of molten salts can be well described by linear functions of temperature (Sada et al., 1984; Horvath, 1985; Janz, 1988; Dutcher et al., 2010). We thus follow

**Table 1.** Concentrations of solution studied in our simulation and the calculated values of surface tension.

| No. | Number of water | Number of NaCl | Concentration ($mol\,kg^{-1}$) in bulk region[b] | $x_{NaCl}$ in bulk region | Concentration ($mol\,kg^{-1}$) of whole solution | $x_{NaCl}$ of whole solution | Surface tension ($mN\,m^{-1}$) |
|---|---|---|---|---|---|---|---|
| 1 | 4142 | 0 | 0 | 0 | 0 | 0 | $62.24 \pm 0.044$ |
| 2 | 4058 | 42 | 0.657 | 0.037 | 0.575 | 0.0325 | $63.48 \pm 0.03$ |
| 3 | 3976 | 83 | 1.235 | 0.067 | 1.159 | 0.0635 | $64.8 \pm 0.014$ |
| 4 | 3824 | 159 | 2.41 | 0.123 | 2.309 | 0.119 | $67.41 \pm 0.089$ |
| 5 | 3728 | 207 | 3.16 | 0.156 | 3.08 | 0.1528 | $69.49 \pm 0.006$ |
| 6 | 3656 | 243 | 3.85 | 0.184 | 3.69 | 0.1776 | $70.76 \pm 0.1$ |
| 7 | 3550 | 296 | 4.8 | 0.219 | 4.63 | 0.213 | $73.61 \pm 0.055$ |
| 8 | 3452 | 345 | 6.04 | 0.261 | 5.552 | 0.245 | $76.06 \pm 0.14$ |
| 9 | 3388 | 377 | 6.75 | 0.283 | 6.182 | 0.265 | $77.5 \pm 0.11$ |
| 10 | 3314 | 414 | 7.47 | 0.304 | 6.94 | 0.288 | $79.7 \pm 0.19$ |
| 11 | 3222 | 460 | 8.57 | 0.334 | 7.931 | 0.317 | $82.06 \pm 0.25$ |
| 12 | 3108 | 517 | 9.745 | 0.36 | 9.24 | 0.351 | $84.35 \pm 0.143$ |
| 13 | 3038 | 552 | 10.66 | 0.384 | 10.09 | 0.371 | $85.67 \pm 0.183$ |
| 14 | 2960 | 591 | 11.83 | 0.409 | 11.09 | 0.3935 | $86.9 \pm 0.04$ |
| 15 | 2868 | 637 | 13.49 | 0.44 | 12.339 | 0.419 | $87.83 \pm 0.25$ |
| 16 | 2762 | 690 | 15.34 | 0.47 | 13.879 | 0.448 | $88.03 \pm 0.88$ |
| 17 | 2636 | 753 | 17.37 | 0.504 | 15.87 | 0.481 | $88.77 \pm 0.42$ |
| 18 | 2486 | 828 | 19.98 | 0.54 | 18.503 | 0.519 | $90.35 \pm 0.6$ |
| 19 | 2368 | 887 | 24.6 | 0.59 | 20.81 | 0.549 | $93.4 \pm 2.157$ |
| 20 | 2232 | 955 | 26.74 | 0.61 | 23.77 | 0.581 | $97.6 \pm 1.46$ |
| 21 | 2122 | 1010 | 30.396 | 0.64 | 26.44 | 0.607 | $102.53 \pm 0.46$ |
| 22[a] | 2109 | 421 | 11.48 | 0.4018 | 11.09 | 0.3935 | $86.9 \pm 0.59$ |

[a] The solution slab in this system is 3 nm × 3 nm × 10 nm and the simulation box is 3 nm × 3 nm × 30 nm.
[b] There is a little difference between the concentration in the bulk region and the one of the whole system due to surface effects. The values used in the main text are the ones in the bulk region.

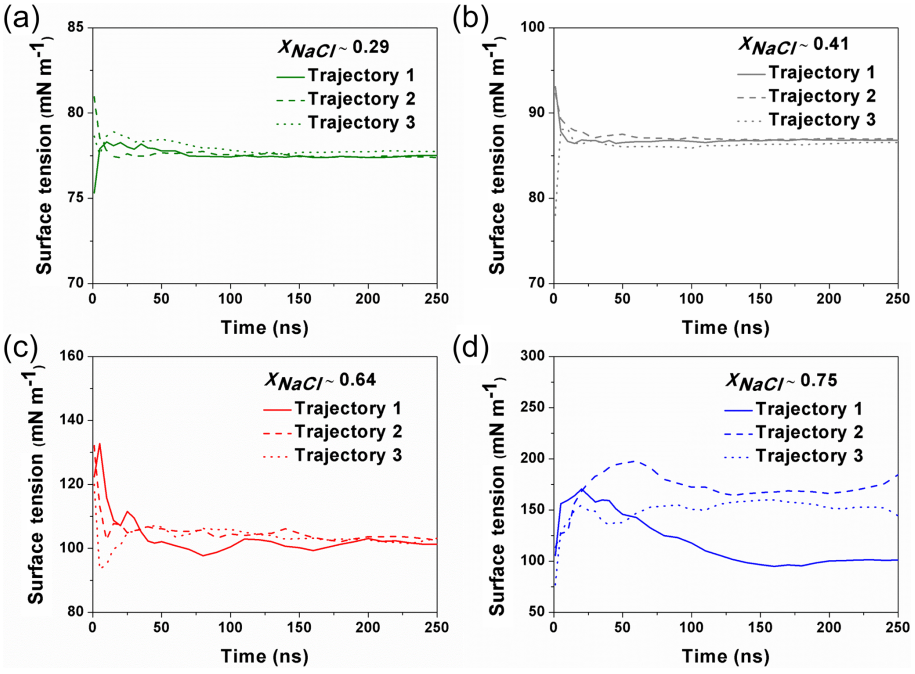


**Figure 1.** The calculated surface tension at different simulation time from different trajectories. For the solution with $x_{NaCl} \leq 0.64$ **(a–c)**, the surface tension become steadily stabilized after ~ 100–150 ns, and different individual simulation runs converge to a similar result. When $x_{NaCl} > 0.64$ (**d**; here $x_{NaCl} = 0.75$), the surface tension keeps fluctuating and the final values from different individual simulations cannot be converged even after 250 ns.

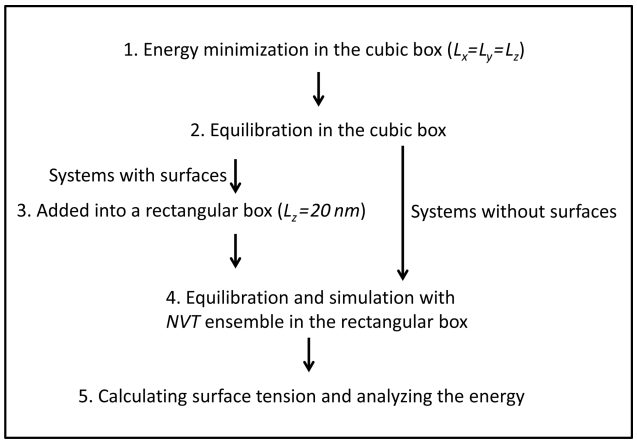


**Figure 2.** Schematic diagram of the different steps performed in the MD simulation.

the approach of Dutcher et al. (2010) assuming a linear relationship between surface tension of molten NaCl and temperature. With this approach, we retrieve the surface tension of molten NaCl at 298.15 K by extrapolating the simulated surface tension of molten NaCl in the temperature range of 1000 to 1700 K. Note that, in principle, non-linearity could still be possible at very high degrees of supercooling (e.g., close to or at room temperature) for the molten salts, which may introduce uncertainties to the offset obtained by the extrapolation.

The simulation procedure we followed is the following (Fig. 2): (1) systems were firstly energetically minimized by the steepest descent method (Stillinger and Weber, 1985). (2) Solutions were equilibrated in the NVT ensemble (constant-temperature, constant-volume) and NPT ensemble (constant-temperature, constant-pressure) (pressure = 1 bar) with periodic boundary conditions in three directions. The temperature was controlled by using the Nosé–Hoover thermostat (Nosé, 1984; Hoover, 1985). The box volume change due to the variation in density at different temperatures, and in our case the length of the cubic box varied from 4.9 to 5.1 nm. (3) The box was elongated along the $z$ direction with $L_z = 20$ nm to create two interfacial regions. (4) The solution was equilibrated and simulated with the NVT ensemble in the rectangular parallelepiped box at the corresponding temperature. (5) Systems without surfaces were also simulated for further energy analysis, and the trajectories obtained from step 2 were simulated with NPT ensemble. (6) All simulations were carried out for at least 200 ns, which is much longer than that in previous studies (a few nanoseconds; Jungwirth and Tobias, 2000; Neyt et al., 2013), because the system that we were dealing with is much more concentrated. A 1 fs time step was adopted and conformations for analysis were saved every 2 ps. Both electrostatic interactions and van der Waals interactions were calculated using the particle mesh Ewald (PME) algorithm, which has been proven to be a good choice for accurate calculation of long-range interactions (Essmann et al., 1995; Fischer et al., 2015). To test the reproducibility, all the systems were simulated 3 times, and the respective statistical error bars were provided.

In our simulation, the Joung–Cheatham (JC) force field for NaCl (Joung and Cheatham III, 2009) with SPC/E water model (Berendsen et al., 1987) was applied to simulate the NaCl solution and molten NaCl. The solubility at 298.15 K based on the JC force field with SPC/E model has been determined as $3.7 \pm 0.2\,\mathrm{mol\,kg^{-1}}$ (Moučka et al., 2013; Mester and Panagiotopoulos, 2015; Espinosa et al., 2016), which to the best of our knowledge is the value closest to the experimental value of solubility ($\sim 6.15\,\mathrm{mol\,kg^{-1}}$). Therefore, this force field is appropriate to use to study the concentration dependence of properties. More details about the history of the attempts to correctly calculate the quantity by molecular simulation can be found in the review by Nezbeda et al. (2016).

### 2.2 Calculation of surface tension

Based on results from MD simulations, the surface tension was calculated by using the mechanical definition of the atomic pressure (Alejandre et al., 1995):

$$\sigma_{\mathrm{MD}} = 0.5 L_z \left[ \langle P_{zz} \rangle - 0.5 \left( \langle P_{xx} \rangle + \langle P_{yy} \rangle \right) \right], \quad (1)$$

where $\sigma_{\mathrm{MD}}$ can represent the surface tension of molten NaCl ($\sigma_{\mathrm{NaCl}}$), NaCl solution ($\sigma_{\mathrm{NaCl,sol}}$) or pure water ($\sigma_{\mathrm{water}}$); $L_z$ is the length of the simulation cell in the longest direction (along $z$ axis) and $P_{aa}$ ($a = x,\ y,\ z$) denotes the diagonal component of the pressure tensor. The $\langle \ldots \rangle$ refers to the time average. The factor 0.5 outside the squared brackets takes into account the two interfaces in the system. Only the stable values were taken as our calculated surface tension.

### 2.3 Energy analysis

The excess surface enthalpy denotes the additional enthalpy in the system due to the creation of surfaces. It can be calculated as the difference of enthalpy between solutions with and without surfaces (Bahadur et al., 2007),

$$\Delta H = H_{b\_s} - H_b, \quad (2)$$

where $H_{b\_s}$ is the total enthalpy of simulated systems with surfaces and $H_b$ is the total enthalpy of simulated systems without surfaces. As the kinetic energy is the same for systems with or without surfaces and the difference of $pV$ can be ignored, $\Delta H$ can be presented as

$$\Delta H = E_{b\_s} - E_b, \quad (3)$$

where $E_{b\_s}$ and $E_b$ are the potential energy of the system with and without surfaces.

Then the surface tension can be determined by the excess surface free energy per unit area as in Eq. (4) (Davidchack

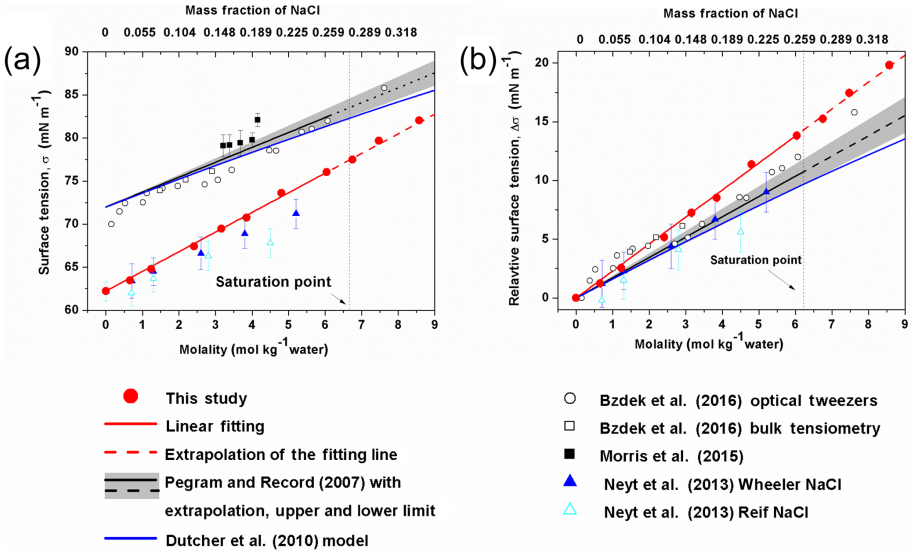


**Figure 3.** Surface tension **(a)** and relative surface tension **(b)** defined as $\Delta\sigma = \sigma_{\text{solution}} - \sigma_{\text{water}}$ as a function of the concentration of NaCl. The $\sigma_{\text{water}}$ in the Morris et al. (2015) study was not determined, thus the corresponding $\Delta\sigma$ is not shown in **(b)**.

and Laird, 2003):

$$\sigma = \frac{\Delta G}{A} = \frac{\Delta H - T \cdot \Delta S}{A}, \tag{4}$$

where $\Delta G$ is the increased part of free energy due to the creation of surfaces, $A$ is the total area of the surface we created, so $A = 2 \times a$ and $a$ is the area of each created surface. $\Delta S$ is the excess surface entropy. We then can retrieve $\Delta S$ by using the data of enthalpy and surface tension:

$$\Delta S = \frac{\Delta H - \sigma \cdot A}{T}, \tag{5}$$

where $\Delta H$ and $T \cdot \Delta S$ per unit area ($\frac{\Delta H}{A}$ and $\frac{T \cdot \Delta S}{A}$) are obtained as the enthalpic and entropic part of the contributions to the net surface tension, which will be used to explain the change of surface tension along with the mass fraction of NaCl ($x_{\text{NaCl}}$).

## 3 Results and discussion

### 3.1 Water-dominated regime ($x_{\text{NaCl}} <\sim 0.39$)

In Fig. 3a, the calculated surface tension of NaCl aqueous solution ($\sigma_{\text{NaCl,sol}}$) is compared with experimentally determined values (Jarvis and Scheiman, 1968; Johansson and Eriksson, 1974; Aveyard and Saleem, 1976; Weissenborn and Pugh, 1995; Matubayasi et al., 2001; Pegram and Record, 2006, 2007; Morris et al., 2015; Bzdek et al., 2016) in the subsaturated concentration range (molality of NaCl solution from 0 to 6.15 mol kg$^{-1}$ and $x_{\text{NaCl}}$ from 0 to $\sim$ 0.265). At 298.15 K, both model simulation (red solid points and fit line in Fig. 3a) and experimental observation (black line in Fig. 3a) reveal a linear dependence of surface tension on solution concentration at molality scale, with a very similar slope (2.1 versus $1.73 \pm 0.17$, respectively). Systematic underestimation, however, exists in the simulated $\sigma_{\text{NaCl,sol}}$. The previous MD simulations by Neyt et al. (2013) have also reported a similar result for the solution whose concentration ranges from 0 to 5.2 mol kg$^{-1}$ by using the same water model (SPC/E) but two different NaCl force fields, i.e., Wheeler NaCl (solid dark-blue triangle in Fig. 3a) and Relf NaCl (open light-blue triangle in Fig. 3a). Bhatt et al. (2004) also used the Wheeler NaCl model and SPC/E water model revealing a linear dependence and underestimation. We also subtracted the experimentally determined and the MD-simulated surface tension of pure water ($\sigma_{\text{water}}$) from the observed and modeled $\sigma_{\text{NaCl,sol}}$, respectively. The relative increase in surface tension ($\Delta\sigma = \sigma_{\text{NaCl,sol}} - \sigma_{\text{water}}$) from models and experiments converge nicely (Fig. 3b), and the former is only a little higher than the latter. The MD simulation is able to reproduce the increment in the growth of surface tension from pure water due to the addition of solute NaCl, although the predicted absolute value of $\sigma_{\text{NaCl,sol}}$ is systematically underestimated, which may mainly be attributed to the discrepancy between observed $\sigma_{\text{water}}$ and the modeled ones from the SPC/E water model.

By performing MD simulations in the supersaturated concentration range, we found that this linear relationship still holds beyond the saturation point until $x_{\text{NaCl}}$ of $\sim$ 0.39 (Fig. 4). As mentioned above, the laboratory experiments with elevated NaCl aqueous droplet and the optical tweezer method show that the linear relationship between $\sigma_{\text{NaCl,sol}}$ and NaCl concentration (molality scale) can be extended to $\sim$ 8 mol kg$^{-1}$ (Fig. 3; Bzdek et al., 2016), corresponding to

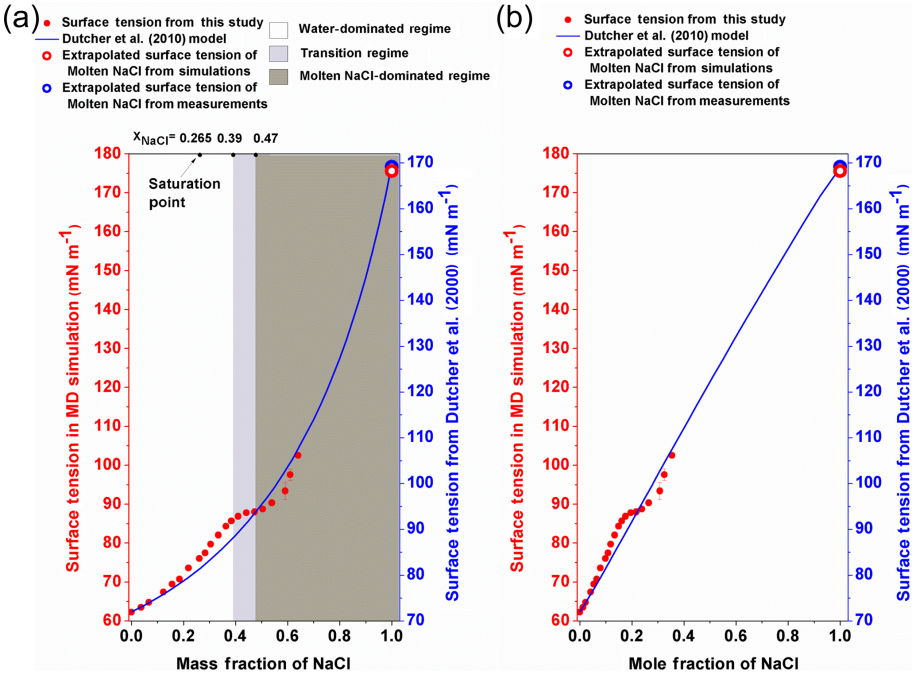


**Figure 4.** The surface tension of different-concentration NaCl solution. **(a)** The surface tension of NaCl solution against the mass fraction of NaCl. The left red $y$ axis is for the data from MD simulation (red circle), and the right blue $y$ axis is for the Dutcher et al. (2010) model (blue solid line). The white, light grey and dark grey areas shade the water-dominated, transition and molten NaCl-dominated regimes, respectively. **(b)** The surface tension of NaCl solution is plotted against the mole fraction of NaCl.

$x_{NaCl}$ of $\sim 0.33$ (Fig. 4), which is consistent with our simulations.

### 3.2 Transition regime ($x_{NaCl}$ from $\sim 0.39$ to $\sim 0.47$)

It was often found that surface tensions of single inorganic electrolyte aqueous solutions were linear functions of concentration (at the molality scale) over the moderate concentration range (Horvath, 1985; Dutcher et al., 2010). However, these simple relationships may not hold when the solutions become more concentrated. As shown in Fig. 4, starting from $x_{NaCl} \sim 0.39$, the simulated $\sigma_{NaCl,sol}$ remains almost unchanged until $x_{NaCl}$ of $\sim 0.47$ (concentration upon efflorescence). This inflection point of $\sigma_{NaCl,sol}$ at $x_{NaCl}$ of $\sim 0.39$ is supported by those determined by the DKA approach (Cheng et al., 2015), where there is a large deviation of surface tension from the monotonic linear increase. Note that beyond $x_{NaCl}$ of $\sim 0.47$, the simulated surface tension increases again (Fig. 4). This second inflection point, right at the concentration upon efflorescence, may imply a potential correlation with crystallization processes.

### 3.3 Molten NaCl-dominated regime ($x_{NaCl} > \sim 0.47$)

Beyond the second inflection point ($x_{NaCl} > 0.47$), the simulated $\sigma_{NaCl,sol}$ gradually increases more and more strongly (Fig. 4). Unfortunately, due to the large fluctuation in the surface tension simulation (Fig. 1), we are not able to extend our surface tension calculation in this way beyond $x_{NaCl}$ of $\sim 0.64$. However, according to Dutcher et al. (2010), it is expected that the surface tension of the solution would ultimately approach the surface tension of the hypothetical molten solute (i.e., $x_{NaCl} = 1$) at the same temperature. This hypothesis has been found to be consistent with the DKA retrieval for a highly concentrated ammonium sulfate aqueous solution with molality of $\sim 380\,\mathrm{mol\,kg^{-1}}$ (Cheng et al., 2015). We thus also try to constrain the growth of $\sigma_{NaCl,sol}$ by MD-simulated surface tension of molten NaCl ($\sigma_{NaCl}$) at 298.15 K.

Similar to the experimental results of Janz (1988), the simulated $\sigma_{NaCl}$ is also linearly correlated with temperature from 1000 K (the simulated melting point of NaCl) to 1700 K, as shown in Fig. 5. Following Dutcher et al. (2010), a surface tension of $\sim 175.58\,\mathrm{mN\,m^{-1}}$ is obtained for the hypothetical molten NaCl at 298.15 K by linear extrapolation of the MD simulated $\sigma_{NaCl}$ at higher temperature, which is very close to the $\sim 169.7\,\mathrm{mN\,m^{-1}}$ extrapolated from the experimental results (Dutcher et al., 2010). Combined with $\sigma_{NaCl} = \sigma_{NaCl,sol}(x_{NaCl} = 1) = \sim 175.58\,\mathrm{mN\,m^{-1}}$, the simulated $\sigma_{NaCl,sol}$ in the concentration range of $x_{NaCl} > 0.47$ shows the tendency to ultimately approach the surface tension of melting NaCl at 298.15 K, similar to the blue curve in Fig. 4 from the Dutcher et al. (2000) study.

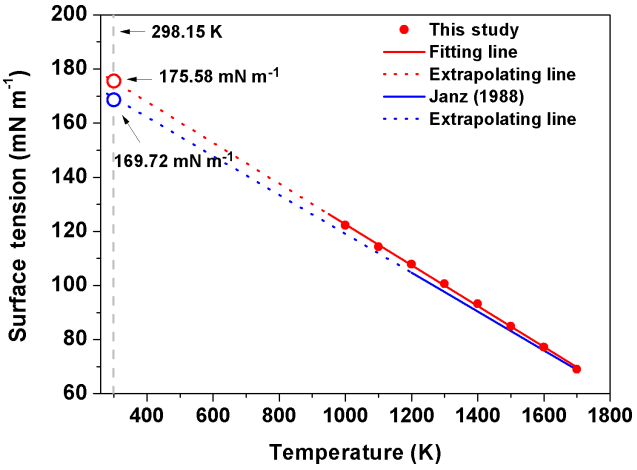


**Figure 5.** The surface tension of molten NaCl at different temperatures. The equation in Janz's study (1988) is $\sigma_{\mathrm{NaCl}} = -0.07188 \cdot T + 191$ (blue solid line). The fitting line based on our data is $\sigma_{\mathrm{NaCl}} = -0.0755 \cdot T + 198.09$ (red solid line). The red and blue open circles represent the extrapolated value of surface tension in simulation and reality, respectively.

### 3.4 Physical chemistry behind the regimes

In energetic analyses, surface tension was decomposed into excess surface enthalpy ($\frac{\Delta H}{A}$) and excess surface entropy ($\frac{T \cdot \Delta S}{A}$). Note that the increase in excess surface entropy ($\frac{T \cdot \Delta S}{A}$) or decrease in $-\frac{T \cdot \Delta S}{A}$ will negatively contribute to the growth of $\sigma_{\mathrm{NaCl,sol}}$. The analyses show that the monotonic increase in surface tension in water-dominated concentration ranges ($x_{\mathrm{NaCl}}$ from 0 to $\sim 0.39$) is driven by the increase in $\frac{\Delta H}{A}$ when the solution becomes concentrated (Fig. 6). When the solution gets concentrated, $\frac{\Delta H}{A}$ first increases slightly with enhanced increasing rate at $x_{\mathrm{NaCl}} > \sim 0.2$ and in the supersaturated regime up to $x_{\mathrm{NaCl}}$ of $\sim 0.39$. $-\frac{T \cdot \Delta S}{A}$ behaves differently, it remains almost constant at about $-45\,\mathrm{mN\,m^{-1}}$ first and only starts to decrease at $x_{\mathrm{NaCl}} \sim 0.2$. This way, in this concentration range ($x_{\mathrm{NaCl}}$ from 0 to $\sim 0.39$), the increase in excess surface enthalpy outnumbers the increase in excess surface entropy and thus this physicochemical regime can be understood as an excess surface enthalpy-driving process.

The stable surface tension in the transition-regime concentration range ($x_{\mathrm{NaCl}}$ from $\sim 0.39$ to $\sim 0.47$) is attributed to the fact that $-\frac{T \cdot \Delta S}{A}$ and $\frac{\Delta H}{A}$ are both almost unchanged. Figure 6 shows that in the concentration above $x_{\mathrm{NaCl}}$ of $\sim 0.39$, the increase in $\frac{\Delta H}{A}$ significantly slows down and stabilizes at $\sim 145\,\mathrm{mN\,m^{-1}}$ when the mass fraction approaches the efflorescence point. During this period, $-\frac{T \cdot \Delta S}{A}$ keeps nearly unchanged, which results in a corresponding $\sigma_{\mathrm{NaCl,sol}}$ almost independent of the solution concentration change.

Here, we present a potential explanation for the stability of surface tension in this region from the structural analysis.

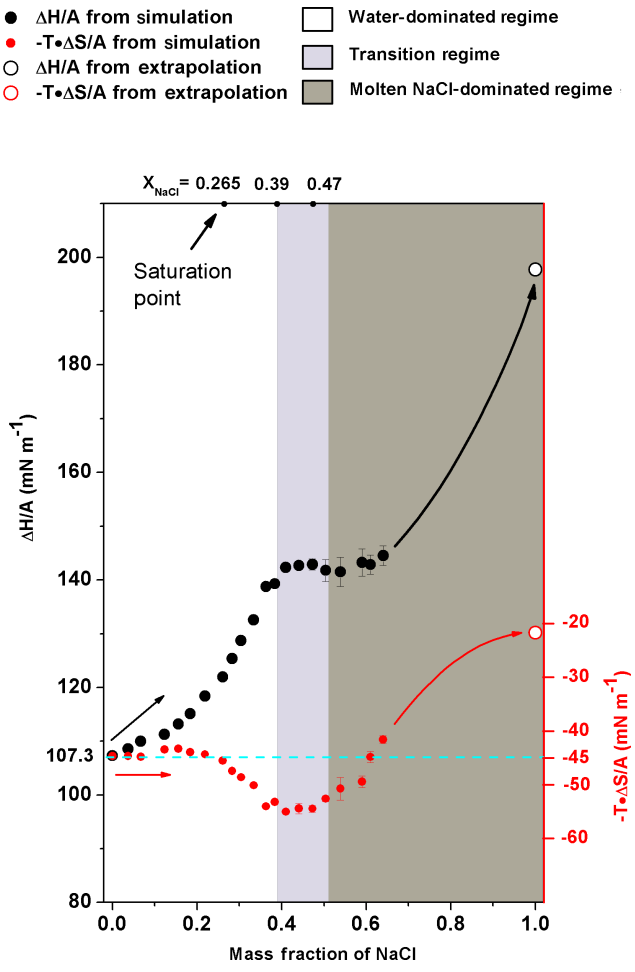


**Figure 6.** The excess surface enthalpy and entropy per unit area ($\frac{\Delta H}{A}$ and $\frac{T \cdot \Delta S}{A}$) of different NaCl solution concentrations. $\frac{\Delta H}{A}$ (black circles) and $-\frac{T \cdot \Delta S}{A}$ (red circles) are shown as a function of mass fraction of NaCl. The solid circles are obtained from simulation directly, and the open circles are obtained from the extrapolation of corresponding properties of molten NaCl. The cyan dashed line is only an auxiliary line for clearer view. Shaded areas are the same as in Fig. 4.

The ratio of $Na^+$ concentration at different positions to the average concentration of the whole system ($C_z/C_{\mathrm{average}}$) in different solutions is shown in Fig. 7a. The three blue-toned lines represent the ratio of solution in the transition regime with $x_{\mathrm{NaCl}}$ from $\sim 0.39$ to $\sim 0.47$. All of them have apophyses (significant rise) near the surface and these apophyses almost overlap with each other. This phenomenon suggests that the solute in these solutions enriches close to the surface and the degree of enrichment is almost the same for the different-concentration solution. Here, we denote the significant difference of the solute concentration in bulk region and on surface as a type of liquid–liquid partitioning. To check if this partitioning is dependent on the size of the solution slab, we calculate the corresponding value of a $3\,\mathrm{nm} \times 3\,\mathrm{nm} \times 10\,\mathrm{nm}$

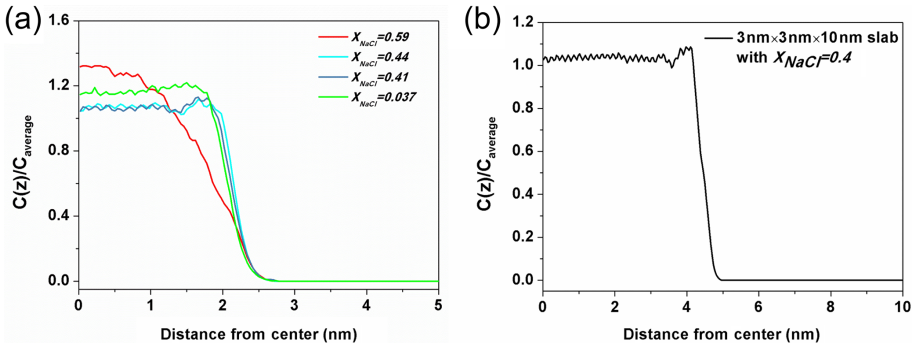


**Figure 7.** The ratio of $Na^+$ concentration at different positions ($C_z$) to the average concentration of the whole system ($C_{\text{average}}$). **(a)** The solution with $x_{\text{NaCl}} = 0.59$ (red line) is on behalf of the solution in the molten NaCl-dominated regime (red line), the solution $x_{\text{NaCl}} = 0.44$ and 0.41 (blue lines) represent the solution in transition regime and the solution $x_{\text{NaCl}} = 0.037$ (green line) represents the solution in the water-dominated regime. **(b)** The density profile obtained from a 3 nm × 3 nm × 10 nm solution slab in which NaCl mass fraction is about 0.4.

solution slab with $x_{\text{NaCl}}$ of 0.4 (Fig. 7b). There is still an apophysis near the surface, thus we can claim that the partitioning is independent of the size of the solution slab in the simulation. Note that this surface enrichment of NaCl does not mean that NaCl is enriched right on top of the solution surface. Actually the density profile of water extends about 0.2 nm beyond that of NaCl towards the vapor region. By contrast, the solution with $x_{\text{NaCl}} > 0.47$ or $< 0.39$ do not have this type of partitioning as shown by the red and green lines. This comparison implies that the stability of surface tension of solution with $x_{\text{NaCl}}$ from $\sim 0.39$ to $\sim 0.47$ is related to the "bulk-surface" partitioning. This interpretation is only a conjecture, and more studies are needed to further examine this phenomenon and interpretation. The shallow minimum in the density profile for $x_{\text{NaCl}}$ between 0.39 and 0.47 to the left of the maximum is somewhat unexpected, and one might expect equilibration problems. However, we have checked that this structural feature develops already during the first 10 ns of the MD simulation, and does not change at all during the residual 200 ns. Surface enrichment of NaCl can be expected, however, when the solubility limit of the water-rich solution in the bulk is reached. Very roughly, such phenomena are analogous to interfacial wetting phenomena such as surface melting of crystals (Frenken and Van der Veen, 1985), which is sometimes observed when the temperature is raised towards the triple point. In our case, the enrichment zone of NaCl (which is about 0.4 nm thick in Fig. 7) would be a precursor effect to the (metastable) NaCl-rich bulk solution. Tentatively, one may correlate the formation of the enrichment zone with the stability of the surface entropy in this region via the entropy of mixing. At the same time, the surface enhancement of ions may be related to the phenomenon of efflorescence.

As shown in Fig. 6, when a solution gets more concentrated from $x_{\text{NaCl}}$ of $\sim 0.47$ to $\sim 0.64$, the $\frac{\Delta H}{A}$ slightly increases from the plateau of $\sim 145\,\text{mN}\,\text{m}^{-1}$ but the change is only $\sim 5\,\text{mN}\,\text{m}^{-1}$. The $-\frac{T\cdot\Delta S}{A}$ keeps increasing. So during this period, both the surface excess enthalpy and entropy terms contribute to the growth of $\sigma_{\text{NaCl,sol}}$. To constrain the energetic analyses, the $\frac{T\cdot\Delta S}{A}$ and $\frac{\Delta H}{A}$ were also calculated for the molten NaCl at 298.15 K. According to Fig. 5, we have $\sigma_{\text{NaCl}} = -0.0755\cdot T + 198.09$; then we can get $\frac{\Delta S_{\text{NaCl}}}{A} = 0.0755\,\text{mN}\,\text{m}^{-1}\,\text{K}^{-1}$ because of $\frac{\Delta S(T)}{A} = \frac{-\text{d}\sigma(T)}{\text{d}T}$ (Landau and Lifshitz, 1969). Therefore, for molten NaCl ($x_{\text{NaCl}} = 1.0$), $\frac{T\cdot\Delta S_{\text{NaCl}}}{A}$ at 298.16 K is $22.15\,\text{mN}\,\text{m}^{-1}$, and $\frac{\Delta H_{\text{NaCl}}}{A}$ at 298.15 K is $198.09\,\text{mN}\,\text{m}^{-1}$ (Fig. 6). Here, we used the derivative of the temperature–surface tension relation to calculate the excess surface entropy, and more discussions about the comparison of these methods can be found in the Supplement (Fig. S1). As can be seen in Fig. 6, it is expected that the excess surface enthalpy term will still have a large amount (about more than $50\,\text{mN}\,\text{m}^{-1}$) to grow until approaching $\frac{\Delta H}{A}$ of molten NaCl at 298.15 K. It is similar for the surface excess entropy term while the increment is smaller. Thus, the fast increase in $\sigma_{\text{NaCl,sol}}$ in the concentration of $x_{\text{NaCl}}$ from $\sim 0.47$ to 1 can be assumed to be a process driven by excess surface enthalpy and excess surface entropy.

## 4 Conclusion

The analysis based on the calculated surface tension confirms the basic concept of the Dutcher et al. (2010) semiempirical model, while unfolding a more detailed global landscape of concentration dependence of surface tension of aqueous NaCl solution and its driving forces: (1) a water-dominated regime ($x_{\text{NaCl}}$ from 0 to $\sim 0.39$; at low concentrations ions are solvated by the water molecules, which means that water-structures/hydration shells are formed around ions); (2) a transition regime ($x_{\text{NaCl}}$ from $\sim 0.39$ to $\sim 0.47$); and (3) a molten NaCl-dominated regime ($x_{\text{NaCl}}$ from $\sim 0.47$ to 1, at very high salt concentration water molecules are solvated by the ions, which means that a salt-structure is formed around the water molecules). Note that our result may not exactly reflect the real mode of surface tension of NaCl solution along

the concentration, but it does imply the concept of a non-monotonic change of surface tension. One must be aware that for nucleation processes in the atmosphere other chemical compounds also matter, and will require future study. Also, mixed salt solutions would be very interesting, and can in principle be studied with similar simulation methods as applied here; however, this task must be left to future work.

*Data availability.* Readers who are interested in the data should contact the authors: Yafang Cheng (yafang.cheng@mpic.de), Hang Su (h.su@mpic.de) or Xiaoxiang Wang (xiaoxiang.wang@mpic.de).

*Supplement.* The supplement related to this article is available online at: https://doi.org/10.5194/acp-18-17077-2018-supplement.

*Author contributions.* YC and HS conceived and led the study. XW performed the MD simulation and analyzed the data. XW, YC, KB and HS interpreted the results. UP and CC discussed the results and commented on the manuscript. XW, KB, YC, CC and HS wrote the manuscript with input from all coauthors.

*Competing interests.* The authors declare that they have no conflict of interest.

*Acknowledgements.* This study is supported by the Max Planck Society (MPG). Xiaoxiang Wang acknowledges the support from China Scholarship Council (CSC, 201406190170). Yafang Cheng acknowledges the Minerva Program from MPG.

The article processing charges for this open-access publication were covered by the Max Planck Society.

Edited by: Maria Cristina Facchini
Reviewed by: two anonymous referees

## References

Abraham, M. J., Murtola, T., Schulz, R., Páll, S., Smith, J. C., Hess, B., and Lindahl, E.: GROMACS: High performance molecular simulations through multi-level parallelism from laptops to supercomputers, SoftwareX., 1, 19–25, 2015.

Alejandre, J., Tildesley, D. J., and Chapela, G. A.: Molecular dynamics simulation of the orthobaric densities and surface tension of water, J. Chem. Phys., 102, 4574–4583, 1995.

Aveyard, R. and Saleem, S. M.: Interfacial tensions at alkane-aqueous electrolyte interfaces, J. Am. Chem. Soc., 72, 1609–1617, 1976.

Bahadur, R., Russell, L. M., and Alavi, S.: Surface tensions in NaCl-water-air systems from MD simulations, J. Phys. Chem. B, 111, 11989–11996, 2007.

Berendsen, H., Grigera, J., and Straatsma, T.: The missing term in effective pair potentials, J. Phys. Chem., 91, 6269–6271, 1987.

Bhatt, D., Newman, J., and Radke, C.: Molecular dynamics simulations of surface tensions of aqueous electrolytic solutions, J. Phys. Chem. B, 108, 9077–9084, 2004.

Biskos, G., Malinowski, A., Russell, L., Buseck, P., and Martin, S.: Nanosize effect on the deliquescence and the efflorescence of sodium chloride particles., Aerosol Sci. Tech., 40, 97–106, 2006.

Bzdek, B. R., Power, R. M., Simpson, S. H., Reid, J. P., and Royall, C. P.: Precise, contactless measurements of the surface tension of picolitre aerosol droplets, Chem. Sci., 7, 274–285, 2016.

Chen, Y., Cheng, Y., Ma, N., Wolke, R., Nordmann, S., Schüttauf, S., Ran, L., Wehner, B., Birmili, W., van der Gon, H. A. C. D., Mu, Q., Barthel, S., Spindler, G., Stieger, B., Müller, K., Zheng, G.-J., Pöschl, U., Su, H., and Wiedensohler, A.: Sea salt emission, transport and influence on size-segregated nitrate simulation: a case study in northwestern Europe by WRF-Chem, Atmos. Chem. Phys., 16, 12081–12097, https://doi.org/10.5194/acp-16-12081-2016, 2016.

Cheng, Y., Su, H., Koop, T., Mikhailov, E., and Pöschl, U.: Size dependence of phase transitions in aerosol nanoparticles, Nat. Commun., 6, 5923, 2015.

Davidchack, R. L. and Laird, B. B.: Direct calculation of the crystal–melt interfacial free energies for continuous potentials: Application to the Lennard-Jones system, J. Chem. Phys., 118, 7651–7657, 2003.

Dutcher, C. S., Wexler, A. S., and Clegg, S. L.: Surface tensions of inorganic multicomponent aqueous electrolyte solutions and melts, J. Phys. Chem. A, 114, 12216–12230, 2010.

Espinosa, J., Young, J., Jiang, H., Gupta, D., Vega, C., Sanz, E., Debenedetti, P., and Panagiotopoulos, A.: On the calculation of solubilities via direct coexistence simulations: Investigation of NaCl aqueous solutions and Lennard-Jones binary mixtures, J. Chem. Phys., 145, 154111, https://doi.org/10.1063/1.4964725, 2016.

Essmann, U., Perera, L., Berkowitz, M. L., Darden, T., Lee, H., and Pedersen, L. G.: A smooth particle mesh Ewald method, J. Chem. Phys., 103, 8577–8593, 1995.

Finlayson-Pitts, B.: The tropospheric chemistry of sea salt: A molecular-level view of the chemistry of NaCl and NaBr, Chem. Rev., 103, 4801–4822, 2003.

Fischer, N. M., van Maaren, P. J., Ditz, J. C., Yildirim, A., and van der Spoel, D.: Properties of organic liquids when simulated with long-range Lennard-Jones interactions, J. Chem. Theory Comput., 11, 2938–2944, 2015.

Frenken, J. W. M. and Van der Veen, J. F.: Observation of surface melting, Phys. Rev. Lett., 54, 134–137, 1985.

Ghorai, S., Wang, B., Tivanski, A., and Laskin, A.: Hygroscopic properties of internally mixed particles composed of NaCl and water-soluble organic acids, Environ. Sci. Technol., 48, 2234–2241, 2014.

Harkins, W. D. and Brown, F.: The determination of surface tension (free surface energy), and the weight of falling drops: The surface tension of water and benzene by the capillary height method, J. Am. Chem. Soc., 41, 499–524, 1919.

Hoover, W. G.: Canonical dynamics: equilibrium phase-space distributions, Phys. Rev. A, 31, 1695, https://doi.org/10.1103/PhysRevA.31.1695, 1985.

Horvath, A. L.: Handbook of aqueous electrolyte solution physical properties, estimation and correlation methods, Ellis Horwood Series in Physical Chemistry, Ellis Horwood Limited, New York, 1985.

Janz, G. J.: Thermodynamic and transport properties for molten salts: correlation equations for critically evaluated density, surface tension, electrical conductance, and viscosity data, Amer. Inst. of Phys., New York, 1988.

Jarvis, N. L. and Scheiman, M. A.: Surface potentials of aqueous electrolyte solutions, J. Phys. Chem., 72, 74–78, 1968.

Johansson, K. and Eriksson, J. C.: $\gamma$ and $\mathrm{d}\gamma/\mathrm{d}T$ measurements on aqueous solutions of 1, 1-electrolytes, J. Colloid Interf. Sci., 49, 469–480, 1974.

Joung, I. S. and Cheatham III, T. E.: Molecular dynamics simulations of the dynamic and energetic properties of alkali and halide ions using water-model-specific ion parameters, J. Phys. Chem. B, 113, 13279–13290, 2009.

Jungwirth, P. and Tobias, D. J.: Surface effects on aqueous ionic solvation: A molecular dynamics simulation study of NaCl at the air/water interface from infinite dilution to saturation, J. Phys. Chem. B, 104, 7702–7706, 2000.

Kumar, A.: Aqueous guanidinium salts: Part II. Isopiestic osmotic coefficients of guanidinium sulphate and viscosity and surface tension of guanidinium chloride, bromide, acetate, perchlorate and sulphate solutions at 298.15 K, Fluid Phase Equilibr., 180, 195–204, 2001.

Landau, L. D. and Lifshitz, E. M.: Statistical physics, Pergamon press, Oxford, 1969.

Levin, Y. and Flores-Mena, J.: Surface tension of strong electrolytes, EPL, 56, 187–192, 2001.

Lewis, E. R. and Schwartz, S. E.: Sea salt aerosol production: mechanisms, methods, measurements, and models-A critical review, American Geophysical Union, Washington, D.C., 2004.

Li, Z. and Lu, B. C.-Y.: Surface tension of aqueous electrolyte solutions at high concentrations – representation and prediction, Chem. Eng. Sci., 56, 2879–2888, 2001.

Li, Z.-B., Li, Y.-G., and Lu, J.-F.: Surface tension model for concentrated electrolyte aqueous solutions by the Pitzer equation, Ind. Eng. Chem. Res., 38, 1133–1139, 1999.

Martin, S. T.: Phase transitions of aqueous atmospheric particles, Chem. Rev., 100, 3403–3454, 2000.

Matubayasi, N., Tsunetomo, K., Sato, I., Akizuki, R., Morishita, T., Matuzawa, A., and Natsukari, Y.: Thermodynamic quantities of surface formation of aqueous electrolyte solutions: IV. Sodium halides, anion mixtures, and sea water, J. Colloid Interf. Sci., 243, 444–456, 2001.

Mester, Z. and Panagiotopoulos, A Z.: Mean ionic activity coefficients in aqueous NaCl solutions from molecular dynamics simulations, J. Chem. Phys., 142, 044507, https://doi.org/10.1063/1.4906320, 2015.

Morris, H. S., Grassian, V. H., and Tivanski, A. V.: Humidity-dependent surface tension measurements of individual inorganic and organic submicrometre liquid particles, Chem. Sci., 6, 3242–3247, 2015.

Moučka, F., Nezbeda, I., and Smith, W. R.: Molecular force field development for aqueous electrolytes: 1. Incorporating appropriate experimental data and the inadequacy of simple electrolyte force fields based on Lennard-Jones and point charge interactions with Lorentz–Berthelot rules, J. Chem. Theory Comput., 9, 5076–5085, 2013.

Neyt, J.-C., Wender, A., Lachet, V., Ghoufi, A., and Malfreyt, P.: Prediction of the concentration dependence of the surface tension and density of salt solutions: atomistic simulations using Drude oscillator polarizable and nonpolarizable models, Phys. Chem. Chem. Phys., 15, 11679–11690, 2013.

Nezbeda, I., Moučka, F., and Smith, W. R.: Recent progress in molecular simulation of aqueous electrolytes: Force fields, chemical potentials and solubility, Mol. Phys., 114, 1665–1690, 2016.

Nosé, S.: A molecular dynamics method for simulations in the canonical ensemble, Mol. Phys., 52, 255–268, 1984.

Pegram, L. M. and Record, M. T.: Partitioning of atmospherically relevant ions between bulk water and the water/vapor interface, P. Natl. Acad. Sci. USA, 103, 14278–14281, 2006.

Pegram, L. M. and Record, M. T.: Hofmeister salt effects on surface tension arise from partitioning of anions and cations between bulk water and the air-water interface, J. Phys. Chem. B, 111, 5411–5417, 2007.

Richardson, C. and Snyder, T. D.: A study of heterogeneous nucleation in aqueous solutions, Langmuir, 10, 2462–2465, 1994.

Sada, E., Katoh, S., Yoshii, H., Yamanlshl, T., and Nakanlshl, A.: Performance of the gas bubble column in molten salt systems, Ind. Eng. Chem. Proc. Des. Dev., 23, 151–154, 1984.

Stillinger, F. H. and Weber, T. A.: Computer simulation of local order in condensed phases of silicon, Phys. Rev. B, 31, 5262–5271, 1985.

Vargaftik, N., Volkov, B., and Voljak, L.: International tables of the surface tension of water, J. Phys. Chem. Ref. Dat., 12, 817–820, 1983.

Wagner, R., Höhler, K., Möhler, O., Saathoff, H., and Schnaiter, M.: Crystallization and immersion freezing ability of oxalic and succinic acid in multicomponent aqueous organic aerosol particles, Geophys. Res. Lett., 42, 2464–2472, 2015.

Weissenborn, P. K. and Pugh, R. J.: Surface tension and bubble coalescence phenomena of aqueous solutions of electrolytes, Langmuir, 11, 1422–1426, 1995.

Weissenborn, P. K. and Pugh, R. J.: Surface tension of aqueous solutions of electrolytes: relationship with ion hydration, oxygen solubility, and bubble coalescence, J. Colloid Interf. Sci., 184, 550–563, 1996.

Wexler, A. S. and Clegg, S. L.: Atmospheric aerosol models for systems including the ions $H^+$, $NH_4^+$, $Na^+$, $SO_4^{2-}$, $NO_3^-$, $Cl^-$, $Br^-$, and $H_2O$, J. Geophys. Res.-Atmos, 107, ACH 14-1–ACH 14-14, https://doi.org/10.1029/2001JD000451, 2002.

Supplement of Atmos. Chem. Phys., 18, 17077–17086, 2018
https://doi.org/10.5194/acp-18-17077-2018-supplement


Atmospheric Chemistry and Physics
Open Access
EGU

*Supplement of*

# Molecular dynamics simulation of the surface tension of aqueous sodium chloride: from dilute to highly supersaturated solutions and molten salt

**Xiaoxiang Wang et al.**

*Correspondence to:* Yafang Cheng (yafang.cheng@mpic.de) and Hang Su (h.su@mpic.de)

**Supplement**

There are three ways to calculate the excess surface entropy, i.e. the direct method, the numerical derivative and the derivative of temperature-surface tension ($T-\sigma$) relation (Sega and Dellago, 2017; Sega et al., 2018). The direct method was employed to calculate $\frac{\Delta H}{A}$ and $\frac{T\cdot\Delta S}{A}$ in our paper (Fig. 6). In this method, we simulated liquid layers with and without surfaces. The difference of enthalpy per area of liquid with surfaces and the one of liquid without surfaces is the excess surface enthalpy ($\frac{\Delta H}{A}$). And $\frac{T\cdot\Delta S}{A}$ can be calculated as $\frac{T\cdot\Delta S}{A}=\frac{\Delta H}{A}-\sigma$. The numerical derivative method is based on the value of $\sigma$ of the studied liquid at different temperatures. We need to use the equation $\sigma(T)=\sigma(T_0)+a\times(T-T_0)+b\times(T-T_0)^2$ to fit the data of $\sigma(T_0)$, $\sigma(T_0-10\ K)$ and $\sigma(T_0+10\ K)$ to get the fitting parameters a and b for a given $T_0$, i.e., $a(T_0)$ and $b(T_0)$, respectively. As $\frac{\Delta S(T)}{A}=\frac{-d\sigma(T)}{dT}$ (Landau and Lifshitz, 1969), we have $\frac{\Delta S}{A}(T_0)=-a(T_0)$. And we can get $\frac{\Delta S}{A}$ at different temperature one by one. For $\frac{\Delta H}{A}$, we can calculate by $\frac{\Delta H}{A}=\sigma+\frac{T\cdot\Delta S}{A}$. The derivative of $T-\sigma$ relation method is also based on the value of $\sigma$ of at different temperatures. After obtaining these values, we can get an equation to describe the relationship between $\sigma$ and T, i.e. $\sigma(T)$. After that the excess surface entropy can be easily calculated by $\frac{\Delta S(T)}{A}=\frac{-d\sigma(T)}{dT}$ (Landau and Lifshitz, 1969). And similarly, $\frac{\Delta H}{A}=\sigma+\frac{T\cdot\Delta S}{A}$.

A very recent paper (Sega et al., 2018) compared excess surface entropy based on these methods and reported that results based on the direct method might not be applicable at high temperature because of its significant deviations to the excess surface entropy derived with the derivative of $T-\sigma$ relation when the temperature is high. Thus we used the derivative of $T-\sigma$ relation method to calculate $\frac{\Delta H}{A}$ and $\frac{T\cdot\Delta S}{A}$ of molten NaCl, but not the direct method. Note again that the majority of data in Fig. 6 (except the points for $x_{NaCl}$ of 1.0) are obtained by the direct method at 298.15 K. We also performed independent calculation of the excess surface entropy and enthalpy of pure water at temperatures from 278.15 K to 348.15 K based on the aforementioned three methods. As shown in the Fig. S1, results from these three methods well agree with each other, which means that results based on the direct method at room temperature can be trusted.

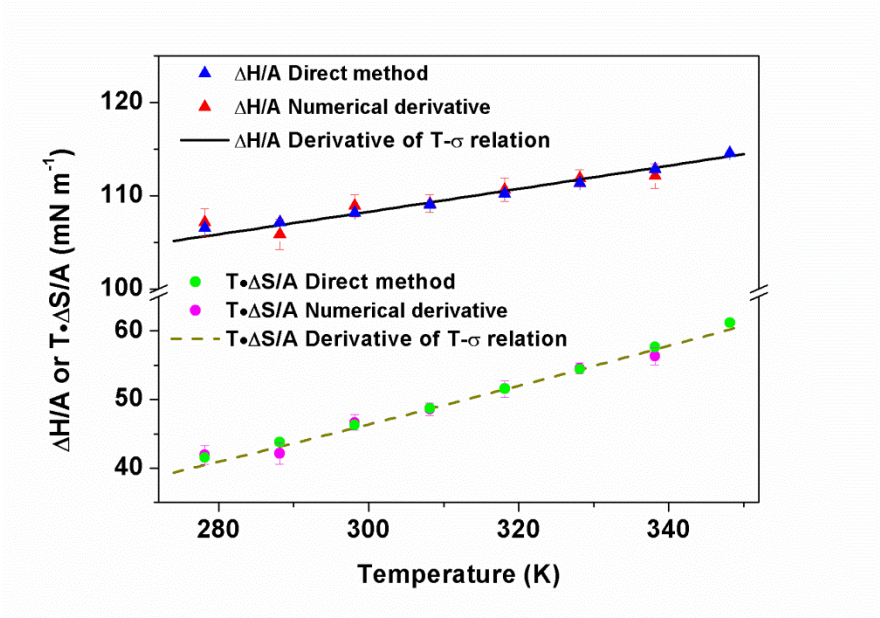


Figure S1. $\frac{\Delta H}{A}$ and $\frac{T \cdot \Delta S}{A}$ of pure water at temperatures from 278.15 K to 348.15 K obtained from different methods.

**References:**

Landau, L. D., and Lifshitz, E. M.: Statistical physics, Pergamon press, 1969.

Sega, M., and Dellago, C.: Long-range dispersion effects on the water/vapor interface simulated using the most common models. J. Phys. Chem. B, 121(15), 3798-3803, 2017.

Sega, M., Horvai, G., and Jedlovszky, P.: On the calculation of the surface entropy in computer simulation. J. Mol. Liq., 262, 58-62, 2018.

## B.3 Wang et al., to be submitted

# Studying the Vapor Pressure and Surface Tension of Water Nano-droplets by MD Simulations

Xiaoxiang Wang[1], Chuchu Chen[1], Kurt Binder[2], Ulrich Pöschl[1], Hang Su[1,3 *], Yafang Cheng[1,3 *]

[1] Max Planck Institute for Chemistry, Multiphase Chemistry Department, Hahn-Meitner-Weg 1, 55128 Mainz, Germany

[2] Institut für Physik, Johannes Gutenberg-Universität, Staudinger Weg 7, 55128 Mainz, Germany

[3] Center for Air Pollution and Climate Change Research, Institute for Environmental and Climate Research, Jinan University, 510632 Guangzhou, China

* Corresponding author. Email: yafang.cheng@mpic.de (Y.C.); h.su@mpic.de (H.S.)

### Author contributions

Y.C. and H.S. conceived and led the study. X.W. performed the MD simulation and analyzed the data. X.W., Y.C., K.B. and H.S. interpreted the results. U.P. and C.C. discussed the results and commented on the manuscript. X.W., Y.C., K.B. and H.S. wrote the manuscript with inputs from all coauthors.

# Studying the Vapor Pressure and Surface Tension of Water Nano-droplets by MD Simulations

Xiaoxiang Wang[1], Chuchu Chen[1], Kurt Binder[2], Ulrich Pöschl[1], Hang Su[1,3 *], Yafang Cheng[1,3 *]

[1] Max Planck Institute for Chemistry, Multiphase Chemistry Department, Hahn-Meitner-Weg 1, 55128 Mainz, Germany

[2] Institut für Physik, Johannes Gutenberg-Universität, Staudinger Weg 7, 55128 Mainz, Germany

[3] Center for Air Pollution and Climate Change Research, Institute for Environmental and Climate Research, Jinan University, 510632 Guangzhou, China

* Corresponding author. Email: yafang.cheng@mpic.de (Y.C.); h.su@mpic.de (H.S.)

**Abstract**

The vapor pressure and surface tension of water nano-droplets play key roles in many different processes. There are still many different debates about the size dependence of these properties. In this paper, we used molecular dynamics (MD) simulation to address some questions involved these debates. We found SPC water model is the best model to reproduce the vapor pressure of water among 6 studied models. The vapor pressure of nano-droplets with different size was calculated, and we found the value of $\ln\frac{P_{sat}(r)}{P_{sat\_0}}$ increases from 0.46 to 2.1 when the radius decreases from ~1.92 nm to ~0.4 nm. Then a method of retrieving surface tension based on the data of vapor pressure from MD simulations was developed. The size dependence of surface tension was analyzed by using a modified form of Tolman equation. The Tolman length is conjectured to be -0.12 nm. Additionally, a compression in the nano-droplet was found, and this compression might be related to the size dependence of vapor pressure and surface tension.

## 1. Introduction

The vapor pressure and surface tension of water nano-droplets are highly important for several different subjects (*1, 2*). Firstly, they are of fundamental interests in areas like classical nucleation theory (*3*) and behaviors of water clusters (*4*). In the atmospheric science, these two properties play as essential roles in several different processes. For example, Li et al. showed that kinetics of ice nucleation in the atmosphere were affected by these properties at the nanoscale (*5*). Findings about these properties may have implications for the process of new particle formation (*6, 7*). Besides studies of atmospheric science, the comprehension of these two properties has received attentions from material science because of their significance in many processes, e.g. the micelle formation (*8-10*).

One of the most important issues about these properties is the size dependence. The Kelvin equation (*11*) provides the vapor pressure of a droplet as a function of the radius of this droplet (Eq. 1).

$$P_{sat}(r) = P_{sat\_0} \cdot \exp(\frac{2\sigma V_m}{rRT}) \quad (1)$$

Here, $P_{sat}(r)$ and $P_{sat\_0}$ are the vapor pressure ($P_{sat}$) over a nano-droplet with radius $r$ and the one over a planar surface; $V_m$ is the molar volume of water. $\sigma$ is the surface tension of the liquid in the droplet, and this value is also dependent on the size. This dependence becomes to be important when the size of droplet is very small. This can be accounted for through the Tolman equation (*12*) (Eq. 2).

$$\sigma(r) = \sigma_\infty/(1 + \frac{2\delta}{r}) \quad (2)$$

Here, $\sigma(r)$ and $\sigma_\infty$ are the surface tension over a nano-droplet with radius $r$ and the one over a planar surface, and $\delta$ is the so called Tolman length. However, there are still a lot debate about the sign and value of $\delta$. Therefore, uncertainty of these equations occurs, especially as the radius approaches the nanometer and sub-nanometer scale. Note that Eq. 1 is supposed to describe the leading behavior of $\sigma(r)$ as $r \to \infty$, but on the nanoscale this relation may break down.

The molecular dynamics (MD) simulation is a useful tool to research issues involving vapor pressure and surface tension. For example, Vega and Miguel study

the vapor pressure and surface tension of most popular models of water by using different methods (*13*). However, very few studies focused on both properties of nano-droplets due to the limitation of techniques. Gibbs ensemble (GE) method and Grand Canonical (GC) method, which are widely used methods for Monte Carlo (MC) simulations, may help people to overcome current challenges, while they are not well-developed for MD simulations. Factorovich et al. have tried to use GC method in MD simulations to calculate the vapor pressure of water nano-droplets with different diameters, while the model they used, mW water model, is a coarse-grained model. Thus the conclusion of this study remains questionable (*14*). In this paper, we integrated MD simulations and the Kelvin equation to develop a simple method to transfer the data of vapor pressure to the value of surface tension and address following scientific questions: 1) what kind of water model can reproduce the vapor pressure of water best; 2) how does the vapor pressure change along the size of water nano-droplet; 3) how is the size dependence of the surface tension of water nano-droplets.

## 2. Methods

### 2.1. Force fields, initial structures, and setups for simulations

To find the proper water model to use for simulation and calculating the ratio of $P_{sat}(r)$ to the one over the planar surface, we performed the calculation of the $P_{sat\_0}$ from simulations of 6 models of water, such as the traditional SPC, SPC/E, TIP3P, TIP4P water models, and TIP4P-like models including the TIP4P/Ew and TIP4P/2005. Parameters about these models are summarized in Table 1, and schematic representations of 3-point models (SPC, SPC/E and TIP3P) and 4-point models (TIP4P, TIP4P/EW and TIP4P/2005) are shown in Figure 1. We then determined that the calculated vapor pressure based on SPC is closest to the experimental value among all calculated values (more details are shown in the section 3.2). Indeed, several studies have also examined the vapor pressure of different water models at different temperature (*15-18*). By comparing results from these studies, we can also find SPC water model is the best one to reproduce the vapor pressure of real water.

Therefore, simulations of nano-droplets and subsequent analyses were carried out based on SPC water model.

For the calculation of vapor pressure over the planar surface, planar water slabs were constructed and simulated. A Water cube with lengths at x-, y- and z-directions of 5 nm ($L_x = L_y = L_z$ = 5 nm) was generated firstly. Subsequently, the cube was added into the cuboid cell with an elongated length along the z-direction ($L_z$ = 20 nm, $L_x = L_y$ = 5 nm) to create two surfaces (Figure 2). It should be noted that performing simulations with explicit interfaces have been used by many researchers to study the vapor−liquid equilibria (*19*). At the same time, 3 nm×3 nm×3 nm and 8 nm×8 nm×8 nm water slabs were also prepared in 3 nm×3 nm×10 nm and 8 nm×8 nm×30 nm cells to check if the size of simulation cell can affect the result. Nano-droplets with different number of water molecules were created, and these droplets, naturally, have different values of diameter. Then these nano-droplets were put into bigger cells (e.g. $L_x = L_y = L_z$ = 10 nm) and suspended in the vacuum.

All simulations were carried out with the GROMACS v5.1 package. Initial structures were firstly energetically minimized. Then the structures were equilibrated and simulated in the NVT ensemble with periodic boundary conditions in all three directions. The temperature was controlled at 298.15 K by using the Nose-Hoover thermostat. All simulations were carried out for at least 50 ns by using a 1 fs time step, and configurations for analysis were saved every 2 ps. Both electrostatic interactions and van der Waals interactions were calculated using the Particle Mesh Ewald (PME) algorithm, because PME has been found to give an accurate calculation of long-range interactions. At least, 3 independent runs were performed for each case.

### 2.2. Count the gaseous water molecules and vapor pressure

The vapor pressure of water can be characterized by the number density of gaseous water. In this study, water molecules, whose interactions with other water molecules equal zero (Figure 3), are considered to be the molecule in the gas phase (gaseous water). After counting the number of gaseous water, the number density,

$\rho_{N\_gas}$, is calculated by Eq. 3.

$$\rho_{N\_gas} = \frac{N_{gas}}{V_{gas}} \quad (3)$$

Here, $N_{gas}$ is the average number of water molecules in the gas phase along the time. $V_{gas}$ is volume of gas phase in the simulation cell. As we know, gaseous water is ideal gas at room temperature, thus we can calculate the value of $P_{sat}$ by Eq. 4.

$$P_{sat} = \frac{\rho_{N\_gas} RT}{N_A} \quad (4)$$

Here, $R$ is the gas constant, and $T$ is the temperature in Kelvin. $N_A$ is the Avogadro constant.

### 2.3. Surface tension of nano-droplets and planar surface

Kelvin equation (Eq. 1) describes vapor pressure of different size droplets, and surface tension of the studied liquid is required for the description. Thus we can retrieve the data of surface tension of different size nano-droplets by Eq. 5.

$$\sigma(r) = \ln\left(\frac{P_{sat}(r)}{P_{sat\_0}}\right) \cdot \frac{rRT}{2V_m} \quad (5)$$

In this study, the radius of nano-droplets is quantified as the distance from the center to the surface, and the position of surface is the place whose density is half of the density in bulk area. As a few water molecules can evaporate into the gas phase, the radius can be varied. This variation is presented as the error bar of radius, although it is quite limited. After getting $\sigma(r)$ of different nano-droplets, the relationship between $\sigma$ and $r$ would be studied.

The surface tension of planar surface was also calculated by using pressure tensor method (Eq. 6), applied to a liquid slab coexisting with vapor.

$$\sigma = \frac{1}{2} L_z \left[\langle P_{zz} \rangle - \frac{1}{2}\left(\langle P_{xx} \rangle + \langle P_{yy} \rangle\right)\right] \quad (6)$$

Here, $L_z$ is the length of the simulation cell (see Figure 2a) in the longest direction (along z-direction, $L_z$ = 20 nm in this case) and $P_{aa}$ $(a = x, y, z)$ denotes the diagonal component of the pressure tensor. The $\langle \cdots \rangle$ refers to time average. The factor $\frac{1}{2}$ outside the squared brackets takes into account the two interfaces in the

system. Note that in simulations one always needs to worry about systematic errors due to the finite size of the simulation box. However, in the case of water at room temperature careful study of size effects (*20*) has shown that for $L \geq 3\,\mathrm{nm}$, $L_z \geq 10\,\mathrm{nm}$ size effects on the surface tension of the planar interface are completely negligible. In principle, the situation for the nano-droplet simulation (Figure 2B) is more subtle: for very large box, a droplet of finite radius r coexisting with supersaturated vapor (with pressure given by Eq. 1) is a state of unstable equilibrium (the system is a state right on top of the nucleation barrier). However, since we work in the NVT ensemble, for box linear dimension L of practical interest one can show that the equilibrium between the droplet and surrounding actually is thermodynamically stable (*21*). While the particle number $N_{droplet}$ in the droplet and $N_{gas}$ in the vapor can slightly fluctuate, the constraint $N_{droplet} + N_{gas} = N$ turns the unstable equilibrium into a stable one.

## 3. Results

### 3.1. Vapor pressure of different water models

By monitoring the position of water molecules in simulated systems, we found for all six water models that molecule can evaporate from the liquid phase to the gas phase as water molecules in the real world. Figure 4 shows the time evolution of number density of gaseous water molecules (all 6 models) recorded every 20 picosecond. The value varies from 0 to 1.3 $\times 10^{-2}$ molecules $nm^{-3}$ for all studied models. As the number density of gaseous water molecules keeps changing, it is not reasonable to use the number of gaseous water molecules in one configure/snapshot (which varies only from 0 to 4 here) to present the vapor pressure. Therefore, we propose to use an average value along the simulation time, and this time-averaged value is actually the term of $\rho_{N\_gas}$ in Eq. 4. The average values over different-length time for SPC water model, as an instance, are presented in Figure 5. It can be seen clearly that the average value becomes stable when the simulation time is longer than 30 ns. Therefore, we chose 50 ns as the time window to calculate the average value in

this study.

According to Eq. 4, the vapor pressure of different water models was calculated. The vapor of water over a planar surface at 298.15 K is 3.1686 kPa (*22*), and this value is equivalent to $7.69\times10^{-4}$ gaseous water molecules $nm^{-3}$. The vapor pressure of SPC, SPC/E, TIP3P, TIP4P, TIP4P/EW and TIP4P/2005 is shown in Table 2, accompanying the number density of gaseous water molecules. Our results are quite close to the values from other studies which are based on different methods (Table 2). It can be seen the result based on SPC water model is closest to the measured value, although it is a little higher than the latter. Thus, we used this water model in the next steps. One may concern that the size of water slab and simulation cell may affect the value of the vapor pressure of models. We calculated the vapor pressure over a 3 nm×3 nm× 3 nm SPC water slab in a 3 nm×3 nm× 10 nm cell, and the one over a 8 nm×8 nm× 8 nm slab in a 8 nm×8 nm× 30 nm cell. Values of vapor pressure obtained based on these slabs and cells are also about 3.46 kPa (Figure 6), and it indicates the vapor pressure of SPC water model is independent on the size of simulated water slab and simulation cell. More than hundreds models of water have been developed since the first realistic interaction potential of water was proposed in 1933, and some other models might be able to reproduce the value of vapor pressure better than SPC (*23, 24*). Determining the best model for studies involved vapor pressure is still an open topic.

### 3.2. Vapor pressure of nano-droplets

By using Eq. 4, the vapor pressure of water nano-droplets with different radius based on SPC water model was obtained (Table 3). The natural logarithm of the relative vapor pressure ($\ln\frac{P_{sat}(r)}{P_{sat\_0}}$) is shown in Figure 7A as a function of the radius. The value of $\ln\frac{P_{sat}(r)}{P_{sat\_0}}$ increases from 0.46 to 2.1 when the radius decreases from ~1.92 nm to ~0.4 nm. The results from Factorovich et al.'s study based on mW coarse-grained model of water were also shown in Figure 7A for the comparison (*14*). The values for droplets with similar size from our study are similar the ones from

Factorovich et al.'s study (*14*), although we used different water models. This may be an accidental coincidence; we do not imply that the $\ln\frac{P_{sat}(r)}{P_{sat\_0}}$ is independent on the selection of water models, and more studies should be done to examine this viewpoint. The values of $\ln\frac{P_{sat}(r)}{P_{sat\_0}}$ from our study and Factorovich et al.'s study (*14*) are also shown against the inverse of radius in Figure 7B, and we find the $\ln\frac{P_{sat}(r)}{P_{sat\_0}}$ increases as the inverse of radius increases.

### 3.3. Size dependence of surface tension and Tolman length

The surface tension of each studied nano-droplets was calculated (Table 3). All values are lower than the measured value, 71.9 mN/m, and it can be expected because the surface tension of the majority of water models based on different method underestimates the value of real water. Therefore, we will focus on the relationship between the surface tension and size of droplets rather than these values themselves. According to Figure 8A, we can find that the size effect is very weak when the radius is larger than 0.52 nm. However, the value drops significantly along the size when the radius is smaller than 0.4 nm. This phenomenon is similar to the one in Factorovich et al.'s study (*14*). Based on these calculated values of surface tension, the analysis of size dependence is performed.

As mentioned above, Tolman suggested that the surface tension of spherical droplets can be written as a simple function of radius of the droplets (Eq. 2) (*12*). Currently, many debates are carried out about $\delta$, although it is agreed that this value should be of the order of the inter-molecular distance. The value of water proposed by Tolman was 0.1 nm originally (*25*). Graziano obtained values ranges from 0.1031 to 0.0665 nm at temperatures from 270 K to 370 K using MD simulations (*26*). By use of the Gibbs-Tolman-Kening-Buff equation, a value of 0.14 nm was reported by Xue et al (*27*). According to these studies, the surface tension should decrease as the decrease of radius. However, a work based on MD simulations for the TIP4P/2005 water model reported a negative $\delta$ of -0.056 nm, and in this case, the surface tension should increase when the droplet becomes smaller (*28, 29*). A pronounced decrease of

the surface tension with decreasing radius was also found by Lau et al. for the TIP4P/2005 water model (*30*). Wilhelmsen et al. used square gradient theory and got a similar result (*31*). Two experimental assessments of δ have also been performed. Holten et al. estimated a value of +0.06 nm via nucleation experiments in an expansion wave tube (*32*). By contrast, Azouzi et al. using cavitation experiments in quartz inclusions obtained a value of −0.047 nm (*33*). This inconsistency might be explained by the different assumptions in the data processing. Besides the debates about $\delta$, the validity of Eq. 2 is also disputed. Tolman neglected higher-order terms (*12*) in the derivation, however, several previous studies suggested the contribution of a term of $\frac{1}{r^2}$ is non-negligible for droplet radii of a few nanometers (*34-36*). The Tolman equation should be rewritten as Eq. 7,

$$\sigma(r) = \sigma_\infty / [1 + \frac{2\delta}{r} + 2\left(\frac{l}{r}\right)^2] \quad (7)$$

where $l$ also is a parameter that has the dimension of length.

We fitted our data with both Eq. 2 and Eq. 7. By using Eq. 2, we got that $\sigma_\infty$ is 66.2 mN $m^{-1}$ and $\delta$ is 0.036. Correspondingly, the curve is presented in Figure 8A. For the fitting of Eq. 7, the obtained $\sigma_\infty$ by using pressure tensor method (54.5 mN/m) was introduced into the equation. Regarding the planar water slab as a droplet with an infinite radius, the relationship between the inverse of surface tension ($\frac{1}{\sigma(r)}$) and the inverse of radius ($\frac{1}{r}$) is drawn in Figure 8B with the fitting curve based on Eq. 7. $\delta$ is -0.12 nm , and $l$ is 0.23 nm. The values of surface tension of 20-water and 50-water droplets are significantly larger than the values of 100-water, 500-water and 1000-water droplets, and we can claim that the quality of the fitting to Eq. 7 is more convincing. In particular, fitting to Eq. 1 is incompatible with the correct value $\sigma_\infty = 54.5\ \mathrm{mN/m}$ for the SPC water model. The value of $\delta$ should then be negative for the real water when the description in terms of the SPC model is trusted.

### 3.4. Structural analysis

The density profile of water slab along z-direction was calculated first (Figure 9).The simulation cell is divided into slabs with a thickness of 0.2 Å, and the density of each slab is statistically averaged along the simulation time. The density profiles were fitted to a hyperbolic tangent function

$$\rho(z) = \frac{1}{2}(\rho_L + \rho_V) - \frac{1}{2}(\rho_L - \rho_V)\tanh[\frac{z-z_0}{d}] \quad (8)$$

where $\rho_L$ and $\rho_V$ are densities of the liquid and vapor, $z_0$ is the position of the Gibbs dividing surface, and $d$ is a parameter describing the surface thickness. The $\rho_L$ is 0.976 kg $L^{-1}$, and it is lower than the value for real water. However, it is almost the same as the ones reported by previous studies (*13*, *37*).

The density profiles of nano-droplets against the distance from the center are shown in Figure 9. Profiles for droplets with radius from 0.52 nm to 1.92 nm are compatible with the hyperbolic tangent form, i.e. (i) a larger density value in the inner part; (ii) a decline of density as the distance to the center increases; (iii) density is approaching to zero. It can be seen that the densities in the inner part for all droplets (~1 kg $L^{-1}$) are larger than $\rho_L$ (0.976 kg $L^{-1}$). This result indicates a compression in the nano-droplet induced by the curvature, though such effect is small. Similar result was also reported by Li et al. based on SPC/E water model (*38*). Note that the equilibrium that we study implies that the droplet and the surrounding vapor have the same chemical potential. Since the vapor is an ideal gas, and its pressure is considerably enhance in comparison with the saturation pressure, we can conclude that also the chemical potential is correspondingly enhanced, and this causes also a density increase of the liquid water in the "bulk" of the droplet. Note that an enhancement of the density in the bulk of the droplet with decreasing droplet radius must be expected, since the chemical potential of the droplet (which must be the same as the chemical potential of the surrounding gas in equilibrium) is enhanced due to the enhanced pressure in the gas, but the observed densities in the droplet are considerably larger than one would predict from this argument. An interesting issue is the broadening of the interfacial profile with increasing droplet radius that one can infer from Figure 9. Following Schmitz et al. (*39*) and Lau et al. (*30*), we fit the radial

density profile to Eq. 9.

$$\rho(r) = \frac{1}{2}(\rho_L + \rho_V) - \frac{1}{2}(\rho_L - \rho_V)\tanh[\frac{2}{D}(r - r_0)] \quad (9)$$

Note that $\rho_V \approx 0$ and $r_0$ is strictly less than the droplet radius resulting from the Gibbs dividing surface, and all calculated values are shown in Table 3. Figure 10 plots the squared width $D^2$ versus $\ln(r_0)$, to demonstrate the logarithmic increase expected from capillary wave theory (for planar interfaces, this is discussed in our previous study (*20*) in more detail). For droplets, this was observed first for the simplistic lattice gas model (*39*). Besides it, Lau et al. verified it in the case of water nano-droplets based on TIP4P/2005 water model at 293 K, and related results are also shown in Figure 10. For the density of water in the bulk area of nano-droplets, the density increases as the radius decreases from 1.92 nm to 0.71 nm. For the 20-water droplet (with radius of 0.52 nm), its density in the bulk area is similar to the one of the 0.71 nm droplet. Although the present model does not describe all properties of water with quantitative accuracy, we feel that the general features of our results can be carried over to real water. For the smallest droplet whose radius is 0.4 nm, the density profile departs from this standard behavior. The density is not homogeneous and presents a peak. Coincidentally, the surface tension of this droplet is also significantly different from the value of other droplets.

## 4. Conclusion

In our study, the vapor pressure of six water models were calculated by MD simulations, and the SPC water model presented the best performance to reproduce the vapor pressure of water. Based on SPC water model, we then calculated the vapor pressure of water nano-droplets with different size. The value of $\ln\frac{P_{sat}(r)}{P_{sat\_0}}$ increases from 0.46 to 2.1 when the radius decreases from ~1.92 nm to ~0.4 nm. According to the Kelvin equation, the surface tension of these droplets was also estimated. The surface tension has a parabolic trend, e.g. it increases firstly and then decreases. The Tolman length conjecture was conjectured to be negative (-0.12 nm, here). Last but not least, the density profiles of water slabs and nano-droplets were analyzed.

**References**


1. P. Peeters, J. Hrubý, M. E. van Dongen, High pressure nucleation experiments in binary and ternary mixtures. *J. Phys. Chem. B* **105**, 11763-11771 (2001).
2. S. Rajamani, T. M. Truskett, S. Garde, Hydrophobic hydration from small to large lengthscales: Understanding and manipulating the crossover. *P. Natl. Acad, Sci.* **102**, 9475-9480 (2005).
3. V. I. Kalikmanov, in *Nucleation theory*. (Springer, 2013), pp. 17-41.
4. J. Paul, C. Collier, R. Saykally, J. Scherer, A. O'keefe, Direct measurement of water cluster concentrations by infrared cavity ringdown laser absorption spectroscopy. *J. Phys. Chem. A* **101**, 5211-5214 (1997).
5. T. Li, D. Donadio, G. Galli, Ice nucleation at the nanoscale probes no man's land of water. *Nat. Commun*, **4**, 1887 (2013).
6. M. O. Andreae, The aerosol nucleation puzzle. *Science* **339**, 911-912 (2013).
7. R. Zhang, A. Khalizov, L. Wang, M. Hu, W. Xu, Nucleation and growth of nanoparticles in the atmosphere. *Chemical Reviews* **112**, 1957-2011 (2011).
8. L. Mishchenko, B. Hatton, V. Bahadur, J. A. Taylor, T. Krupenkin, J. Aizenberg, Design of ice-free nanostructured surfaces based on repulsion of impacting water droplets. *ACS nano* **4**, 7699-7707 (2010).
9. D. Chandler, Interfaces and the driving force of hydrophobic assembly. *Nature* **437**, 640 (2005).
10. L. Maibaum, A. R. Dinner, D. Chandler, Micelle formation and the hydrophobic effect. *J. Phys. Chem. B* **108**, 6778-6781 (2004).
11. W. Thomson, On the equilibrium of vapour at a curved surface of liquid. *Proceedings of the Royal Society of Edinburgh* **7**, 63-68 (1872).
12. R. C. Tolman, The effect of droplet size on surface tension. *J. Chem. Phys.* **17**, 333-337 (1949).
13. C. Vega, E. De Miguel, Surface tension of the most popular models of water by using the test-area simulation method. *J. Chem. Phys.* **126**, 154707 (2007).
14. M. H. Factorovich, V. Molinero, D. A. Scherlis, Vapor pressure of water nanodroplets. *J. Am. Chem. Soc.* **136**, 4508-4514 (2014).

15. G. C. Boulougouris, I. G. Economou, D. N. Theodorou, Engineering a molecular model for water phase equilibrium over a wide temperature range. *J. Phys. Chem. B* **102**, 1029-1035 (1998).
16. J. R. Errington, A. Z. Panagiotopoulos, A Fixed Point Charge Model for Water Optimized to the Vapor− Liquid Coexistence Properties. *J. Phys. Chem. B* **102**, 7470-7475 (1998).
17. . (National Institute of Standards and Technology, 2018).
18. C. Vega, J. Abascal, I. Nezbeda, Vapor-liquid equilibria from the triple point up to the critical point for the new generation of TIP4P-like models: TIP4P/Ew, TIP4P/2005, and TIP4P/ice. *J. Chem. Phys.* **125**, 034503 (2006).
19. I. Nezbeda, Simulations of Vapor–Liquid Equilibria: Routine versus Thoroughness. *Journal of Chemical & Engineering Data* **61**, 3964-3969 (2016).
20. X. Wang, K. Binder, C. Chen, T. Koop, U. Pöschl, H. Su, Y. Cheng, Second inflection point of water surface tension in deeply supercooled regime revealed by entropy anomaly and surface structure using molecular dynamics simulations. *Phys. Chem. Chem. Phys.*, (2019).
21. K. Binder, M. Kalos, "Critical clusters" in a supersaturated vapor: Theory and Monte Carlo simulation. *J. Stat. Phys.*, **22**, 363-396 (1980).
22. A. Wexler, Vapor pressure formulation for water in range 0 to 100 C. A revision. *J. Res. Natl. Bur. Stand. A* **80**, 775-785 (1976).
23. R. M. Shields, B. Temelso, K. A. Archer, T. E. Morrell, G. C. Shields, Accurate predictions of water cluster formation, $(H_2O)n=2-10$. *J. Phys. Chem. A* **114**, 11725-11737 (2010).
24. I. Shvab, R. J. Sadus, Atomistic water models: Aqueous thermodynamic properties from ambient to supercritical conditions. *Fluid Phase Equilibr.* **407**, 7-30 (2016).
25. R. C. Tolman, The superficial density of matter at a liquid-vapor boundary. *J. Chem. Phys.* **17**, 118-127 (1949).
26. G. Graziano, Significance of the Tolman length at a molecular level. *Chemical*

*Physics Letters* **497**, 33-36 (2010).

27. Y.-Q. Xue, X.-C. Yang, Z.-X. Cui, W.-P. Lai, The effect of microdroplet size on the surface tension and Tolman length. *J. Phys. Chem. B* **115**, 109-112 (2010).
28. M. N. Joswiak, N. Duff, M. F. Doherty, B. Peters, Size-dependent surface free energy and Tolman-corrected droplet nucleation of TIP4P/2005 water. *J. Phys. Chem. Lett.* **4**, 4267-4272 (2013).
29. M. N. Joswiak, R. Do, M. F. Doherty, B. Peters, Energetic and entropic components of the Tolman length for mW and TIP4P/2005 water nanodroplets. *J. Chem. Phys.* **145**, 204703 (2016).
30. G. V. Lau, I. J. Ford, P. A. Hunt, E. A. Müller, G. Jackson, Surface thermodynamics of planar, cylindrical, and spherical vapour-liquid interfaces of water. *J. Chem. Phys.* **142**, 114701 (2015).
31. Ø. Wilhelmsen, D. Bedeaux, D. Reguera, Communication: Tolman length and rigidity constants of water and their role in nucleation. *J. Chem. Phys.* **142**, 171103 (2015).
32. V. Holten, D. Labetski, M. Van Dongen, Homogeneous nucleation of water between 200 and 240 K: New wave tube data and estimation of the Tolman length. *J. Chem. Phys.* **123**, 104505 (2005).
33. M. E. M. Azouzi, C. Ramboz, J.-F. Lenain, F. Caupin, A coherent picture of water at extreme negative pressure. *Nature Physics* **9**, 38 (2013).
34. S. K. Das, K. Binder, Universal critical behavior of curvature-dependent interfacial tension. *Phys. Rev. Lett.* **107**, 235702 (2011).
35. K. Binder, B. J. Block, P. Virnau, A. Tröster, Beyond the van der Waals loop: What can be learned from simulating Lennard-Jones fluids inside the region of phase coexistence. *Am. J. Phys.* **80**, 1099-1109 (2012).
36. B. J. Block, S. K. Das, M. Oettel, P. Virnau, K. Binder, Curvature dependence of surface free energy of liquid drops and bubbles: A simulation study. *J. Chem. Phys.* **133**, 154702 (2010).
37. H. Berendsen, J. Grigera, T. Straatsma, The missing term in effective pair

potentials. *J. Phys. Chem.* **91**, 6269-6271 (1987).

38. X. Li, T. Hede, Y. Tu, C. Leck, H. Ågren, Glycine in aerosol water droplets: a critical assessment of Köhler theory by predicting surface tension from molecular dynamics simulations. *Atmos. Chem. Phys.* **11**, 519-527 (2011).

39. F. Schmitz, P. Virnau, K. Binder, Monte Carlo tests of nucleation concepts in the lattice gas model. *Phys. Rev. E* **87**, 053302 (2013).

## Figures and Tables

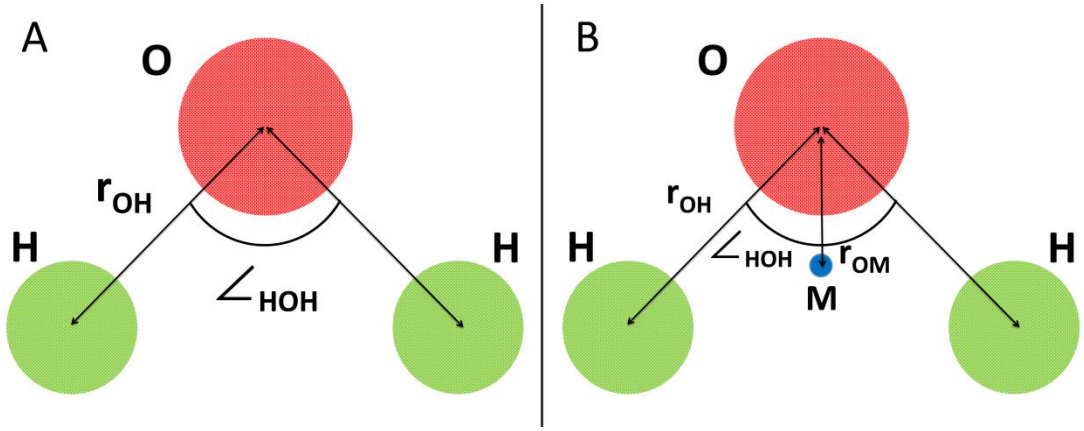


Figure 1. Schematic representations of (A) 3-point models (i.e. SPC, SPC/E and TIP3P) and (B) 4-point models (i.e. TIP4P, TIP4P/EW and TIP4P/2005).

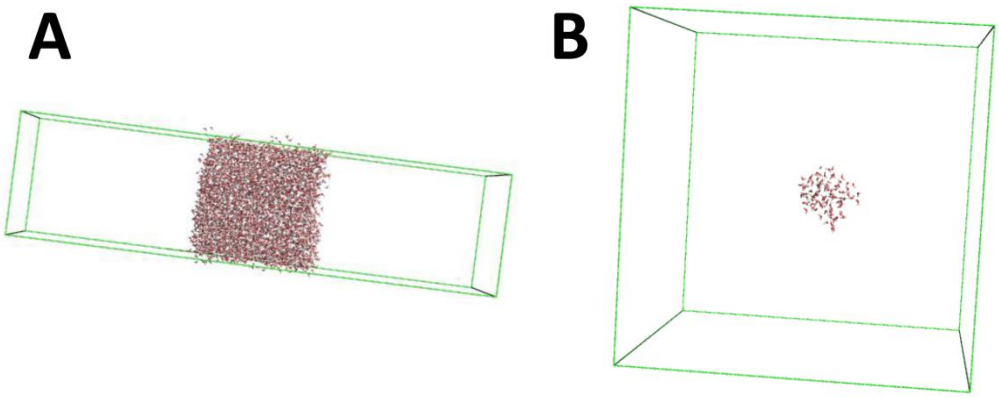


Figure 2. Simulation cell for counting the number of water molecules in the vapor. (A) For simulations of planar surface. (B) Simulations for nano-droplets.

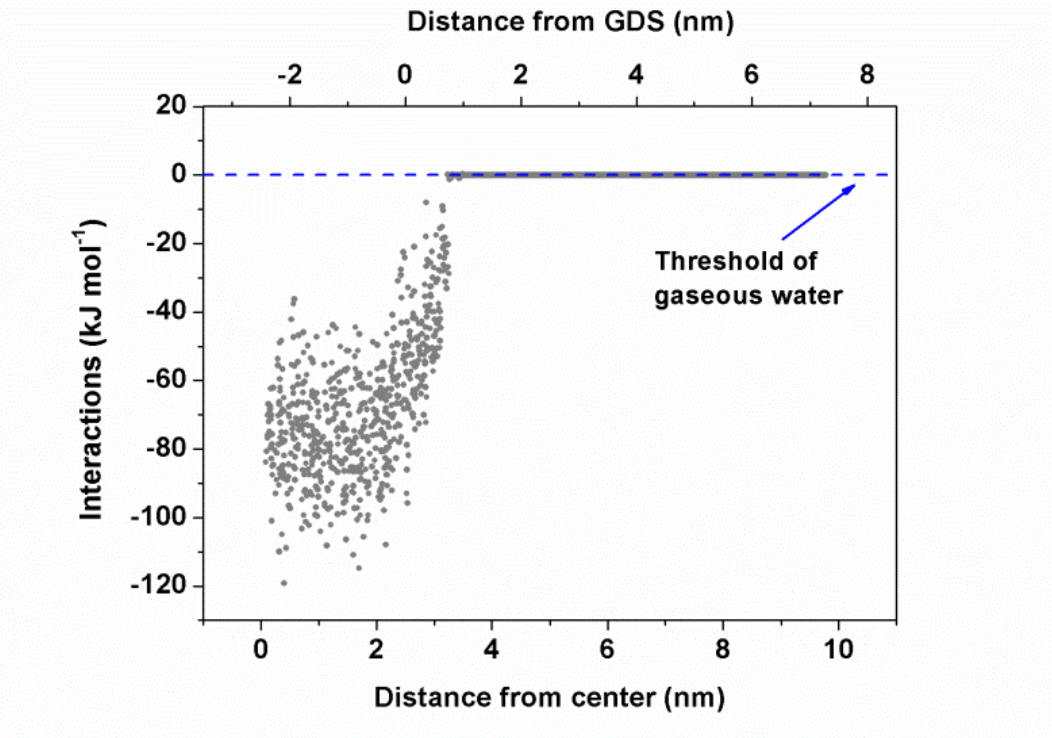


Figure 3. The interaction between a selected molecule and other molecules as a function of the distance between them. GDC means the Gibbs dividing surface.

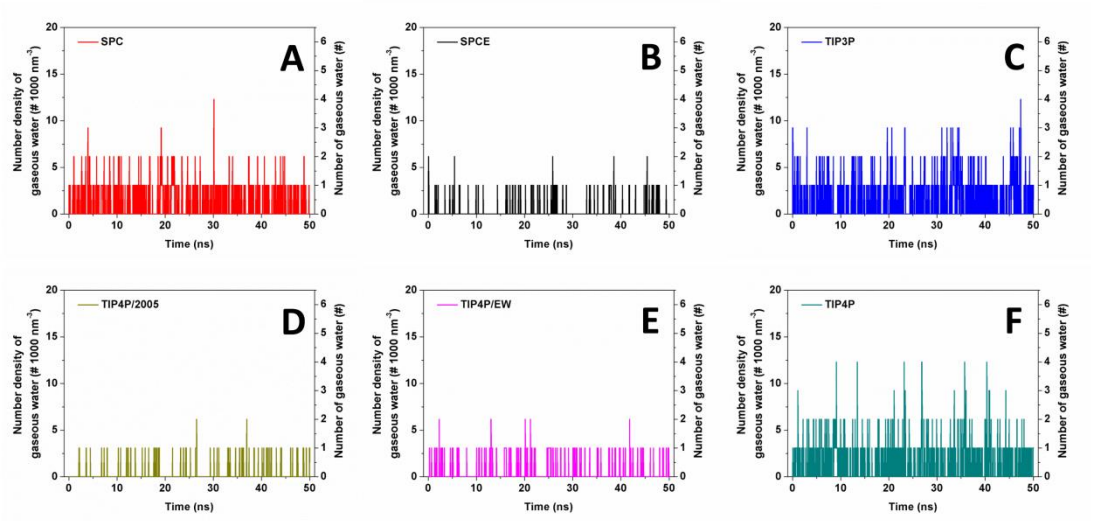


Figure 4. Number density of gaseous water molecules over the planar surface based on different water models. The type of model is specified in the left upper corner of each panel. A box volume of $5\ \text{nm} \times 5\ \text{nm} \times 20\ \text{nm}$ and a total number $N = 4142$ of water moelcules was used throughout.

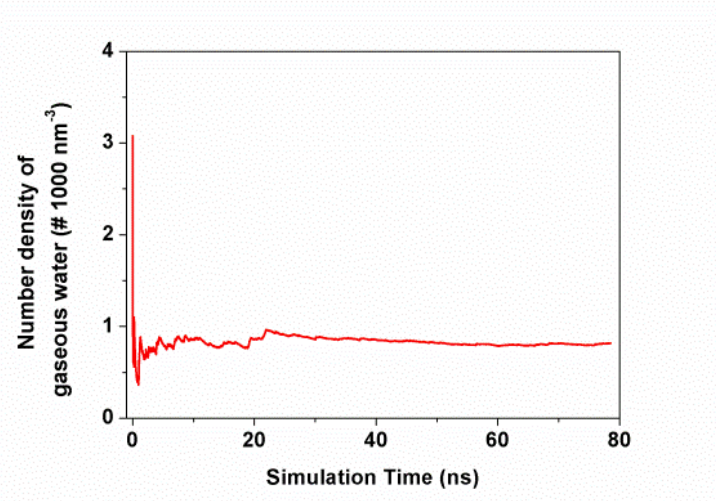


Figure 5. Time-average number density of gaseous water molecules over the planar surface based on SPC model.

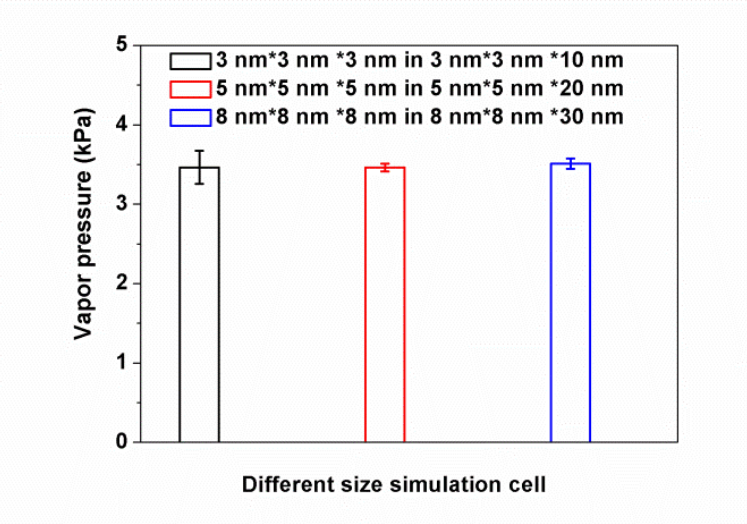


Figure 6. The vapor pressure based on SPC water model in different simulation cells.

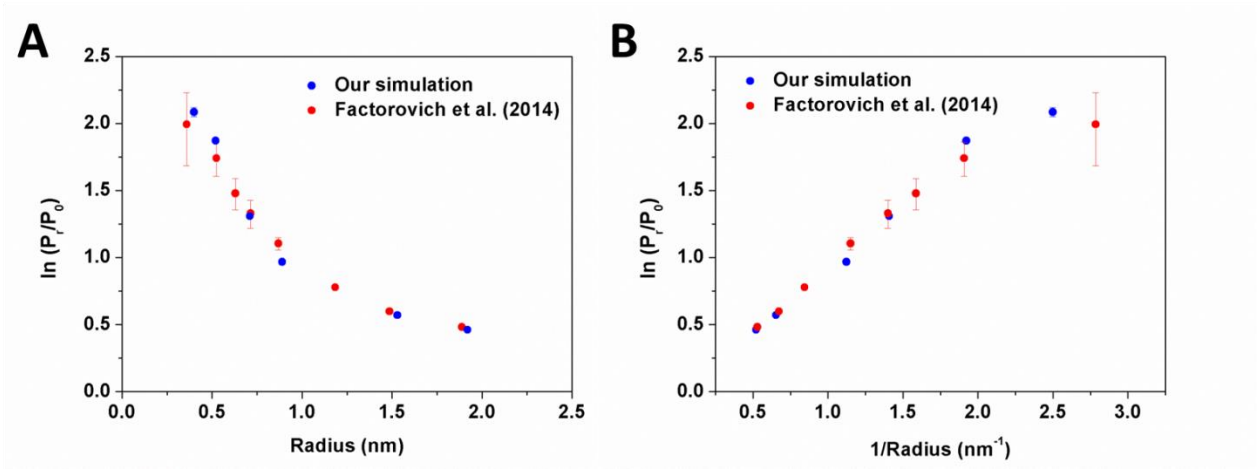


Figure 7. The relationship between the relative vapor pressure and size of nano-droplets.

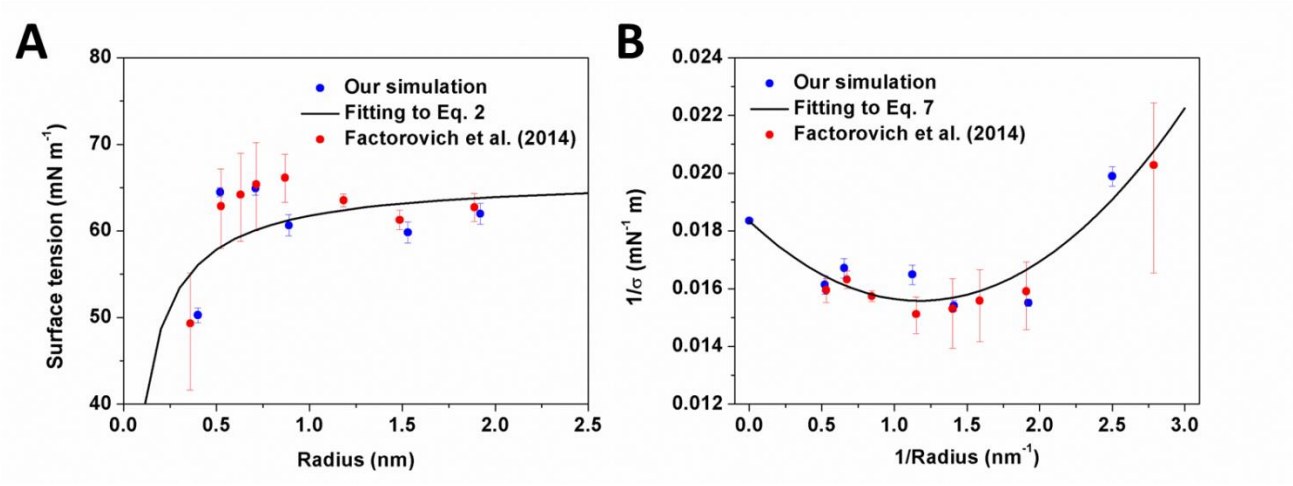


Figure 8. The relationship between the surface tension and size of nano-droplets.

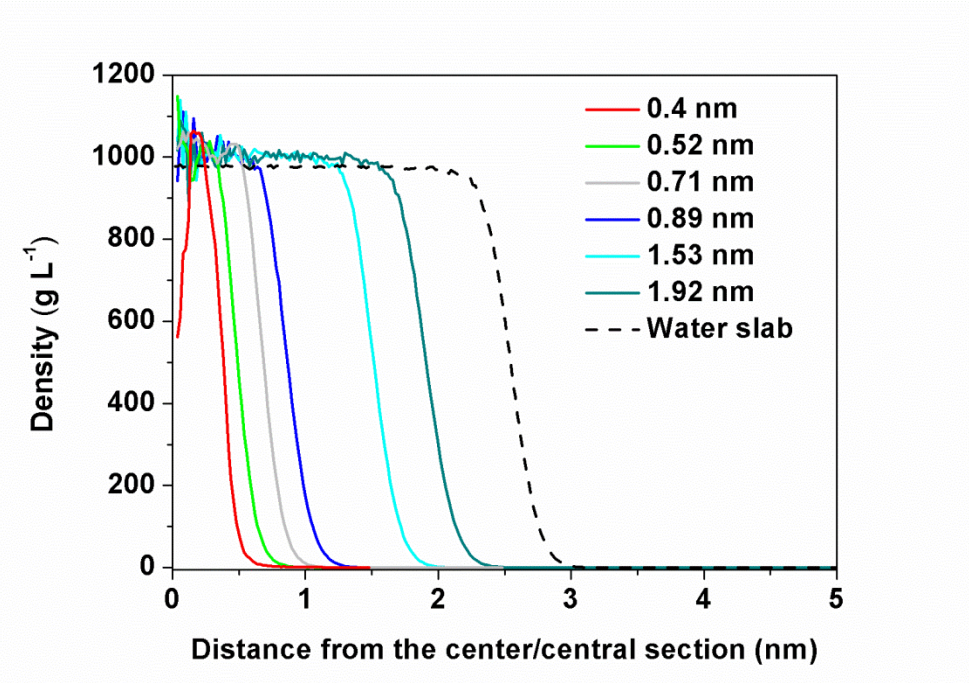


Figure 9. Density profile of water nano-droplets and slab.

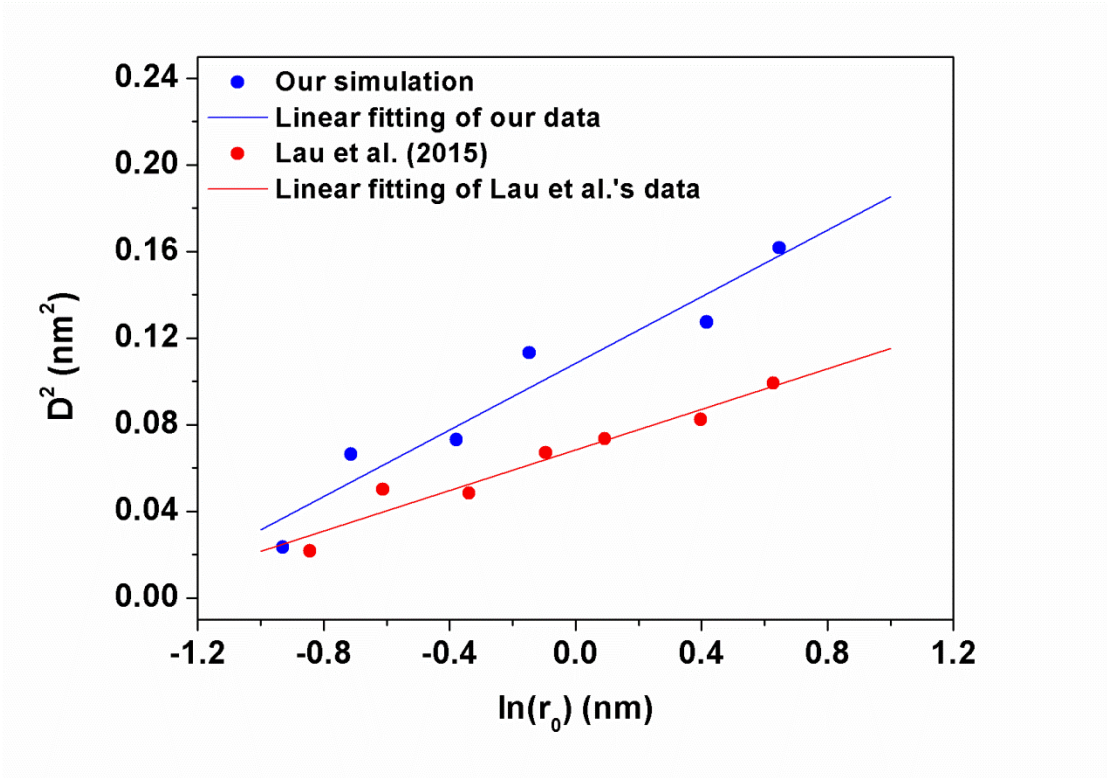


Figure 10. The relationship between the squared width $D^2$ and $\ln(r_0)$. The linear relation can be found in our data (SPC water at 298.15 K, blue circles and line) and Lau et al.'s data (TIP4P/2005 at 293K, red circles and line). As the density profile of 9-water droplets does not have a standard behavior, $D$ and $r_0$ of 9-water droplet were not calculated.

Table 1. Parameters of studied water models.

| Water model | $r_\sigma$ (nm) | $\epsilon$ (kJ $mol^{-1}$) | $r_{OH}$ (nm) | $r_{OM}$ (nm)[a] | q(O) (e) | q(H) (e) | q(M) (e)[a] | ∠HOH |
|---|---|---|---|---|---|---|---|---|
| SPC | 0.3166 | 0.65 | 0.1 | 0 | -0.82 | 0.41 | 0 | 109.47 ° |
| SPC/E | 0.3166 | 0.65 | 0.1 | 0 | -0.8476 | 0.4238 | 0 | 109.47 ° |
| TIP3P | 0.315061 | 0.6364 | 0.09572 | 0 | -0.834 | 0.417 | 0 | 104.52 ° |
| TIP4P | 0.3154 | 0.64852 | 0.09572 | 0.015 | 0 | 0.52 | -1.048 | 104.52 ° |
| TIP4P/EW | 0.316435 | 0.680946 | 0.09572 | 0.0125 | 0 | 0.52422 | -1.04844 | 104.52 ° |
| TIP4P /2005 | 0.31589 | 0.7749 | 0.09572 | 0.01546 | 0 | 0.5564 | -1.1128 | 104.52 ° |

a. Only 4-point models have these parameters.

Table 2. The vapor pressure of water at 298.15 K from MD simulations and measurements.

| Water model | Number density of water (# per 1000 $nm^3$) | Vapor pressure (kPa) | Literature data (kPa) at 300 K[a] |
|---|---|---|---|
| Measurement | 0.769 | 3.1690 | |
| SPC | 0.84 ±0.012 | 3.4616 ±0.0495 | / |
| SPC/E | 0.21 ±0.005 | 0.8654 ±0.0206 | 1 (*16*), 1.017 (*17*) |
| TIP3P | 1.38 ±0.268 | 5.6869 ±1.1044 | 5.123 (*17*) |
| TIP4P | 1.14 ±0.038 | 4.6979 ±0.1565 | 5.137 (*17*) |
| TIP4P/EW | 0.30 ±0.042 | 1.2363 ±0.1731 | 1.13 (*18*) |
| TIP4P /2005 | 0.17 ±0.009 | 0.7006 ±0.0371 | 0.778 (*18*) |

a. We do not find related data at 298.15 K, therefore the data at 300 K are shown here for the reference.

Table 3.Radius, vapor pressure and surface tension of different nano-droplets.

| Number of water molecules | Radius (nm) | $\ln\frac{P_{sat}(r)}{P_{sat\_0}}$ | Surface tension (mN/m) | Gibbs dividing radius ($r_0$, nm) | D (nm) | $\rho_L$ (g $L^{-1}$) |
|---|---|---|---|---|---|---|
| 9 | 0.4 | 2.1±0.047 | 50.77±1.14 | - | - | - |
| 20 | 0.52 | 1.87±0.015 | 64.47±0.52 | 0.49 | 0.2575 | 1035.5 |
| 50 | 0.71 | 1.31±0.015 | 64.89±0.75 | 0.685 | 0.27034 | 1037 |
| 100 | 0.89 | 0.97±0.019 | 60.64±1.23 | 0.863 | 0.3365 | 1025.6 |
| 500 | 1.53 | 0.57±0.012 | 59.82±1.21 | 1.516 | 0.3569 | 1010.2 |
| 1000 | 1.92 | 0.46±0.009 | 61.98±1.23 | 1.91 | 0.402 | 1005.1 |

**Curriculum Vitae**

**Basic information**

Name: Xiaoxiang Wang
Gender: Male
Date and country of birth: 21st, September, 1989. China
E-mail: xiaoxiang.wang@mpic.de (business); wxxgzs@163.com (private)
Phone: +49-6131-305-7203
Cell phone: +49 15751146632
Address: Lucy-Hillebrand-Straße 10, Room 4104-1, 55128, Mainz

**Education**

- Johannes Gutenberg-Universität Mainz, Germany, 2014 - , PhD of Chemistry
- Max Planck Institute for Chemistry, Germany, 2014 - , PhD of Chemistry
- Nanjing University, China, 2011-2014, Master of Environmental Engineering
- Guangzhou University, China, 2007-2011, Bachelor of Environmental Science

**Research Interest**

- Molecular Dynamics Simulation
- Phase Transition of Aerosol Particles
- Size Effect of Atmospheric Nanoparticles

**Publications**

20 Peer-review papers (as the first author in 5 papers)
See:
https://scholar.google.com/citations?hl=zh-CN&user=bLI18w8AAAAJ&view_op=list_works&sortby=pubdate

**Professional Service**

- Member of European Geosciences Union
- Member of American Chemical Society
- Member of GCCCD (Die Gesellschaft Chinesischer Chemiker und Chemieingenieure in der Bundesrepublik Deutschland)
- Reviewer: Environmental Science & Technology, Applied Microbiology and Biotechnology, SAR and QSAR in Environmental Research

**Awards**

- Best Paper in Conference of Chinese Society for Environmental Science (2012)
- Chinese National Award of Graduate Student (2013)
- Wang Baozhen Prize for Talent Master Students in Environmental Science (2014)